Band Limited Motion Control
of CNC Machine Tools

Von
Xinmei Zhang

Band 20

BAND LIMITED MOTION CONTROL

OF CNC MACHINE TOOLS

Vom Promotionsausschuss der
Technischen Universität Hamburg-Harburg
zur Erlangung des akademischen Grades
Doktor-Ingenieurin
genehmigte Dissertation

von
M.Sc. **Xinmei Zhang**
aus
Jiangsu, China

2010

1. Gutachter:	Prof. Dr. Klaus Rall
	Institut für Werkzeugmaschinen,Roboter und Montageanlagen
2. Gutachter:	Prof. Dr. Wolfgang Papiernik
	Siemens Automation and Drives
Tag der mündlichen Prüfung:	07. Mai. 2010

Acknowledgments

First and foremost, I would like to express my sincere gratitude to Prof. Rall. He not only guided me throughout the work but also taught me a lot of useful things which I did not know. He was also very supportive and generous in providing me with various opportunities. What I learned from him is a treasure for my future life.

I cannot fully express my gratitude to the incomparable Prof. Papiernik, for his initialization of the project, for guiding me with his wide and deep knowledge in the control area, and for his generosity, faith, help and patience.

My thanks also go to Mr. Cairns. He read the dissertation and corrected my English with patience and care.

I would like to thank the Siemens Automation and Drives for funding my work and providing the needed hardware and software for testing the result of this work.

My sincere appreciations to the entire team at the Institute of Machine Tools, Robotics and Assembly Lines, with special thanks to Yu Da, S. Tessmer, U. Schmeller and Dr. Wollnack for their help. For their generous assistance in the research of the thesis, I would like to acknowledge Ruangrit Ekachaiworasin and Carlos Gonzalez Vazquez.

My gratitude also goes to my friends in Hamburg, who made my life valuable. Specially I would like to thank Ine and Christian Hensgens, for encouraging me, for supporting me, and for giving me the feeling of confidence. I would like to thank my parents and parents-in-law. Thank you Mom and Dad, for supporting me anyways and always! Thank you Heidi and Dieter, for your understanding and endless help. My final thanks go to Mark and Jonas, to whom I owe so much...

Abstract

Machine tools are restricted by many factors to fulfilling the requirements of high speed and high accuracy. Among those factors, an elastic drive system with low eigenfrequency is very common. To allow the elastic drive system to achieve the high speed and high accuracy demands, efforts are invested in every phase of the drive system in this work.

Vibrations, especially resonance vibrations, inhibit the drive system from being fast and accurate. The mostly used method to reduce the vibration in the elastic drive system is the tuning of controller parameter. Optimal controller parameters for rigid system are studied thoroughly. However, for the controller parameters of the elastic system, the trial and error method must be used. In this work, two simple and practical formulas are first developed to set the controller parameter in velocity loop. These two formulas are also tested and verified in real machine tools. Meanwhile, input shaper, an effective feedforward method to eliminate vibrations, is integrated in the cascade control loop to provide another choice.

Parameter identification of the drive system is very helpful to understand the mechanical system and for further use. From measured frequencies of the drive system, the mechanical parameters of the system of high order can be quickly and accurately identified through the algorithms developed in this work. From the identified parameters, the drive system can be simulated near reality.

Besides the method of reducing vibration through feedback and feedforward controllers, another way to achieve high speed and high accuracy of machine tools is to avoid resonance vibration. An effective way to avoid resonance vibration is to let the command signal have no resonance frequencies content of the drive system. The command signal of each axis should avoid at least the lowest eigenfrequency of that corresponding axis. Normally the axes of the machine tools do not have the same eigenfrequencies. In this work, Wavelet Synthesis and iterative trajectory process are developed for this purpose. Severe vibrations are prevented from appearing through this method.

The algorithm and methods provided in this thesis are simulated and tested on a test rig. The simulation and test results show that the methods are effective in allowing the whole drive system to be quick and accurate.

Table of Contents

List of Figures

List of Tables

Nomenclature

a :	wavelet scale	-
${}^{i}a_j$:	denominator coefficient of transfer function	
a_i:	acceleration in ith axis	m/s^2
$\hat{a}$:	maximum acceleration	m/s^2
$\vec{a}$:	acceleration vector	m/s^2
A_1:	magnitude of first impulse of input shaper	-
A_2:	magnitude of second impulse of input shaper	-
${}^{i}b_j$:	numerator coefficient of transfer function	
b:	wavelet translation factor	-
$D_{0,1,\cdots,n}$:	torsional damping constant	$Nm/(rad/s)$
D:	torsional damping constant	$Nm/(rad/s)$
e :	Euler number	
$e(t)$:	controlled error signal	
E :	amplitude error	
F :	frequency	Hz
F_0 :	characteristic frequency	Hz
F_{ar}:	anti-resonance frequency	Hz
F_b :	dimensionless bandwidth indication	-
F_s :	sampling frequency	Hz
F_a :	scaled frequency	Hz
F_c :	dimensionless center frequency of wavelet	-
F_{dp} :	damped poles frequency	Hz
F_{dz} :	damped zeros frequency	Hz
F_d:	(damped) natural frequency	Hz
F_r:	resonance frequency	Hz
F_z :	zeros frequency	Hz
f_n :	denominator of transfer function	

g_n :	numerator of transfer function	
G :	amplitude of response	
G_v :	transfer function of velocity loop	
G_{sys} :	transfer function of controlled system	
G_{OL} :	transfer function of open loop	
$\hat{j}$:	maximum jerk	m/s^3
j_i:	jerk in ith axis	m/s^3
$\vec{\mathbf{j}}$:	jerk vector	$m/s-3$
$J_{0,1,\cdots,n}$:	moment of inertia	kgm^2
k_r:	proportional controller in velocity loop	$Nm/(rad/s)$
k_v:	proportional controller in position loop	$1/s$
k_p:	general proportional controller	-
$K_{0,1,\cdots,n}$;	torsional stiffness constant	Nm/rad
K:	torsional stiffness constant	Nm/rad
K_E:	voltage constant	Vs/rad
L :	length of rod	m
M_M:	torque to the motor	Nm
M_L:	torque to load	Nm
$M_{0,1,\cdots,n}$:	torque	Nm
$p_{1,2,\cdots,n}$:	poles	
$\vec{\mathbf{p}}'$:	path unit tangent vector	
$\vec{\mathbf{p}}''$:	curvature vector	
$\vec{\mathbf{p}}'''$:	third derivative of path vector	
$\vec{\mathbf{p}}$:	path vector	
Q :	coefficient of input shaper	
r :	frequency ratio	-
R :	radius of rod	m
s :	path parameter	m
$\dot{s}$:	path velocity	
$\ddot{s}$:	path acceleration	
$\dddot{s}$:	path jerk	
s_0 :	initial path parameter	

s_f :	final path parameter	
$\dot{s}_{max}$:	maximum path velocity	
$\ddot{s}_{max}$:	maximum path acceleration	
$\dddot{s}_{max}$:	maximum path jerk	
t_0 :	time period	s
t_d:	constant of derivative controller	
t_i':	constant of integral controller	
t_i:	time constant of PI controller	s
t_s :	sampling time period	s
T_d:	damped time period of the system	s
$\hat{T}_{Ei}$:	estimated equivalent time of current control loop	s
T_{Ei}:	equivalent time of current control loop	s
T_{En}:	equivalent time of velocity control loop	s
$T_{E\varphi}$:	equivalent time of position control loop	s
T_i :	time position of input shaper	s
T_n:	time period of the second order system	s
T_M:	time constant of motor	s
T_L:	time constant of load	s
v_i:	velocity in ith axis	m/s
$\hat{v}$:	maximum velocity	m/s
$\vec{\mathbf{v}}$:	velocity vector	m/s
$w(\tau)$:	window function	
$x(\tau)$:	input signal	
$z_{1,2,\cdots,n}$:	zero of the transfer function	
$\theta_{0,1\cdots,n}$:	radial angle	rad
$\dot{\theta}_{0,1,\cdots,n}$:	angular velocity	rad/s
$\ddot{\theta}_{0,1,\cdots,n}$:	angular acceleration	rad/s^2
ω_0 :	characteristic radial frequency	rad/s
ω_{dn} :	damped poles radial frequency	rad/s
ω_d :	natural radial frequency	rad/s
ω_r :	resonance radial frequency	rad/s
ω_n :	poles radial frequency	rad/s

ω_M :	angular velocity of the motor	rad/s
ω_L :	angular velocity of the load	rad/s
ω_{ref} :	reference angular velocity	rad/s
ω_z :	zeros radial frequency	rad/s
ω_{zn} :	damped zeros radial frequency	rad/s
ξ:	damping ratio	-
ξ_n:	damping ratio of poles in mass-spring-system	-
ξ_z:	damping ratio of zeros in mass-spring-system	-
θ_M :	angular position of the motor	rad
θ_L :	angular position of the load	rad
$\dot{\theta}_M$:	angular velocity of the motor	rad/s
$\dot{\theta}_L$:	angular velocity of the load	rad/s
$\psi_{a,b}$:	mother wavelet	
δ_w :	frequency resolution of mother wavelet	-
δ_t :	time resolution of mother wavelet	-
Δ_w :	frequency resolution of wavelet	Hz
Δ_t :	time resolution of wavelet	s

Acronyms

AC:	**A**lternating **C**urrent
AVO:	**A**bsolute **V**alue **O**ptimum
BCS:	**B**asic **C**oordinate **S**ystem
CNC:	**C**omputer **N**umerical **C**ontrol
D:	**D**erivative
DC:	**D**irect **C**urrent
DR:	**D**ouble **R**atio
EMF:	**E**lectro**M**agnetic **F**ield
ERA:	**E**igensystem **R**ealization **A**lgorithm
FT:	**F**ouier **T**ransform
FFT:	**F**ast **F**ourier **T**ransform
HSM:	**H**igh **S**peed **M**achining
I:	**I**ntegral
IS:	**I**nput **S**haping
MCS:	**M**achine **C**oordinate **S**ystem
NC:	**N**umerical **C**ontrol
P:	**P**roportional
SI:	**S**pecified **I**nsensitivity
SO:	**S**ymmetrical **O**ptimum
STFT:	**S**hort **T**ime **F**ourier **T**ransform
WT:	**W**avelet **T**ranform
ZV:	**Z**ero **V**ibration
ZVD:	**Z**ero **V**ibration **D**erivative

Glossary of some frequently related technical terms

Characteristic frequency (F_0):

is the frequency of an undamped system, at which the system oscillates in a free vibration situation. It is also called undamped natural frequency. It equals eigenfrequency and resonance frequency for the system without damping.

Natural Frequency(F_d):

is the frequency at which a damped system will oscillate in a free vibration situation. It is less than the characteristic frequency. The relationship between the characteristic frequency and natural frequency can be expressed by $F_d = F_0 * \sqrt{(1 - \xi^2)}$. It is also called damped natural frequency.

Eigenfrequency:

is the frequency at which the system will oscillate in a free vibration situation. For an undamped system, the eigenfrequency is the characteristic frequency of the system. For a damped system, the eigenfrequency is the damped natural frequency.

Resonance Frequency, or Resonant Frequency (F_r):

is the frequency at which a system tends to oscillate at maximum amplitude. For an undamped system, resonance frequency is the characteristic frequency of the system. For a damped system, resonance frequency is $F_r = F_0 * \sqrt{(1 - 2 * \xi^2)}$. When the damping of the system is small, the difference between the resonance frequency and natural frequency is small.

Pole Frequency:

is the frequency of the Pole in Pole-Zero Plot of the system. Pole frequency is the characteristic frequency.

Damped Pole Frequency (F_{dp}):

is the frequency of the imaginary part of the Pole in Pole-Zero Plot of the system. Damped pole frequency is also the damped natural frequency.

Zero Frequency:

is the frequency of the Zero in Pole-Zero Plot of the system.

Damped Zero Frequency (F_{dz}):

is the frequency of the imaginary part of the Zero in Pole-Zero Plot of the system.

System Frequency:

is the frequency of the controlled mechanical system.

Introduction

1.1 Motivation

Good quality and low cost of a product are always required by all customers. Those two factors of a product are mainly determined by the production machines. Good quality of a product is assured by high precision of the machine tools. Low price of a product can be achieved by increased productivity through high manufacturing speed together with minimized auxiliary process times and process stability. Therefore, high precision and speed are two demands for modern machine tools to provide products that satisfy customers [76].

Byrne presented curves in [8], as shown in Figure 1.1, tracing the development in manufacturing capability in terms of achievable machining accuracy during the last 60 years. Ultra-precision machine tools under computer control can position the tool relative to the workpiece to a resolution and positioning accuracy in the order of 1nm. For "precision machining", the accuracy could now achieve $10nm$ with the help of accurate machine elements. In "normal machining", e.g. CNC turning and milling machines, accuracies of 10 to 100 μm can be achieved. Besides knowing those concrete values of accuracies that machine tools can achieve, the tendencies to higher accuracies of machine tools also catch the eyes.

Precision manufacturing relies, to a significant extent, on the quality and accuracy of a machine tool. One important factor which affects the accuracy of a machined component is the error caused by the vibration of the machine tool. The commonly approved solution is to use rigid components to improve the accuracy of the machine system.

High Speed Machining (HSM) is also a mainstream trend. Origin of interest in HSM was the work done by Salomon in 1931 [20]. His definition of HSM is based on chip removal temperature reduction with high cutting speed (5-10 times higher than in conventional machining) in a machining process. Though later researchers have unfortunately not been able
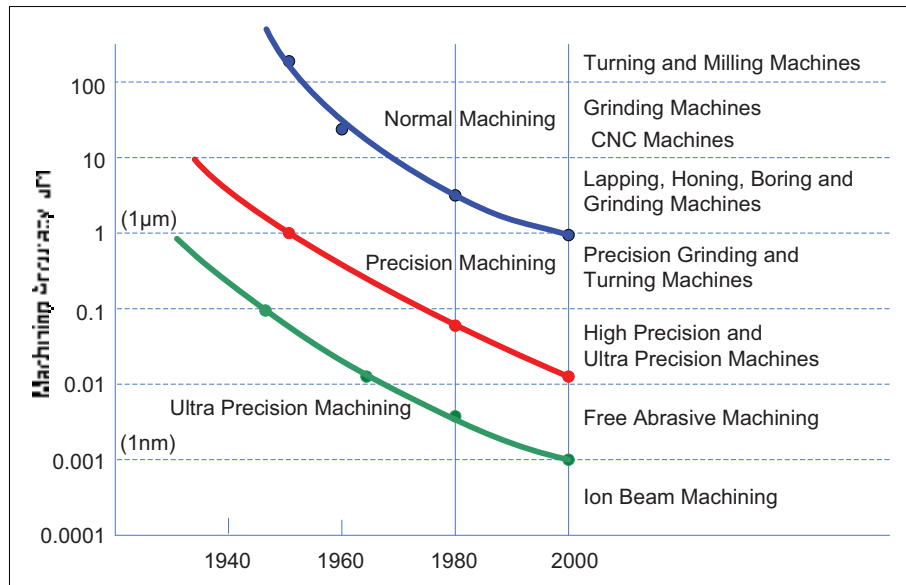
Figure 1.1: Development of achievable "Machining" accuracy over the last sixty years [8]

to verify this theory to its full extent, they also confirm that there is a relative decrease of the temperature at the cutting edge that starts at certain cutting speeds for different materials [20]. Table 1.1 [1] gives an example of some cutting speeds [3] for general knowledge of normal and high speed in cutting process. The cutting speed is dependent on the character of the workpiece material. For instance, for cutting gray cast iron, figures greater than 6m/s might be high-speed machining, whereas for softer aluminum alloys, 50 m/s is high-speed.

To perform HSM applications it is necessary to use light, but rigid machine tool to achieve high speed and minimize problematic vibrations. Light and rigid machine tool assures high acceleration, high eigenfrequency of the system, therefor high speed. Rigid machine tool assures no low eigenfrequency in the axis, therefore high accuracy.

Therefore, both precision and high speed machining require rigid machine system. However primarily due to space, weight, and power constraints, this is not always possible. Elasticity is unavoidable in some mechanical systems such as: high speed pick and place robots, coordinate measurement machines, hard drive testing machines, gantry cranes and so on. In machine tools, due to the power trains elements such as belts, spindles, gears and so on, the rigidity of the machine tool is also limited. All those kinds of mechanisms suffer from vibration related problems undergoing point-to-point, trajectory following, and other common motion tasks. The effective use of such systems can only be achieved when such vibrations can be properly handled.

Thus the demands of high quality and low cost of product motivate researchers to find a

---

[1]WC:Tungsten Carbide; PCD: polycrystalline diamond; CBN:cubic boron nitride; sia.: sialon; cer.: ceramic; +:more than

Work material	Solid tool - end mill, drill WC, coated WC, PCD, ceramic		Indexable tool - shell and face mill WC, ceramic, sialon, CBN, PCD	
	Typical velocity (m/s)	High Speed (m/s)	Typical velocity (m/s)	High Speed (m/s)
aluminum	5+ (WC,PCD)	50+ (WC,PCD)	10+	60+ (WC,PCD)
cast iron				
soft	2.5	6	6	20(sia.,cer.)
ductile	1.75	4	4	15(cer.)
steel				
free machining steel	1.75	6	6	10
alloy	1.25	4	3.5	6
stainless	1.75	2.5	2.5	4.5
hardness RC65	0.4	2	0.5(WC) 1.5(CBN,cer.)	0.75(WC) 3(CBN,cer.)
titanium	0.625	1	0.75	1.5
superalloy(Iconel)	0.75	1.25	1.3(WC) 3.5(sia.)	6(sia.,cer.)

Table 1.1: Example of some cutting speeds [3]

way to get rid of vibration for machine tools, or at least reduce them to an insignificant degree, especially those have inherent structure flexibility, so that the aims of high accuracy and high speed can be achieved.

1.2 Problem Description and Aims

The problem of reducing vibrations is a complex one that can be approached in many ways. Kozak [30] presents a simple manner to categorize those approaches by looking at a flexible dynamic system under control as shown in Figure 1.2, which can be found in every control text book.
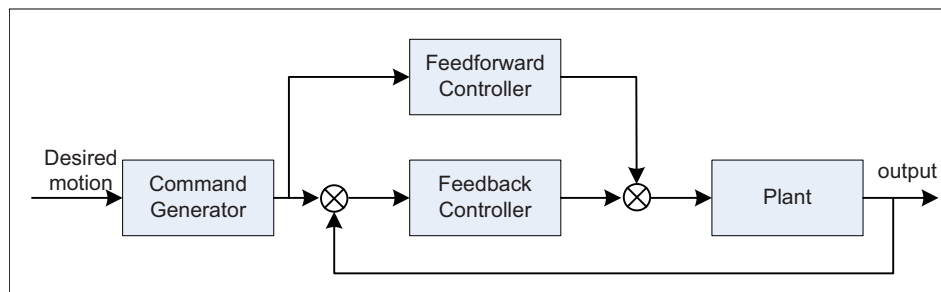
Figure 1.2: Block diagram of a typical closed loop control

There are four primary blocks in the above system. Researchers have made different efforts to reduce system vibration through those four blocks. They are the

1. Plant,

2. Command Generator,

3. Feedback Controller,

4. and the Feedforward Controller.

The Plant Block

The plant is normally the first concern for a researcher to think about when vibration reduction task is presented. The elastic structure of the plant is a source of vibrations. Therefore, making the plant system more rigid and/or adding damper to the plant are two main approaches.

The increasing of the rigidity sometimes comes with the increase of the inertia or mass of the components of the plant. This results in a reduced payload, worse dynamic behavior and increased cost. There are usually many trade-offs that must be considered in order to produce a physically and economically viable mechanism. Moreover, the elasticity that comes from power trains in the mechanical plant restricts the level of rigidity that can be reached.

Adding damper to the plant is usually done by adding damping material to a mechanism. However, modifying a pre-existing plant can be costly and difficult, and making modifications to reduce vibration can potentially change the performance of other aspects of the mechanism, e.g. the stiffness.

In this work, the plant is not targeted for eliminating vibrations, because the aimed solution is to reduce the vibration for any plant. But the knowledge of parameters of the plant is as important as getting rid of vibrations itself. Therefore, parameter identification is the first step. Two main domains of identification exist: frequency domain and time domain identification [1, 19, 36, 42]. The time domain identification is the classical approach to system identification. In the frequency domain identification, the frequency response of the system is used to estimate the plant parameters. However, the existing methods of parameters identification are either too complicated or not suitable for high order systems. As the characteristic parameters of the plant have to be known for the final solution, the first aim of this work is parameter identification for machine tool system of any order.

Aim 1: Identifying parameters of the plant for any order of the system.

The Command Generator Block

System vibrations come in mainly two forms. First form of vibrations are transient and die out after a period of time. The second form of vibrations are steady state vibrations, which are constant in magnitude and frequency, and do not die out. This second form of vibrations are generally caused by some periodic excitation. In general, vibrations can come in any combination of these two types. Vibrations can be caused by many different sources. Command generator is one of the sources. Typical example of command that brings the transient vibration is a step input.

A lot of efforts are dedicated to create or modify commands that cause the system response to satisfy desired transient/steady state performance characteristics [46, 47, 56, 57]. There is at least one distinct advantage of using the command generation approach over the other approaches: systems that suffer from troublesome dynamic behavior, such as vibrations, can be retrofitted to take advantage of command generation schemes at low cost and with generally no modifications needing to be made to the mechanical system and controller.

Limiting jerk, the derivative of acceleration, is now commonly applied to command generator of motion control [32, 33, 37, 55]. It can effectively reduce transient vibrations though not completely. The resulted s-curve of velocity profile, however, has no effect in getting rid of resonance vibration.

Some researchers turn to inverse dynamics [48]. When the system model is inverted, an input can be found by specifying the output. Unfortunately, the selected output trajectory does not always lead to an input, and it can be difficult to find the optimal trajectory. All kinds of time optimal trajectory, though also jerk limited, try to get a time optimal aim, but in the end the vibrations make the plant system a longer time to settle down, not to mention the bad accuracy. This is because the trajectory may contain the eigenfrequency of the plant system, thus inducing the resonance vibration. This initiates the idea of designing the trajectory that is jerk-limited, has no eigenfrequency of the mechanism, and is semi time optimal. This is the second aim that this work will achieve.

Aim 2: Designing trajectory that will not induce resonance vibration and also should be at least semi-time optimal.

The Feedback Controller Block

The feedback controller block contains the functional law used to control the system. It is perhaps the most popular block investigated by engineers for vibration reduction of flexible systems and disturbance rejection. Though more advanced controllers such as state space controller, "intelligent" controller are developed in academic research, the traditional cascade controller is still widely used in manufacturing industry [78]. One drawback of using the more intelligent and complicated controllers is that those controllers often require more or complicated sensors, which can present significant cost and feasibility issues and can potentially introduce stability problems. Therefore, the cascade controller, since its origin, is the principal controller in manufacturing industry.

Determination of the controller parameters in a cascade control loop has been investigated thoroughly [28, 29, 53, 79]. Double ratio, a method based on a damping optimum of a closed control loop, is widely accepted for a rigid plant system [21]. However, the double ratio method has its difficulty in calculating the parameters of PI controller in a cascade control loop for an elastic mechanical system. Lowering down the double ratio value is the most commonly used method for researchers to estimate the best control parameters for an elastic system. Without exception, the parameters are always away from the optimal one. Tuning the controller parameters for elastic system in practice are normally done by trial and error method, which costs time, depends a lot on experience and most of the time is not optimal. Elastic system is always the one that exists in the industry and brings most of the problems. Therefore, the third aim of this work is:

Aim 3: Determining cascaded controller parameters for elastic mechanical system.

The Feedforward Controller Block

The feedforward controller block was developed with the development of cascaded control. In the early days of positioning and contouring controls on ma-

chine tools, the axis position loop gains, which are also known as velocity constants, had to be identical. Otherwise following errors would not be the same on the axes, and workpiece contour errors would occur. Then about some 30 years ago it was found that the use of velocity feedforward could eliminate the need to match axis position loop gains. However this technique only was valid for constant feedrates. If any of the machine axes should have an acceleration or deceleration, position errors would occur. The velocity feedforward correction is added to the input of the velocity servo loop. For the problem of position errors during acceleration/deceleration, an acceleration feedforward concept can be added to the current loop input [7, 78]. Feedforward control is now used not only with cascaded control. It is also a more general concept. Any control without feedback is also considered as feedforward control. Input shaper, which is grouped to command generation by some researchers [43, 60, 68], is in fact a feedforward controller.

Input shaper is very profitable in eliminating vibration. It is also very simple to apply this method to control systems. As a feedforward controller, input shaper also shares the drawbacks with other feedforward controllers. The most obvious drawback is the fact that a feedforward controller has no resistance to disturbance. Moreover, input shaper generates additional problems when the trajectory is not stepwise [65, 67]. Consequently, input shaper is normally used where no disturbance exists and only the shape of the trajectory is important. But if input shaper is put into the cascade control loop instead of after the command generator, the trajectory following problems can be compensated, and the disturbance can be eliminated by the cascaded feedback controller. Hence aim 4 of this work is:

Aim 4: Designing input shaper within cascade control loop, to achieve quick response without vibration for elastic system.

1.3 Overview of the Thesis

This work addresses the vibration reduction problem for the machine tools. From suppressing vibration in a closed control loop with PI controller or input shaper, to identifying the

parameters of mechanical systems, to preventing vibration happening in command generator in a motion controller. This whole process makes sure the machine tools produce products precisely, quickly and economically.

The thesis is arranged as following: Chapter 2 presents basic knowledge of motion controllers and closed control loops for better understanding following chapters. The setup of a test rig is shortly introduced to simulate feed drive system for high speed application. In Chapter 3, the PI parameters of the velocity loop for elastic system is deduced to achieve a good compromise between accuracy and response time for setpoints input and disturbance. After this the input shaper together with the cascaded control loop are designed to obtain quick response and good accuracy for systems without disturbances or little disturbances. Chapter 4 describes the process of mechanical systems modeling and parameter identification. The trajectory that is produced by time optimal planning will be analyzed by time-frequency analysis method in Chapter 5. Then redesigning process of trajectory to get rid of eigenfrequency is developed in this chapter. Experiments are made and presented in Chapter 6, to validate the effectiveness of the process and methods developed in this work. Finally, some conclusions and suggestions for further work are given.

CHAPTER 2

CNC controlled Machine Tools

Important modules of the CNC controlled machine tools are: (i) a mechanism together with actuators, capable of performing motions; (ii) a controller together with a sensing system, capable of controlling these motions; and (iii) computer algorithms, capable of designing motions that the mechanism should follow. These three parts are named mechanical system, servo controller and NC kernel as shown in Figure 2.1.

The NC kernel accepts commands and other inputs to generate a motion profile using parameters such as distance to move, maximum acceleration and maximum velocity. The motion profile is then used to get the setpoints values for each axis of the machine tool by some transformation procedure. The above processes will be explained in greater detail in section 2.1.
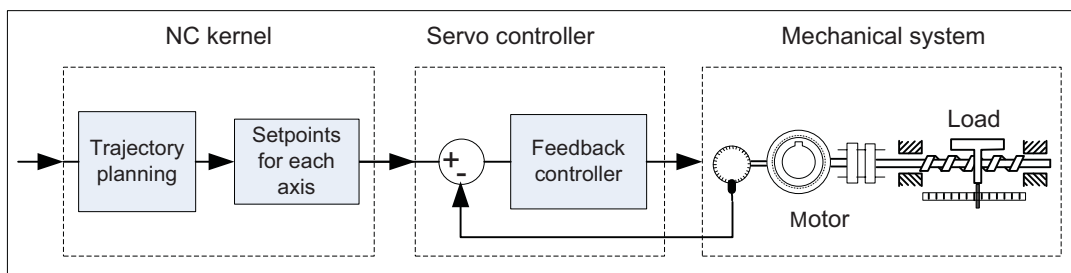
Figure 2.1: Control structure of one axis in CNC machine tool

The servo controller receives the setpoints command from the NC kernel, compares this with the feedback signal from the sensing system, and decides the amount of movement that the motor should follow, thus keeping the mechanical system tracking the setpoints command. The typical servo control scheme is explained in section 2.2.

The mechanical part is the mechanism that carries out the command. In machine tools, the mechanical part for each axis normally has a motor to provide torque/force, a load to follow the movement of the motor, and power train components to transfer movement from the

motor to the load. Depending on the accuracy requirements, the complexity of controller, and the stability of the mechanical system, the measurement system could either be installed on the motor side or the load side. Chapter 2.3 explains more about the mechanism of machine axis.

2.1 Motion Planning and Control

In practical applications the setpoints for each axis need to be generated automatically. The NC kernel has the task to generate setpoints over time for the axes. This process in the NC kernel is also identified as motion planning and control process.

2.1.1 Basic functions of the NC kernel

The motion planning and control process can then be further divided into five parts: contour generation, trajectory planning (including look-ahead function and motion control), interpolation, kinematic transformation and fine interpolation as shown in Figure 2.2 with references to [44, 45].
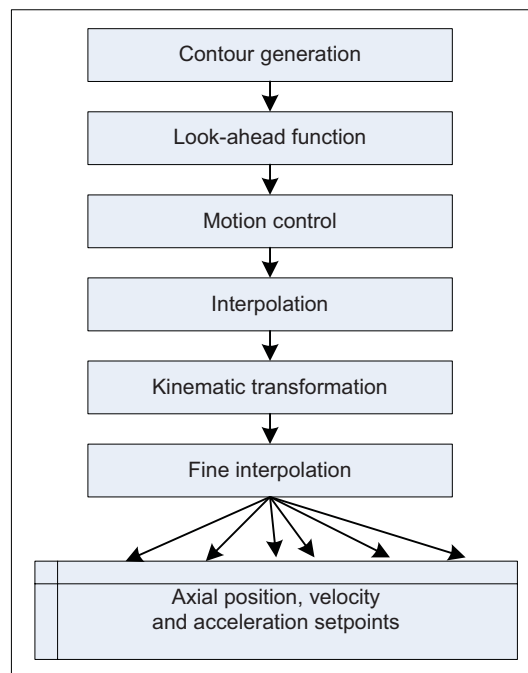
Figure 2.2: Geometry data processing in the NC kernel [44]

Contour is defined by a user part program in the form of linear, circular, helical, polynomial or spline blocks. It is followed by a contour rounding function for the purpose of getting rid of discontinuous transitions between neighboring blocks by making them tangential or C^2

continuous (C^2 continuity requires that the 2nd derivative of two curves are equal at joining joint. Intuitively, two curves are C^2continuous at the joining point if the acceleration does not change when crossing one curve to the other). The processed contour together with the machine data flow into the static and dynamic look-ahead function. The static look-ahead function checks the contour for "critical points" where the programmed path feedrate may not be maintainable and which therefore may have to be reduced to a lower value. The task of the dynamic look-ahead function is then to define a "maximum path velocity" from which braking down to zero velocity is guaranteed without exceeding the possible axis acceleration rates at the end of the blocks in the processor queue. The geometric data then go to the motion controller. The basic task of the motion controller is trajectory planning, which is to transpose the state vector of the motion, which is composed of the scalar path variables jerk, acceleration, and distance, from an existing initial state to a desired final state in the optimum time allowing for defined restrictions. In principle, it can be conceived that the input to a trajectory planning algorithm is the path description and the constraints imposed by the machine dynamics, whereas the output is the path acceleration, path velocity and distance setpoints. The subsequent interpolation then needs to calculate the unit tangent and curvature vectors, in accordance with the selected interpolation type, in order to produce the Cartesian setpoints for the position vector, the velocity and acceleration vectors. Before the Cartesian setpoints can go into the servo control loop, kinematic transformation is needed to transfer the setpoints from Basic Coordinate System (BCS) to Machine Coordinate System (MCS). Up to now, each axis of the machine tool has its reference input. However, the sampling cycle of the setpoints of the axes does not map with the sampling cycle of the servo control loop. Therefore, fine interpolation has to be performed. The calculated velocity and acceleration (torque) are finally passed to the servo control level where velocity, torque and field regulation, pulse width modulation and actuation of the power section are performed. The servo control system acts to make the machine track the reference signal by activating the appropriate actuators of the axes [45] [44].

2.1.2 Trajectory planning

Trajectory planning is the central task of the motion controller. It is the process of computing a sequence of desired positions, velocities and accelerations over time. There are two important requirements which must be fulfilled for the planning of executable trajectory [55].

The first requirement is that a desired trajectory must be able to be realized physically without causing mechanical damage to the machine tools or the environment. In most motion

control devices, this work is partly done by path planning to assure collision avoidance. Avoiding mechanical damage is mainly assured in the trajectory planning phase by applying soft motion control instead of brisk motion control.

The second important demand is that the movement must be "optimal". The evaluation of trajectory planning data should satisfy certain performance criteria, the most important of which is time. Optimization with regard to minimum time yields very important information: a minimum time trajectory represents the utmost limit of ability which a given machine is able to achieve on a prescribed path subject to all relevant constraints and without deviating from the path.

Brisk motion control and soft motion control

Step velocity input, the typical command for testing the system's response, is seldom used in machine tools due to the vibration it brings to the system. Smooth command reduces system vibration by avoiding abrupt changes in the command input. This property, in nature, is realized through limiting the command's first and/or higher order derivatives. In this sense, brisk motion control is a first order smooth velocity command generation, and soft motion control a second order smooth velocity command generation.

In brisk motion control, the acceleration of the plant should not exceed its maximum acceleration limitation, but the acceleration could change suddenly as shown in Figure 2.3 (a), which causes jerky motion. Brisk motion control can cause severe vibrations in the mechanism that may lead to the failure of mechanical parts, besides the jerky motion. Moreover, the possibly limited bandwidth of the actuators may make it impossible to realize discontinuous actuator torques in practice. The jerky character of a machine movement can be reduced by formulating additional movement constraints for jerk, which is the derivative of acceleration.

In soft motion control, as shown in Figure 2.3 (b), the velocity, acceleration and jerk at each time should not exceed its limitation, $\hat{v}$, $\hat{a}$ and $\hat{j}$. Compared with brisk motion control, it needs more time to finish the same task. However, if the settling time is compared, soft motion control may not be slower than brisk motion control, not to mention a smoother manufacturing process and better quality of the product. Therefore, soft motion control is mostly used in applications where accuracy and the absence of vibrations are stressed.
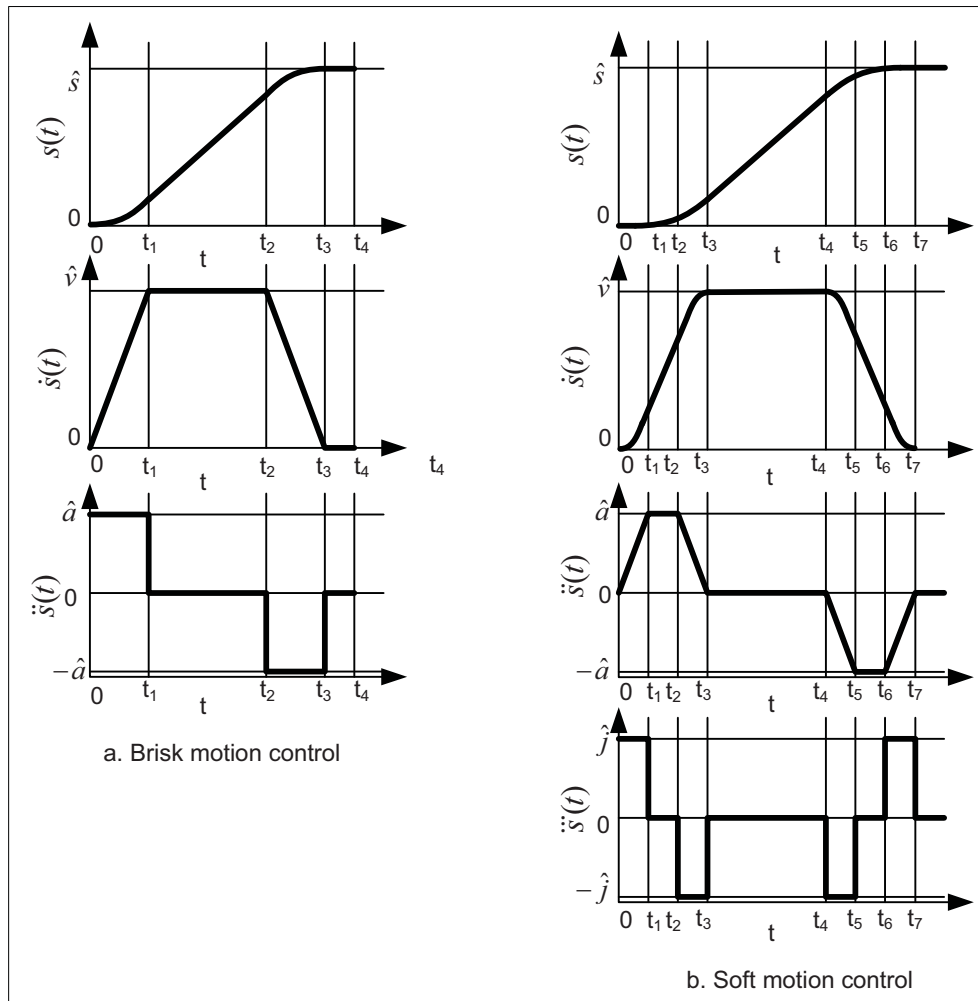
Figure 2.3: Brisk motion control and soft motion control

Path-constrained, jerk-limited, time optimal trajectory planning

Trajectory planning is an optimization problem. In optimization, aims, boundary conditions and constraints are the three elements that need to be addressed.

As stated before, optimum time is the main aim of the trajectory planning. The boundary conditions are simple as all the initial and final states should be zero. The constraints in the trajectory planning are based on the ability of the machine tools besides "path constrained" and "jerk-limited". "Path constrained" illustrates that the trajectory to be designed is for a given path. "Jerk-limited" reveals that the trajectory is the soft motion trajectory.

The constraints for trajectory planning can be summarized as two types [81]: the system constraints imposed by the machine tools themselves (due to the limits on the axis motion constraints), and the path constraints given by the task (geometric constraints). These two kinds of constraints determine that the path motion (including path velocity $\dot{s}$, path acceleration $\ddot{s}$, and path jerk $\dddot{s}$) should be within certain limitations.

The **system constraints** include maximum axis velocity $\hat{v}$, axis acceleration $\hat{a}$, and axis jerk $\hat{j}$ of each axis in machine tool. The axis velocity, acceleration and jerk constraints can be expressed as the velocity, acceleration and jerk bounds on each axis as shown in equations (2.1a),(2.1b),(2.1c).

$$-\hat{v}_i \leq v_i \leq \hat{v}_i, \quad v_i \in \vec{\mathbf{v}}, \tag{2.1a}$$

$$-\hat{a}_i \leq a_i \leq \hat{a}_i, \quad a_i \in \vec{\mathbf{a}}, \tag{2.1b}$$

$$-\hat{j}_i \leq j_i \leq \hat{j}_i, \quad j_i \in \vec{\mathbf{j}}, \tag{2.1c}$$

where

$i = 1 \cdots n$, n is the number of axis,

$\vec{\mathbf{v}}$: the velocity vector,

$\vec{\mathbf{a}}$: the acceleration vector,

$\vec{\mathbf{j}}$: the jerk vector

$$\vec{\mathbf{v}} = \begin{bmatrix} v_1 \\ v_2 \\ \cdots \\ v_n \end{bmatrix} \quad \vec{\mathbf{a}} = \begin{bmatrix} a_1 \\ a_2 \\ \cdots \\ a_n \end{bmatrix} \quad \vec{\mathbf{j}} = \begin{bmatrix} j_1 \\ j_2 \\ \cdots \\ j_n \end{bmatrix}.$$

The **path constraints** are the geometry constraints of a given path. Given a geometric path for the task parameterized as a function of the arc length parameter s: $\vec{\mathbf{p}}(s)$ where $s \in [s_0, s_f]$, the path unit tangent $\vec{\mathbf{p}}'$: $\vec{\mathbf{p}}' = \frac{d\vec{\mathbf{p}}}{ds}$, curvature $\vec{\mathbf{p}}''$: $\vec{\mathbf{p}}'' = \frac{d^2\vec{\mathbf{p}}}{ds^2}$ and the third derivative vector $\vec{\mathbf{p}}'''$: $\vec{\mathbf{p}}''' = \frac{d^3\vec{\mathbf{p}}}{ds^3}$ are among the main constrains influencing the path motion. The trajectory planning problem is greatly simplified by parameterizing the path with the parameter s. This reduces the $4n$ (4 comes from axial path, velocity, acceleration and jerk; n: the number of axes) dimensional problem to four states s, $\dot{s}$, $\ddot{s}$ and $\dddot{s}$ [58]. These four states of s are also named s-plane.

The system and path constraints form the path motion limitation from two aspects:

(i) First, the velocity, acceleration and jerk of each axis should not exceed its ability as listed in equations (2.1). As path motion in the s-plane is preferred instead of axis motion, the relationship between the axis motion and path motion is described by the following equations:

$$v_i = \frac{dp_i}{dt} = \frac{dp_i}{ds}\dot{s} = p'_i\dot{s}, \tag{2.2a}$$

$$a_i = \frac{d^2p_i}{dt^2} = \frac{dp_i}{ds}\ddot{s} + \frac{d^2p_i}{ds^2}\dot{s}^2 = p'_i\ddot{s} + p''_i\dot{s}^2, \tag{2.2b}$$

$$j_i = \frac{d^3p_i}{dt^3} = \frac{dp_i}{ds}\dddot{s} + 3\frac{d^2p_i}{ds^2}\dot{s}\ddot{s} + \frac{d^3p_i}{ds^3}\dot{s}^3 = p'_i\dddot{s} + 3p''_i\dot{s}\ddot{s} + p'''_i\dot{s}^3, \tag{2.2c}$$

where $i = 1 \cdots n$.

Together with equations (2.1), the limitations of $\dot{s}$, $\ddot{s}$ and $\dddot{s}$ are obtained though the following equations:

$$-\hat{v}_i \leq p'_i\dot{s} \leq \hat{v}_i, \tag{2.3a}$$

$$-\hat{a}_i \leq p'_i\ddot{s} + p''_i\dot{s}^2 \leq \hat{a}_i, \tag{2.3b}$$

$$-\hat{j}_i \leq p'_i\dddot{s} + 3p''_i\dot{s}\ddot{s} + p'''_i\dot{s}^3 \leq \hat{j}_i, \tag{2.3c}$$

where $i = 1 \cdots n$.

(ii) Secondly, the path velocity, acceleration and jerk should not exceed the maximum ability of the machine tools determined by axis motion. Therefore, the path motion constraints should also be within the limitations as calculated in (2.4).

$$0 \leq \dot{s} \leq \sqrt{\sum_{i=1}^{n} \hat{v}_i^2}, \tag{2.4a}$$

$$-\sqrt{\sum_{i=1}^{n} \hat{a}_i^2} \leq \ddot{s} \leq \sqrt{\sum_{i=1}^{n} \hat{a}_i^2}, \tag{2.4b}$$

$$-\sqrt{\sum_{i=1}^{n} \hat{j}_i^2} \leq \dddot{s} \leq \sqrt{\sum_{i=1}^{n} \hat{j}_i^2}, \tag{2.4c}$$

where $i = 1 \cdots n$.

The final limitations of $\dot{s}$, $\ddot{s}$ and $\dddot{s}$ are the smallest range determined from equation (2.3) and equation (2.4).

The time optimal trajectory planning problem could be structured now as follows:

Given a geometric path for the task parameterized as a function of the parameter s: $\vec{p}(s)$ where $s \in [0, s_f]$

1. *Objective function*

$$min : T = \int_0^{t_f} 1\, dt \tag{2.5}$$

where t_f is the final time of motion along the path.

2. *Boundary conditions*

$$
\begin{aligned}
\dot{s}_{s=0} &= 0 & \dot{s}_{s=s_f} &= 0 \\
\ddot{s}_{s=0} &= 0 & \ddot{s}_{s=s_f} &= 0 \\
\dddot{s}_{s=0} &= 0 & \dddot{s}_{s=s_f} &= 0
\end{aligned}
\tag{2.6}
$$

3. *Constraints*

   (i) *path velocity constraint:*
   $$
   0 \leq \dot{s} \leq \dot{s}_{max}
   \tag{2.7}
   $$

   (ii) *path acceleration constraint:*
   $$
   \ddot{s}_{min} \leq \ddot{s} \leq \ddot{s}_{max}
   \tag{2.8}
   $$

   (iii) *path jerk constraint:*
   $$
   \dddot{s}_{min} \leq \dddot{s} \leq \dddot{s}_{max}
   \tag{2.9}
   $$

Trajectory planning is done for the path in the s-plane. That is, the trajectory obtained is $s(t), \dot{s}(t), \ddot{s}(t)$ and $\dddot{s}(t)$. To generate the setpoints commands for each axis of the machine tool, the s-plane trajectory has to be transfered to each axis as described in equation (2.2).

Vibration caused by the trajectory

In the trajectory planning phase, the jerk limitation is applied in order to reduce vibrations caused by the excitation of the eigenfrequencies of machine tools. Normally, low jerk trajectories can be tracked more accurately. However, the jerk should not be lowered too much, as it increases the time of motion.

Though the vibration level is reduced for the trajectory with soft motion control compared with brisk motion control in each axis, the vibration problem is still there due to the fact that the eigenfrequencies exist in each axis motion(v_i, a_i, j_i). The existing of eigenfrequencies in each axis can not be detected unless the s-plane trajectory is transfered to axis motion. Therefore, in the trajectory planning phase, it is impossible to avoid or predict the resonance vibration problem.

Resonance vibration could be avoided if the eigenfrequencies of the axis are eliminated from the trajectory. To remove the eigenfrequencies in the trajectory, the first step is to find out

where the eigenfrequencies are in the trajectory. Even if there is an eigenfrequency in the trajectory, this does not imply that it will create the vibration problem: a brief existence of eigenfrequency in the trajectory does not create enough energy to cause vibrations. For example, in industry, experienced technicians would speed up the machine tools very quickly if resonance has to be passed during the run-up or run-down of the machines. In a second step, the area where the eigenfrequency of the axis appears should be redesigned so that the vibration level that it would create is within defined limits. See chapter 4 for more details.

2.2 Servo Control

The concept of servo control has not changed significantly in the last 50 years. The basic reasons for using servo system include the need to improve transient response times, reduce steady state errors, reduce the sensitivity to load parameters and eliminate disturbances.

PID type controller is widely used in servo control because of its simplicity and successful industrial applications. It consists of three parts:

- a proportional (P) part generates a control action which is proportional to the error signal;

- an integral (I) part on the integral of the error signals; and

- a derivative (D) part on the changing rate of the error signal.

The ideal algorithm of a PID controller is:

$$u(t) = k_p[e(t) + \frac{1}{t_i} \int e(t)dt + t_d \frac{d}{dt} e(t)] \tag{2.10}$$

$u(t)$: control command signal; $e(t)$: error signal;
k_p: proportional gain; t_i: integration time constant; t_d: derivative time constant.

More or less, the proportional gain k_p affects the overall response of the closed-loop system to an error $e(t)$. Increasing k_p will increase the bandwidth (faster response) of the closed-loop system, and reduce the steady state error. However, the steady state error cannot be reduced to zero, and with high proportional gain k_p, the closed-loop system tends to become unstable. In order to reach a zero steady state error, an integral action can be used together with the proportional action. However, increasing the integration time t_i causes the system to become more oscillatory in transient and the bandwidth is reduced. The derivative action

has a counter-action to the integral. It reduces the oscillation in transient, and enlarges the bandwidth.

All the feedback control systems rely on sensor measurements, which usually contain high frequency noise. When the derivative action is used in the controller, it tends to amplify this high-frequency noise, and generates an unreasonable high controller command. To avoid this problem at high frequencies, a derivate action is usually combined with filtering techniques. However, both the integral action and the derivative action have some practical problems, which have to be carefully dealt with in the real implementation.

Cascade control has been by far the predominant control structure in machine tools because of its many advantages. Though the theory of advance motion control concepts has been well known for nearly 40 years, applications in the machine tools industries are scarcely found. State space is a strong competitor for the cascade control.

2.2.1 Cascade control

An example for a cascade controller structure for servo control is illustrated in Figure 2.4. It consists of several distinct control loops: the innermost current control loop is enclosed by a velocity control loop, which is further enclosed by the position control loop [21] [45].
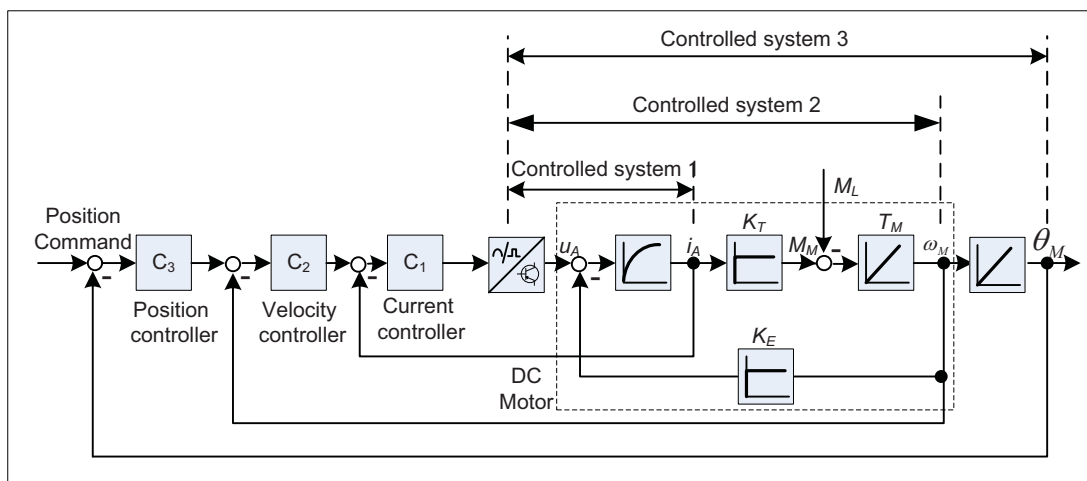
Figure 2.4: Block diagram of cascade control for a feed drive[21]

The inner loop in Figure 2.4 is the current control loop. A transistor power converter acts as the actuating device, which supplies the electrical drive with power. The motor given in Figure 2.4 is a DC motor. The current i_A is the result of the power converter and back EMF (Electromagnetic Field) which is proportional to the motor's velocity with voltage constant K_E. Torque is the result of i_A multiplied with torque constant K_T. Therefore the current

control loop is sometimes also called the force/torque control loop. It is usually realized with PI controllers (C_1 in Figure 2.4). Normally the current loop is built in the motor drive system, and is already tuned to an optimal value before it is put to use. For simplification, the current loop can be approximated by a first-order lag with the equivalent time constant T_{Ei}. The simplified cascade control structure with the equivalent time constant for the current control loop is shown in Figure 2.5.
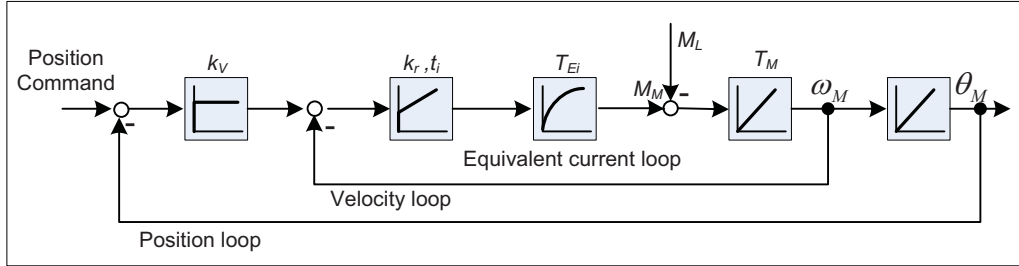
Figure 2.5: Simplified cascade control loop

The velocity control loop is superimposed on the current loop. Mechanical disturbance, M_L in Figure 2.4, enters directly into the speed control loop. The disturbance in the velocity loop will cause error in the output speed. To eliminate the steady state velocity error, the controller in the velocity loop is usually designed as a PI controller (C_2 in Figure 2.4). The performance of the velocity loop is very important for the servo control system, because almost all the disturbances of the system enter this loop. Thus the effects of non-linearity and disturbance input in the velocity loop are dealt with in the velocity loop. In this way, non-linearity and disturbance can be reduced, and with less influence on the outer loop.

It is usually enough to use a proportional controller (C_3 in Figure 2.4) for the position control loop, because there is an integrator in the position loop by nature: the integration of the speed signal gives the position signal, see Figure 2.4. No further disturbances can appear at the input of this integrator either. The integrator also reduces the steady state position error to zero for a step change in the reference position input.

Figure 2.5 shows the simplified cascade control structure for a drive axis. T_{Ei} stands for the equivalent time constant of the simplified current control loop. k_r and t_i are the proportional gain and integral part of the velocity controller respectively. k_v is the proportional gain of the position controller, which is normally called velocity gain.

Although the number of tuning parameters may be higher than that with a single loop control structure, the cascade control structure is usually tuned step-by-step starting from the innermost loop to the outermost loop, ensuring a safe start-up of the entire system. A cascade controller structure requires that the bandwidth (speed of response) of each loop in-

creases from the outer loop to the inner loop, so that the dynamic delay caused in the inner loop could be ignored by the outer loop. As in the case of the cascade servo control structure in Figure 2.5, the current control loop usually has the highest bandwidth, and the position control loop has the lowest bandwidth. Thanks to the advance in power electronics, the current loop is commonly realized with a bandwidth of around 2 kHz.

The advantages of using cascade control are summarized as follows:

- Faster inner controller handles disturbances and/or modeling error in the inner loop, without influencing the outer loop;

- The non-linear property of the system is mostly handled in the inner loop, i.e. the outer loop operates with improved non-linearity;

- The tuning procedure is easier and performance better as the controllers are tuned step-by-step starting from the innermost loop to the outermost loop;

- The internal control variables can easily be limited via the command variables of the corresponding control loop;

- Disturbances are canceled in the loop where they appear. For example, voltage drops in the power supply are canceled in the current control loop. It is not necessary to wait until position errors appear, as they would be in a simple position control loop without cascade.

2.2.2 Feedforward control

Feedforward is often used in the cascade position/velocity loop. Since feedforward works outside the loop, it does not cause an instability problem. Servo control systems use feedforward control to speed up the response to rapidly changing position commands.

The feedforward path speeds up the response by taking the command around the slower position loop directly to the velocity loop. This is velocity feedforward. The velocity feedforward path connects the velocity profile to the velocity loop through the feedforward controller. It can reduce the time required to make a quick move by a factor of two or more.

However, the velocity feedforward was only valid for constant feedrates. If any of the machine axes should accelerate or decelerate, position errors will occur. For the problem of position errors during acceleration, an acceleration feedforward concept can be added to the current loop input.

The acceleration feed forward path connects the acceleration profile to the current loop through the feedforward controller. Besides the position demands during the acceleration process, acceleration feedforward also eliminates the overshoot caused by velocity feedforward without reducing loop gains.

Figure 2.6 shows the feedforward structure together with the simplified cascade control of the drive axis. C_{FV} is the velocity feedforward controller. C_{FA} is the acceleration feedforward controller.
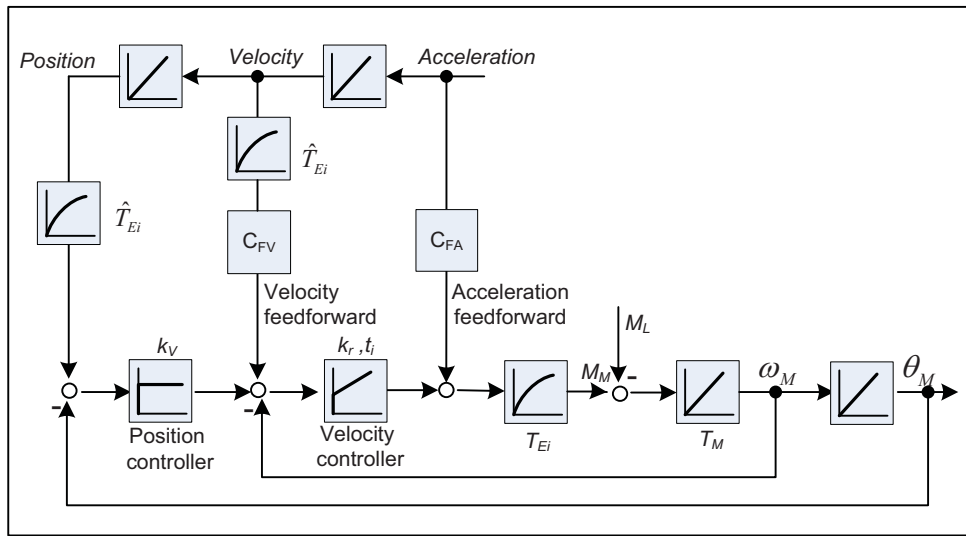
Figure 2.6: Feedforward control of a feed drive

$\hat{T}_{Ei}$ in position and velocity forward routines in Figure 2.6 is a balancing element. The balancing element is set to the equivalent time constant T_{Ei} of the current control loop. As this equivalent time constant of the current loop can not be exact as in reality, the time constant in the balancing element is just an estimated equivalent time constant of the current control loop. This ensures that the transposing of the position/velocity setpoints into position/velocity actual values are the same as that of the velocity/current control loop provided the position/velocity setpoints are delayed by the equivalent time constant of the current control loop before being passed to the position/velocity controller [44].

Higher order feedforward attracts researchers' interest due to its ability to solve the servo errors arising from jerk phases in a motion. Jerk derivative feedforward control together with velocity and acceleration feedforward compensates these servo errors to a minimum as described in [6, 33]. Unfortunately, many servo control systems do not even support acceleration feedforward due to the difficulty in getting acceleration input. Feedforward higher than acceleration is still not practical in the control of machine tools.

2.2.3 State space control

Classical control is appropriate for linear time-invariant systems. It is at its best when dealing with single input/single output systems. It also has some success with nonlinear systems, giving good results at an equilibrium point about which the system behavior is approximately linear. The control method is based on transfer function models of the plant to be controlled. However, when it comes to more complex systems with multiple variables, such as those arising in aerospace applications, classical techniques based on transfer functions tend to become tedious and soon reach their limits. State space control, which appeared in the 1960s, turned out to be more suitable for such applications. It comprehends the concept of the internal system state; thus, the approach deals with the internal dynamics of a system and not only its input/output behavior [34].

State space control is quite powerful. It naturally and automatically handles the coordination of many variables. In addition, the design for high-order systems uses the same linear algebraic formulas as those used for low-order systems. The only difference is that the formulas for high-order systems require a computer to perform the calculations. However, the power that the state space control technique exhibits is due largely to the state space model of the plant. If the model is accurate, then the theory provides excellent results. If the model of the plant is not an accurate reflection of the actual system, unfortunately, the results could be quite poor [75].

Since its appearance, state space control has attracted a lot of interest in machine tools control. However, until today, state space control is seldom installed on machine tools as a control system. One important reason is that the control quality of the state space control depends largely on the identification accuracy of the parameters on the plant. Besides, the state space control is also more complicated to apply to machine tools than simple cascade control.

2.3 Mechanical Systems

Elasticity or compliance in the power train elements between motor and load causes vibration problems. Mechanical vibration can be a problem for almost any machine system, that tries to maximize either command response or dynamic performance, from small ones to large machines, to high precision metal cutting mills and lathes [17] [23].

To compute, predict and eliminate the positioning errors caused by mechanical vibration in CNC machine tools requires an accurate mathematical model which adequately replicates the dynamic behavior of the machine tool.

2.3.1 Mechanical System Modeling

A typical conventinal feed drive consists of a motor connected to a moving mass through some power train connections. For example, in a feed drive, a gear is connected to the motor shaft on the one side; on the gear output, it moves e.g a ball screw. The feed screw then converts the rotational motion into a translational motion and moves the machine table sitting on the guide way. A schematic diagram of a typical feed drive is shown in Figure 2.7.
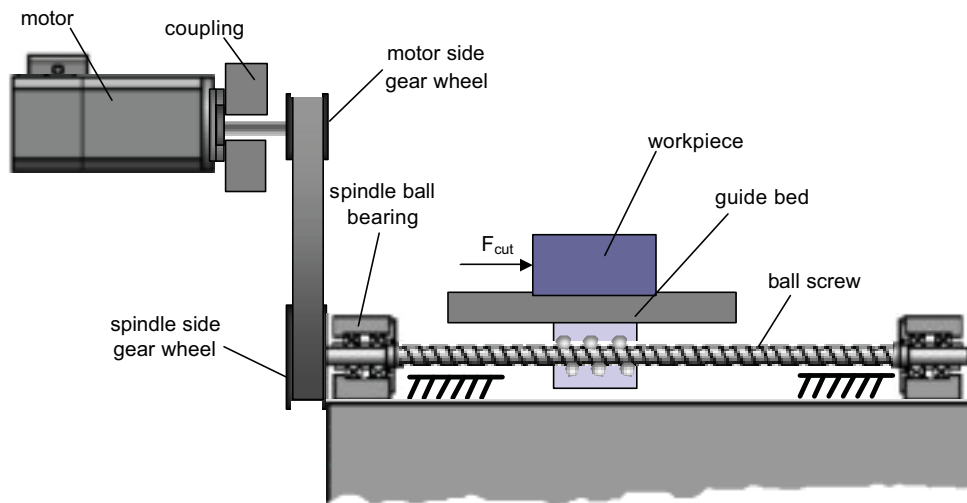
Figure 2.7: Structure of a feed drive axis

The mechanical stiffness of the connections and components in feed drive is limited. Therefore the power train behaves like a spring. In addition to spring forces, the couplings and guide ways can also provide damping forces. Damping forces are usually produced in proportion to the velocity difference between the two connected bodies. Usually, damping forces are intrinsic properties of the materials used to form couplings and of the mechanical interface (joint) of the connected parts. Mechanical damping helps to stabilize the system considerably. Materials commonly used for transmission parts, such as steel, provide very little mechanical damping, but the damping coefficient of joints can be very high.

For the mathematical description of the feed drive, the connections and elements of machine tools are therefore described by masses, springs and dampers. A simplified model, whose masses are connected by springs and dampers, as shown in Figure 2.8, is normally used to model feed drive [45].
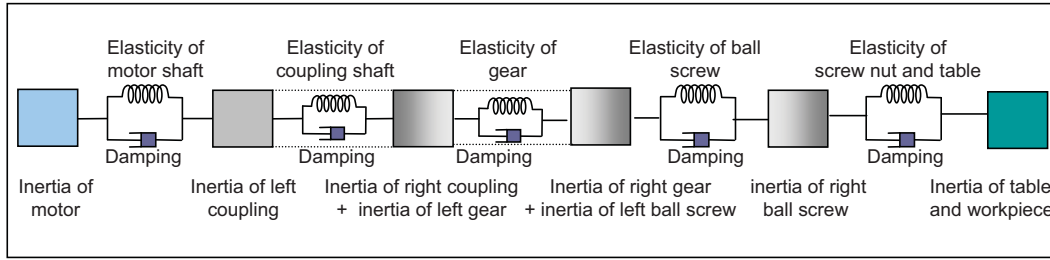
Figure 2.8: Dynamic model of the feed drive [45]

In some cases, for an elastic drive system with low frequency, the above model of the feed drive can be reduced to a mass-spring-mass model without losing accuracy. Normally the inertias of the connection components are small compared to motor and load. These small inertias are added either to the motor inertia or load inertia, according to the positions of the connection components in relative to the dominant elastic part in the feed drive. The stiffness of the components can be treated as a single composed equivalent spring constant that interconnects motor and load. The well-known model for an elastically-coupled motor and load is shown in Figure 2.9, and a block-diagram is shown in Figure 2.10. Here, the equivalent spring constant of the transmission, K, is shown as providing torque to the load in proportion to the difference of motor and load position. A mechanical damping term D is used to produce torque in proportion to velocity difference between motor and load. This is the typical second order system which is widely used to represent the feed drive system [13] [16].
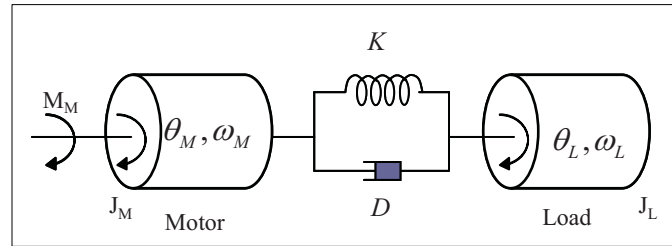
Figure 2.9: Motor and load with an elastic coupling

The equation of motion of the motor is described by

$$J_M\ddot{\theta}_M(t) + D\big(\dot{\theta}_M(t) - \dot{\theta}_L(t)\big) + K\big(\theta_M(t) - \theta_L(t)\big) = M_M(t). \tag{2.11}$$

The equation of motion of the load is described by

$$J_L\ddot{\theta}_L(t) + D\big(\dot{\theta}_L(t) - \dot{\theta}_M(t)\big) + K\big(\theta_L(t) - \theta_M(t)\big) = 0, \tag{2.12}$$

with

θ_M : position of the motor;

θ_L : position of the load;

$\dot{\theta}_M = \omega_M$: velocity of the motor;

$\dot{\theta}_L = \omega_L$: velocity of the load;

M_M : torque to motor;

J_M : inertia of motor;

J_L : inertia of load;

D : damping constant of system;

K : spring constant of the system.

The corresponding block diagram of the above system is shown in Figure 2.10.
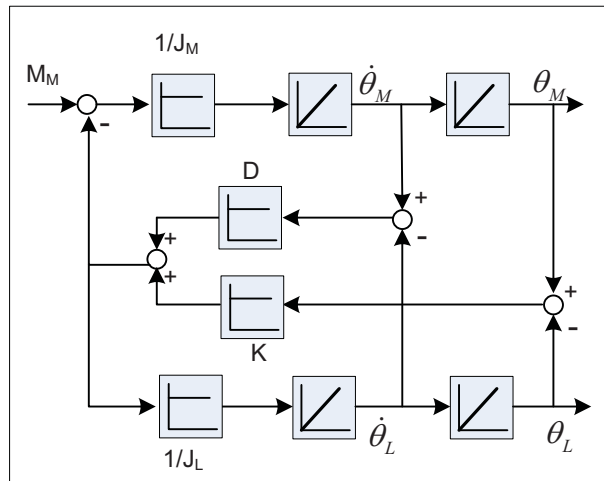
Figure 2.10: Block diagram of elastically coupled motor and load

2.3.2 Test Rig setup

The studies in this work are tested on a demonstration machine: a motor driving a load through an elastic coupling to represent a feed drive system as shown in Figure 2.11. The machine is set up to validate the theoretical findings of this work.

2.3.3 Motion control architecture of the test rig

The test rig consists of two AC motors connected by a rod. The two motors selected are SIEMENS 1FT6 motors with a rated speed of 3000 rpm. The feedback devices are sine-encoder from HEIDENHAIN configured for a resolution of 2048 pulses/revolution. The encoder generates two sinusoidal signals with levels of 1Vpp (peak-to-peak) and a phase

Figure 2.11: View of test rig

difference of pi/2. A third index signal helps to give the absolute motor position. The HEI-DENHAIN encoders for AC motors generally have a natural frequency higher than 2 kHz in the measuring direction, which in most applications exceeds the eigen mechanical frequencies of the machine and therefore have practically no limiting effect on the position and speed control loops. The elastic coupling is a steel rod 10mm in diameter and 850mm long. The rod is connected on both sides to the motors through a torsionally rigid and backlash-free coupling from RADEX. The calculations of the elasticity of the rod, the system's eigen-frequency together with some motor data are listed in Appendix A.

The control architecture of the test rig is also presented in Figure 2.12. A Simodrive 611U by SIEMENS is used to provide the required power for the motors and the amplifiers as well as current loop controller for each motor. A dSPACE DS1005 DSP controller board is used to implement the control algorithms for both motors. The encoder interface of the DS3002 A/D board makes it possible to read in the digital encoder position signal of the two motors of the test rig. A DS2101 D/A output interface sends the control command to the motor amplifiers. Two splitters, which are used to split the signal into two identical parts, are installed to send the signals to the amplifier on the Simodrive and to the DS3002 board on the dSPACE.

The current controller and the power amplifier are implemented in the Simodrive. The position and velocity controller are implemented with the dSPACE DSP controller board. The human-machine-interface is provided by ControlDesk, also by dSPACE, and runs on the host computer. The reference trajectories are produced off-line with the MATLAB functions developed from [15]. The trajectories are jerk-limited.

Experiments are carried out on the test rig to obtain the frequency response of the system. They are done in open velocity loop by the software attached to the Simodrive 611U. The response is shown in Figure 2.13. The resonance frequency of the mechanical system can be identified as 50Hz, and the anti-resonance frequency is 35Hz. Damping is very small. The frequency measurement of the mechanical system in this figure corresponds to the model and mathematical calculation in Appendix A.
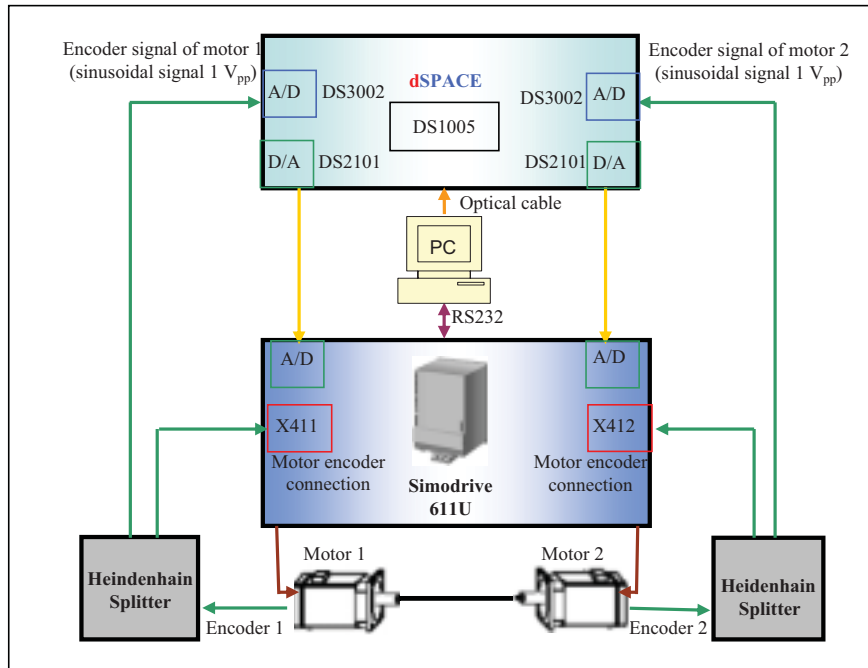
Figure 2.12: Block diagram of elastically coupled motor and load
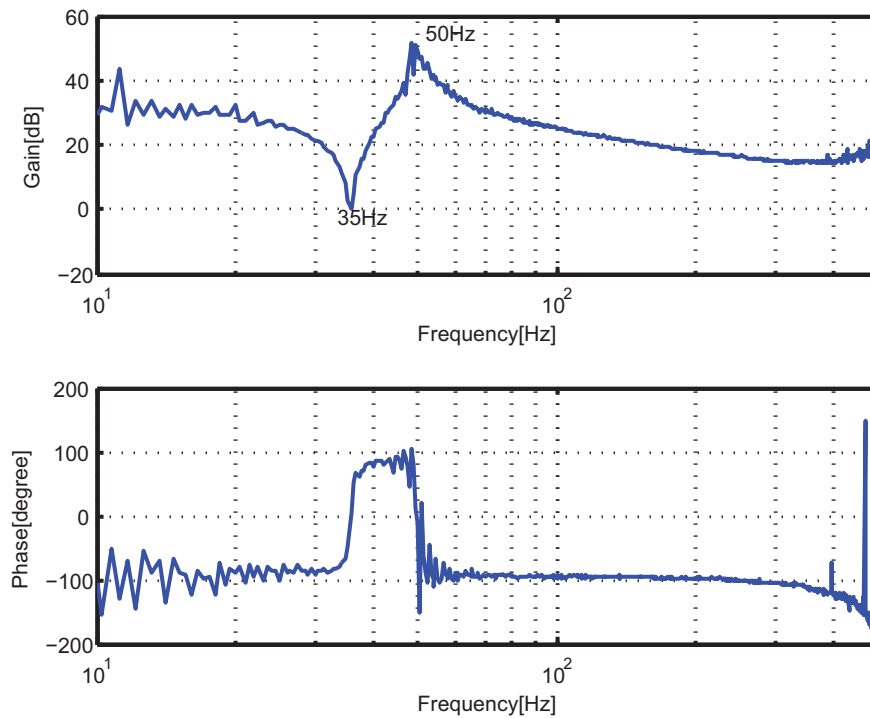
Figure 2.13: Frequency response of the test rig system

Cascade Control with Input Shaper

Methods that have been investigated for controlling elastic structures can be divided roughly into feedback and feedforward approaches. Feedback control methods use measurements and among others estimate the system states to reduce vibration, while feedforward techniques alter the actuator commands or setpoints so that system oscillations are reduced. A variety of design methods for feedback control systems have been developed, but the cascaded configuration is most commonly used for the control of machine tools due to the reasons stated in section 2.2.1. However, the parameters of the PI controller in velocity loop and the P controller in position loop are either determined by some estimates made by the experienced engineer, or by the estimate from the calculation for rigid systems, or by using the trial and error method. In this chapter, effective parameters of controllers for elastic structures are deduced and presented. By using the deduced parameters, the response of the system achieves a good compromise between response time and accuracy.

There are a lot of feedforward control methods that have been investigated for controlling elastic structures. The frequently used feedforward method combined with cascaded control loop for machine tools is the velocity feedforward and acceleration feedforward as introduced in section 2.2.2. Since full information about the velocity and acceleration is not always available, the application of this feedforward method is not always possible.

Input shaper is a feedforward method used to form the input without exciting vibrations. The advantages of input shaper, such as simplicity, ease of implementation, saturation avoidance, etc., compared with other precompensators, are so obvious that much attention is paid to input shaper techniques. However, closed-loop control for an input shaped system has received only scant attention [27], especially the application of input shaper techniques together with the most commonly used cascade control loop. Input shaper together with the cascaded control loop combines the advantages of both. On one hand, it is much better to prevent residual vibration by using a feedforward control scheme than trying to eliminate

these vibrations once they occur. On the other hand, feedforward controllers cannot reject disturbances. This is where the cascaded control loop, as a feedback controller, can be useful. These considerations lead to the idea of using a hybrid control approach, where the input shaper is applied at the input of the velocity control loop. Besides, when time and accuracy are important factors in the application, input shaper together with the cascade control loop can provide a very good solution.

3.1 Designing Parameters of Controllers for Elastic System

In high speed machine tools, mechanical or structural vibration is one of the most critical factors involved in affecting the machine's performance. It can be mostly reduced by fine tuning the servo parameters in the control loop to reach the required precision. Typically the controller parameters of servo-drives are adjusted manually by qualified personnel. In this case, optimum controll can only be achieved with considerable effort and expense. Pritschow etc. [53] developed a self-tuning controller for digitally controlled machine tools based on the theory of evolution strategy. The tuning procedure is still at the trial and error process, but with the help of computer. A good guess of the initial value of the parameters of controllers is a requirement, however.

One of the obvious advantages of the cascade control loop is that the tuning process of the controllers is easy: step-by-step tuning from the innermost to the outermost control loop. Each control loop can be adjusted efficiently and independently.

3.1.1 Designing parameters of controllers in the velocity loop

The published literature lists a number of suggestions on how to determine the values of the controller parameters for velocity loop theoretically. The best known methods are Symmetrical Optimum (SO) [28][29] and Absolute Value Optimum (AVO) [21]. They are designed to maintain the closed-loop magnitude response curve as flat and as close to unity for as large bandwidth as possible. Symmetrical Optimum has the best performance compensating intrinsic disturbance signals. The response to a command step shows a very steep rise phase followed by a considerable overshoot (maximum 43%). The response to a disturbance is fast and the amplitude of the deviation is in the same range as with the AVO method. Absolute Value Optimum provides the fastest response to a command step with very little overshoot (maximum 4%). The response to a disturbance is of moderate speed and the amplitude of the deviation is only half the amplitude obtained with SO.

Double Ratio [79] is another method based on a damping optimum of the closed control loop. The double ratio method is used to determine the free controller parameters contained in the coefficients of the denominator of the closed loop transfer function. The principle of the double ratio method is to set the damping of the system to be 0.707. Optimization based on the damping optimum with double ratios leads to a good command and disturbance response without having to perform extensive calculations. Therefore this method is preferred in getting the controller parameter of the cascade control loop.

If the transfer function of a closed control loop can be written to:

$$F(s) = \frac{b_0 + b_1 s + \cdots + b_m s^m}{a_0 + a_1 s + \cdots + a_n s^n} \quad m \le n, \tag{3.1}$$

then the coefficients of $a_0, a_1, \ldots, a_n$ of the denominator determine the damping ratio and stability of the closed control loop. An optimum response can be achieved by forming the coefficient ratios, starting at the end of the denominator and continuing to the front,

$$\frac{a_n}{a_{n-1}}, \frac{a_{n-1}}{a_{n-2}}, \ldots, \frac{a_1}{a_0}, \tag{3.2}$$

and two adjacent ratios are in the proportion of

$$\frac{\frac{a_n}{a_{n-1}}}{\frac{a_{n-1}}{a_{n-2}}} = \frac{a_n a_{n-2}}{(a_{n-1})^2} \le \frac{1}{2}. \tag{3.3}$$

If the number of free parameters is less than $n - 1$, then only the ratios of the lower order numbers are used. The double ratio method results in a robust response, insusceptible to parameter fluctuations and approximations within the controlled system [21].

Applying the double ratio method to a rigid system in the velocity loop, very simple equations for PI controller can be derived. The equations are also well-known in industry. However, the equations are not suitable for elastic system. For the elastic system, the double ratio method has difficulty in determining the parameters of the PI controller due to the complicated denominator in the transfer function. The most commonly used estimation of the PI controller for the elastic system is to use the PI calculation formula for a rigid system and lower the double ratio of $1/2$ to $1/4$ or even lower. As a result, there is no good estimation of the PI controller. In the following, a very good calculation of the PI controller for the elastic system is deduced based on double ratio method. Simulations and experiments confirm the calculations.

Double ratio for determining parameters for rigid system

As discussed in section 2.2.1, the controller in the velocity loop of the feed drive system is the PI controller. The block diagram of the velocity loop for a rigid feed drive system is drawn in Figure 3.1.
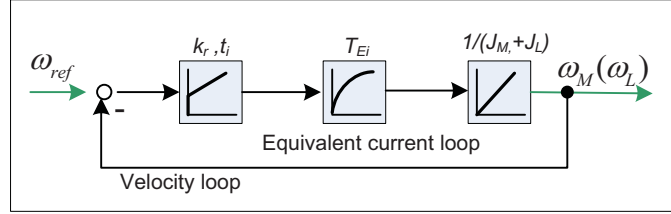
Figure 3.1: Block diagram of the velocity control loop for a rigid system

The corresponding transfer function of the rigid mechanical system with PI control loop is:

$$\frac{\omega_M}{\omega_{ref}} = \frac{1}{t_i'(J_M + J_L)T_{Ei}s^3 + t_i'(J_M + J_L)s^2 + k_r t_i's + 1} \tag{3.4}$$

with

k_r : parameter of P controller;

t_i' : constant of the I controller;

t_i : time constant of the PI controller, $t_i = t_i' * k_r$;

J_M :inertia of motor;

J_L : inertia of load;

T_{Ei} : equivalent time constant of current control loop;

ω_M : motor velocity from measurement;

ω_{ref} : motor velocity from setpoints.

By applying double ratio, it is easy to get the parameters of the PI controller, which is normally used today, for a rigid system. Based on equations (3.4) and (3.3), the parameters of PI controller are deduced to be:

$$k_r = \frac{J_M + J_L}{2T_{Ei}} \tag{3.5}$$

$$t_i' = \frac{8T_{Ei}^2}{J_M + J_L}. \tag{3.6}$$

The time constant of the PI controller t_i is also the time constant of the velocity loop T_{En}, which is calculated as

$$t_i = T_{En} = k_r * t_i' = 4T_{Ei}. \tag{3.7}$$

with

> T_{Ei}: equivalent time constant of current loop,
>
> T_{En}: equivalent time constant of velocity loop.

The above equation says that the equivalent time constant of the velocity loop has nothing to do with the mechanical system's parameters. It only depends on the current control loop. These calculated parameters work well for rigid systems, but it is not suitable for elastic systems. For elastic mechanical systems, a lower ratio is usually used to calculate the parameters of the PI controller, for example using 0.25 instead of 0.5. Thus,

$$k_r = \frac{J_M + J_L}{4T_{Ei}}, \tag{3.8}$$

$$t'_i = \frac{64T_{Ei}^2}{J_M + J_L}, \tag{3.9}$$

and the corresponding $t_i = T_{En} = 16T_{Ei}$. Although the calculated time constant of the velocity loop for the elastic system is already longer than for the rigid system, the above equation still takes no account of the elastic property in the mechanical system.

Simulations in Figure 3.2 show that with k_r and t'_i tuned to the ratio of 0.25, the vibrations on the velocity of the load side are still unbearable. Figure 3.2(a) is the motor and load velocity response to disturbance, and (b) is the velocity response to step input. Clearly, the motor responses under the situations of the step setpoints and disturbance are smaller than the load response. However, due to the elastic property, the load vibrates violently.

a. Response to disturbance   b. Response to step reference
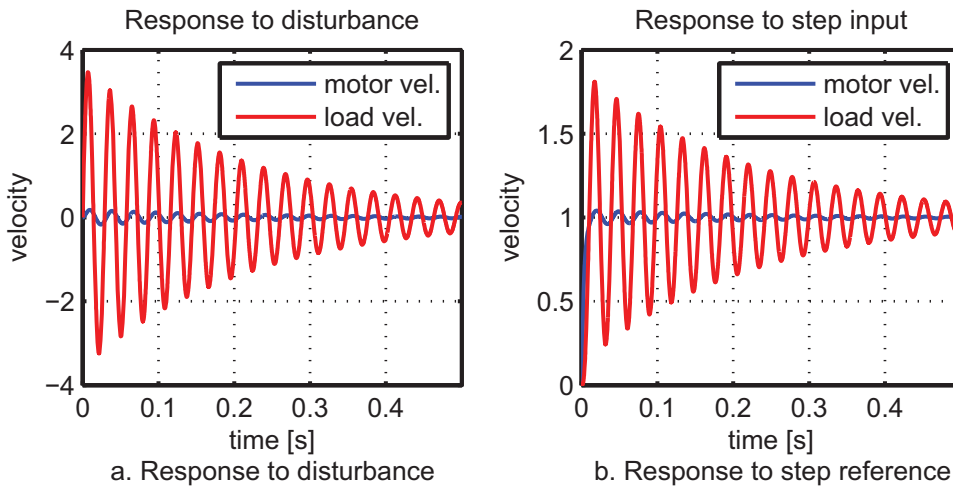
Figure 3.2: Elastic system response with PI controller designed for rigid system with double ratio 0.25 ($J_M = 0.0013 kgm^2$, $J_L = 0.0013 kgm^2$, $F_n = 50Hz$, $\xi = 0.01$. Controller: $k_r = 3.25 Nms/rad$, $t_i = 3.3ms$)

Determining controller parameters for the elastic system

As later on the frequencies and damping ratios of the second order mass-spring-damper system will be distinguished from the poles frequency (characteristic frequency of the mechanical system) and zeros frequency, poles damping ratio and zeros damping ratio, and so on, here these frequencies and damping ratios are explained by the transfer function of the second order mass-spring-damper system. The transfer function is,

$$\frac{\omega_M}{M_M} = \frac{1}{s} \frac{J_L s^2 + Ds + K}{(J_M * J_L)s^2 + (J_M + J_L)Ds + (J_M + J_L)K} \tag{3.10}$$

with

ω_M : velocity of the motor;

M_M : torque to motor;

J_M : inertia of motor;

J_L : inertia of load;

D : damping constant of system;

K : spring constant of the system .

Poles		Zeros	
poles radial frequency	$\omega_n = \sqrt{\frac{K(J_M+J_L)}{J_M J_L}}$	zeros radial frequency	$\omega_z = \sqrt{\frac{K}{J_L}}$
poles frequency	$F_n = \frac{\omega_n}{2\pi}$	zeros frequency	$F_z = \frac{\omega_z}{2\pi}$
poles time period	$T_n = 1/F_n = \frac{2\pi}{\omega_n}$	zeros time period	$T_z = 1/F_z = \frac{2\pi}{\omega_z}$
poles damping ratio	$\zeta_n = \frac{D}{2}\sqrt{\frac{J_M+J_L}{K J_M J_L}}$	zeros damping ratio	$\zeta_z = \frac{D}{2}\sqrt{\frac{1}{K J_L}}$
poles damped radial frequency	$\omega_{dn} = \omega_n \sqrt{1-\zeta_n^2}$	zeros damped radial frequency	$\omega_{dz} = \omega_z \sqrt{1-\zeta_z^2}$
poles damped frequency	$F_{dn} = \frac{\omega_{dn}}{2\pi}$	zeros damped frequency	$F_{dz} = \frac{\omega_{dz}}{2\pi}$
poles damped period	$T_{dn} = \frac{1}{F_{dn}}$	zeros damped period	$T_{dz} = \frac{1}{F_{dz}}$
resonance frequency	$F_r = \frac{\omega_n \sqrt{1-2\zeta_n^2}}{2\pi}$	anti-resonance frequency	$F_{ar} = \frac{\omega_z \sqrt{1-2\zeta_z^2}}{2\pi}$

Table 3.1: Frequencies, time periods, and damping ratios of poles and zeros

The velocity loop of a second order elastic system is shown in the following Figure 3.3.

The transfer function corresponding to the velocity loop with the PI controller for the elastic system is:

$$\frac{\omega_M}{\omega_{ref}} = \frac{\frac{k_r}{T_{Ei}J_M}\left[s^3 + b_2 s^2 + b_1 s + b_0\right]}{s^5 + a_4 s^4 + a_3 s^3 + a_2 s^2 + +a_1 s + a_0} \tag{3.11}$$

with

$b_2 = \frac{1}{k_r t_i'} + \frac{D}{J_L}$,
$b_1 = \frac{1}{k_r t_i'}\frac{D}{J_L}$,
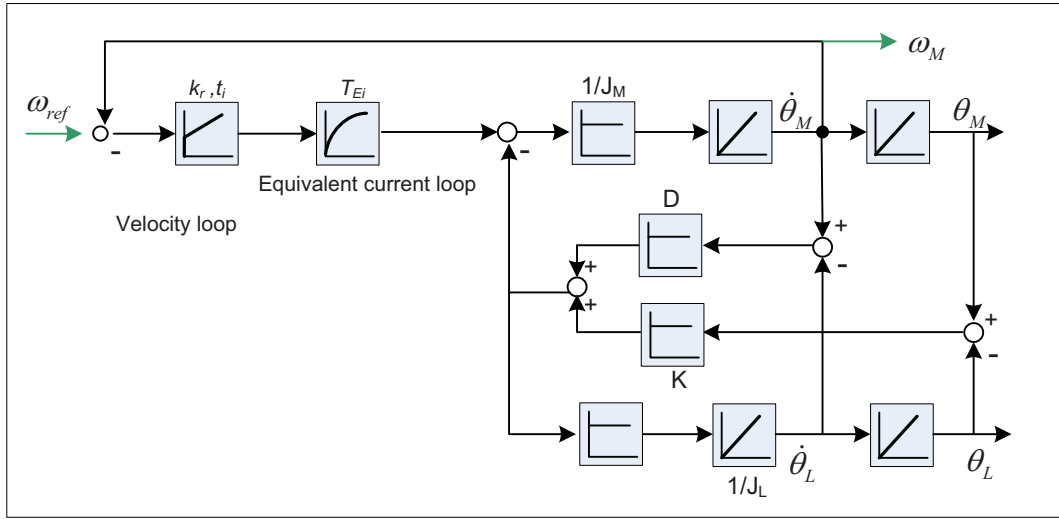
Figure 3.3: Block diagram of velocity control loop for elastic system

$b_0 = \frac{K}{J_L} \frac{1}{k_r t_i'}$,

$a_4 = \frac{1}{T_{Ei}} + JD$,

$a_3 = JK + \frac{JD}{T_{Ei}} + \frac{k_r}{T_{Ei} J_M}$,

$a_2 = \frac{JK}{T_{Ei}} + \frac{1}{T_{Ei} J_M t_i'} + \frac{k_r D}{T_{Ei} J_M J_L}$,

$a_1 = \frac{k_r K + \frac{D}{t_i'}}{T_{Ei} J_M J_L}$,

$a_0 = \frac{K}{T_{Ei} J_M J_L t_i'}$,

$J = \frac{J_M J_L}{J_M + J_L}$,

D : damping constant of the mechanical system,

K : stiffness constant of the mechanical system.

Applying the double ratio method, the 5th order denominator determines 4 double ratios, while only two variables (k_r, t_i') are to be decided. As the lower order of the denominator determines the main character of the system's response in low frequency range, up to $n = 3$ of the denominator of equation (3.2) will be used to calculate k_r, t_i' with double ratio.

According to

$$r_1 = \frac{a_0 a_2}{a_1^2} = \frac{1}{2},\tag{3.12}$$

the following equation is obtained,

$$A + Bt_i' + Ck_r^2 t_i'^2 = 0,\tag{3.13}$$

with

$A = K - \frac{D}{2J_L}$,

$B = \frac{J_M + J_L}{J_L} K^2$,

35

$$C = -\frac{K^2}{2J_L}.$$

According to

$$r_2 = \frac{a_1 a_3}{a_1^2} = \frac{1}{2}, \tag{3.14}$$

the following equation is obtained:

$$(ak_r^2 + bk_r + c)t_i'^2 + dt_i' + e = 0, \tag{3.15}$$

with

$$a = \frac{K}{T_{Ei}J_M^2 J_L} - \frac{1}{2T_{Ei}}\left(\frac{D}{J_M J_L}\right)^2,$$
$$b = \frac{JK^2}{J_M J_L},$$
$$c = \frac{J^2 K^2}{2T_{Ei}},$$
$$d = \left(JK + \frac{JD}{T_{Ei}}\right)\frac{D}{J_M J_L} - \frac{JK}{T_{Ei}J_M},$$
$$e = -\frac{1}{2T_{Ei}J_M^2}.$$

From equations (3.13) and (3.15), it is clear that the parameters of the PI controller can not be calculated simply. Two simplifications are therefore made to make the problem easier to solve:

- $D = 0$. As in an elastic system, especially a drive system with a long rod connection, the damping constant is very small.

- $T_{Ei} = 0$. Thanks to the development of computers, the equivalent time constant of the current control loop nowadays is smaller than $200\mu s$. Compared with the time period of the velocity loop of the mechanical system, which is normally bigger than $0.01s$, the T_{Ei} can be neglected.

Verification of the effect of the above two simplifications is done in section 3.1.1.

Under these two simplifications, the following parameters of k_r in equation (3.16) and t_i' in equation (3.17) for PI controller can be deduced to be

$$k_r = \frac{2}{3}\omega_n \sqrt{2(J_M + J_L)J_M}, \tag{3.16}$$

$$t_i' = \frac{3}{J_M \omega_n^2}. \tag{3.17}$$

The above two equations confirm that the elastic property of the mechanical system determines the parameters of controller in the velocity loop.

As the frequency response of the elastic system can easily be measured, the calculation of the parameters of PI controller in equations (3.16) and (3.17) can be changed to be parameterized with the measured frequency of the mechanical system (ω_n and ω_z) and the known motor inertia J_M, as in equations (3.18) and (3.19).

$$k_r = \frac{2\sqrt{2}}{3} \frac{\omega_n^2 J_M}{\omega_z} \tag{3.18}$$

$$t_i' = \frac{3}{\omega_n^2 J_M} \tag{3.19}$$

Thus, the time constant of the PI controller t_i, which can also be looked as the equivalent time constant of the velocity loop T_{En}, depends only on the frequency of the zeros of the mechanical system, as in equation (3.20).

$$t_i = T_{En} = k_r t_i' = \frac{2\sqrt{2}}{\omega_z} \tag{3.20}$$

If $J_M = J_L$, the relationship between the mechanical system period and time constant of the closed velocity loop can be expressed as in the following equation:

$$T_{En} = \frac{2}{\pi} T_n, \tag{3.21}$$

with T_n: the time period of the eigenfrequency of the system.

Simulations in Figure 3.4 verify the given calculation of the PI controller above. Both disturbance and step response are much better than the PI controller tuned with lowered double ratio for rigid system in the last section in Figure 3.4. To distinguish the k_r and t_i' in equations (3.5), (3.6) for rigid systems and in equations (3.18), (3.19) for elastic systems, the former set of equations is named rigid double ratios, and the later one is called elastic double ratios in this thesis later.

Verification

Two simplifications are made during the calculation of the PI controller for elastic system. The first one is that the damping constant is assumed to be zero. The second one is that the equivalent time constant of the current loop is assumed to be zero compared with the mechanical system's frequency. Thanks to the development of microsystems, $T_{Ei} = 0.2ms$ is

a. Response to disturbance   b. Response to step reference
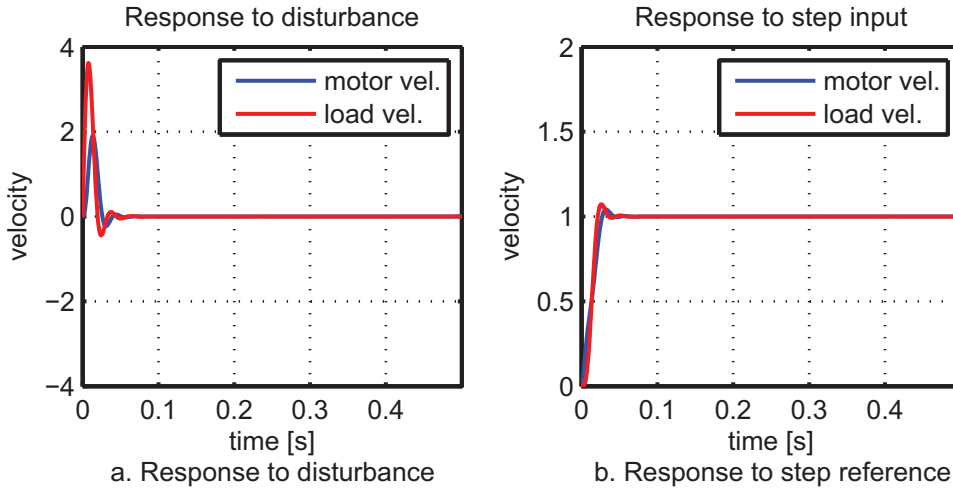
Figure 3.4: Elastic system response with PI controller tuned to elastic double ratio ($J_M = 0.0013kgm^2$, $J_L = 0.0013kgm^2$, $F_n = 50Hz$, $\xi = 0.01$. Controller: $k_r = 0.5445Nms/rad$, $t_i = 12.7ms$)

very common nowadays. By contrast, the time period of an elastic system is around or more than $10ms$, which is much bigger than T_{Ei}. To verify that those two assumptions do not make a big difference to the parameters of the PI controller the following Table 3.2 is presented. The first big column shows the parameters of the mechanical system and the equivalent time of the current control loop. The second big column shows the parameters of the PI calculated iterating with the non-linear equations (3.13) and (3.15) without assumptions. The third column is the PI controller calculated through equations (3.16) and (3.17) with the two assumptions. The fourth one shows a comparison between the parameters of the PI controller calculated without assumptions and with assumptions.

Parameters of the mechanical system					No assumptions		With assumptions		Comparison	
ξ	f_n	J_M	J_L	T_{Ei}	k_{r0}	t_{io}	k_r	t'_i	k_r/k_{ro}	t'_i/t_{io}
0.001	10	1e-3	1e-3	125e-6	0.0834	0.7659	0.0821	0.7599	0.98	0.99
0.001	80	1e-3	1e-3	125e-6	0.6443	0.0126	0.6566	0.0119	1.02	0.94
0.01	10	1e-3	1e-3	125e-6	0.0834	0.7659	0.0821	0.7599	0.98	0.99
0.01	80	1e-3	1e-3	125e-6	0.6422	0.0127	0.6566	0.0119	1.02	0.94
0.1	10	1e-3	1e-3	125e-6	0.0836	0.7611	0.0821	0.7599	0.98	1.00
0.1	80	1e-3	1e-3	125e-6	0.6448	0.0126	0.6566	0.0119	1.02	0.94
0.01	10	3e-3	1e-3	125e-6	0.2040	0.2557	0.2011	0.2533	0.99	0.99
0.01	80	3e-3	1e-3	125e-6	1.5639	0.0043	1.6084	0.0040	1.03	0.93
0.01	10	1e-3	2e-3	125e-6	0.1022	0.7648	0.1005	0.7599	0.98	0.99
0.01	80	1e-3	2e-3	125e-6	0.7948	0.0125	0.8042	0.0119	1.01	0.95
0.1	80	3e-3	1e-3	125e-6	1.5660	0.0043	1.6084	0.0040	1.03	0.93
0.001	80	3e-3	1e-3	125e-6	1.5643	0.0043	1.6084	0.0040	1.03	0.93
0.01	80	3e-3	1e-3	62.5e-6	1.6024	0.0041	1.6084	0.0040	1.00	0.96
0.1	10	1e-3	1e-3	62.5e-6	0.0838	0.7580	0.0821	0.7599	0.98	1.00

Table 3.2: Verifying the parameters of PI controller

Different parameters of the system are tested. From the last two columns in Table 3.2, it is proved that the two simplifications make no big difference in the calculation of the parameters of the PI controller. The worst case has 7% difference by t_i' between the values calculated with realistic parameters and based on the assumptions, due to $J_M = 3J_L$, which is seldom tha case in industry. Therefore, the equations (3.16) and (3.17), or (3.18) and (3.18), based on the two simplifications can be used for calculating the PI parameters for the elastic system.

Although the two formulas are deduced for controller of mass-spring-mass system, the real practical experiences show that they are also suitable for systems with more frequencies. The lowest pole and zero frequencies should be used in the above formulas for systems with more eigenfrequencies.

3.1.2 Designing the parameter of the controller in position loop

In further analysis, the complete transfer function of the closed velocity loop with mechanical system causes difficulty in deriving the parameter for position loop. Therefore, a simplified approximation for the closed velocity loop is required. Like the equivalent time delay for current control loop T_{Ei}, the effective equivalent time delay for the velocity control loop also uses the PT_1 element [21], which in this case is T_{En} as in equations (3.20). Hence, the transfer function of the equivalent velocity control loop is,

$$G_v = \frac{1}{T_{En}s + 1}. \tag{3.22}$$

The closed position loop with simplified equivalent velocity loop is presented in Figure 3.5. In the above figure, k_v is the parameter of the proportional controller in the position loop.
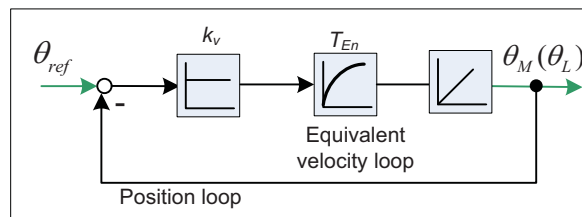
Figure 3.5: Closed position loop with equivalent velocity loop

The parameter k_v, which is also called velocity gain, of the proportional controller P in the position loop decisively determines the dynamic accuracy of a machine tool. The influence of the k_v factor on the tracking error of the axis is analyzed in [5][51][52]. Overshoot in position loop for machine tools is always undesirable. No overshoot at the output of the position loop by tuning the k_v factor is a basic requirement among the requirements for the

dynamic accuracy of the machine tool. According to the stability theory, an output will give no-overshoot when all the poles are along the real axis. This property can be used to find the limitation for the proportional constant k_v.

In the root locus of the open position loop with only equivalent velocity loop as in equation (3.22), one of the poles never leaves the real axis. The other two poles move toward each other, intersect and break away from the real axis. The highest value is given at the break-away point of the poles. The break-away point can be found by using the normal root locus plotting technique, or by the equation $\frac{dG_{OL}}{ds} = 0$, where $G_{OL} = \frac{1}{T_{En}s+1}\frac{1}{s}$ is the position open-loop transfer function or the equivalent velocity control loop with an integral element. The breaking point is found to be

$$s = \frac{-1}{2T_{En}}. \tag{3.23}$$

The corresponding k_v is found to be

$$k_v \leq \frac{1}{4T_{En}}. \tag{3.24}$$

Insert equation (3.20) into equation (3.24), and the k_v factor can be found as to the mechanical systems parameter as in equation (3.25),

$$k_v \leq \frac{\omega_z}{8\sqrt{2}}. \tag{3.25}$$

If $J_M = J_L$, then $\omega_z = \omega_n \sqrt{1/2}$. The above equation can be rewritten as

$$k_v \leq \frac{\omega_n}{16}. \tag{3.26}$$

When the maximum value of the k_v in equation (3.26) is used, the equivalent delay time of the position loop is calculated as

$$T_{E\varphi} = \frac{1}{k_v} = \frac{8}{\pi}T_n, \tag{3.27}$$

where T_n is the mechanical system's period.

Figure 3.6 verifies that the response of the position loop has no over shoot with parameters k_v in equation (3.25), k_r in equation (3.16) and t_i' in equation (3.17).

Position response to step reference
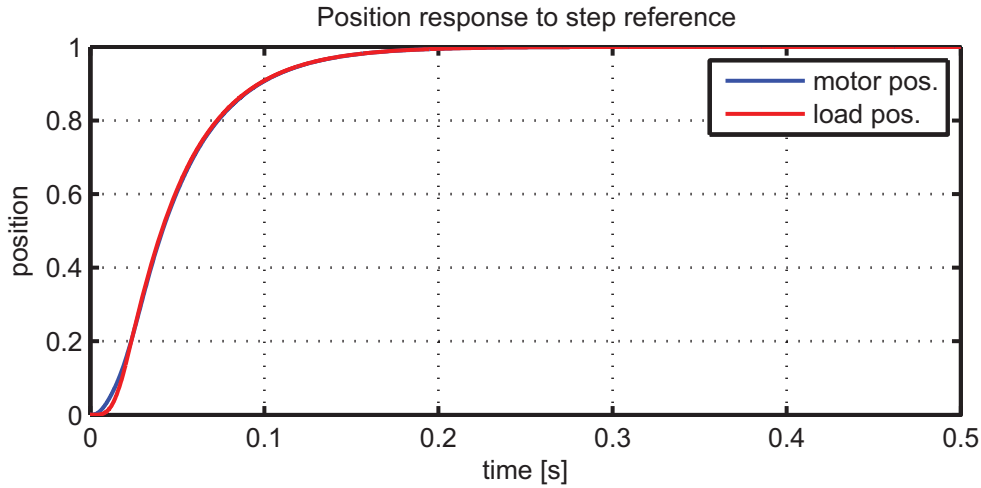
Figure 3.6: Position response to step input with calculated controller parameters ($J_M = 0.0013kgm^2$, $J_L = 0.0013kgm^2$, $F_n = 50Hz$, $\xi = 0.01$. Controller: $k_r = 0.5445Nms/rad$, $t_i = 12.7ms$, $k_v = 19.631/s$)

3.2   Input Shaper

Input shaper was first introduced to control the residual vibration by Singer and Seering in 1989 [60]. It originates from the "posicast" method that was developed by Smith in 1957 [68]. After the year 1989, a lot of papers appeared to address the different aspects of this technology, such as sensitivity, robustness, frequency domain designing, trajectory following, and so on. Besides the Zero Vibration(ZV) [60] method, Zero Vibration Derivative (ZVD)[59] and Specified Insensitivity (SI) [61][67] methods were developed to increase the robustness of the input shaper. Singh and Vadali [63] talked of placing zeros to cancel system residual vibration in frequency domain when they analyzed the robustness of input shaper. Tuttle and Seering [73] began the frequency domain method of designing input shaper. Input shaper designed in frequency domain for multi-mode systems shows more benefit in shaper length and the number of impulses [11][43].

A lot of interest in this technique was followed by a range of further applications with input shapers, from wafer handling robots to an experiment that flew on the Space Shuttle Endeavor [74]. Singer and Singhose [66] found a great improvement in coordinate measurement repeatability by the use of an input shaper. Kapila, Tzes and Yan [27] proposed a method to calculate a full state feedback controller for a closed loop system with an input shaper inside the loop in front of the flexible structure. The output of a hard disk drive head testing machine was significantly improved with shaping. Lim, Stevens and How [35] used a new convex optimization approach to design a multi-mode input shaper for a two-link flexible manipulator which achieves faster step response and lower overshoot in combination with the former standalone PD controller. All of these examples of using input shaper

to suppress residual vibrations are well done and demonstrated for point to point motions. Singhose [65][64][67] verified that input shaper can also be applied to spatial trajectories for trajectory following where only the shape of the movement is important. However, there is a smaller-than-desired radius problem for the circular trajectories as stated in [67]. A solution was also given as by "using an unshaped circle command that has a radius larger than desired". However the reason for this smaller-than-desired radius through input shaper is not analyzed or given, and what is more, no feasible solution to determine the "unshaped circle command that has a radius larger than desired" is given. Rall etc. [54] analyzed the reasons for this effect caused by input shaper in a circular trajectory, and gave an exact solution to this problem. The dynamics of an elastic structure coupled with an input shaper give rise to time delays in the control input. Kapila etc. [27] combined the input shaper and the feed back control loop using time delay control theory without causing any instability problems. But input shaper together with cascade control loop is still left untouched.

3.2.1 Input shaper in time domain

The working principle of input shaper can be explained both in the time domain and the frequency domain. In the time domain, input shaper can be explained by vibration cancellation caused by two impulses with suitable designed amplitudes and time locations. This concept is shown in Figure 3.7. From Figure 3.7 it is known that the vibration due to the impulses of A_1 is canceled by the vibration due to impulse A_2. A_2 should happen at one half of the period of the response period, and with an amplitude that is the same as the vibration due to A_1 at that moment. Those two impulses are produced by an input shaper to convolve with setpoints to the mechanical system [62].

If the two impulses in input shaper are chosen correctly, then the system will respond without vibration to those impulses. If a sequence of impulses causes no residual vibration when applied to a mechanical system, then the command generated by convolving this sequence with any function will have the same effect.

Consider a second order system with one flexible mode. At first a reasonable estimate of the systems characteristic frequency ω_0, and the damping ratio ξ is needed. They can be found by measurements or, if the differential equation i.e. the eigenvalues are known, by the equation

$$\lambda_{1,2} = -\xi\omega_0 \pm j\omega_0\sqrt{1 - \xi^2}. \tag{3.28}$$
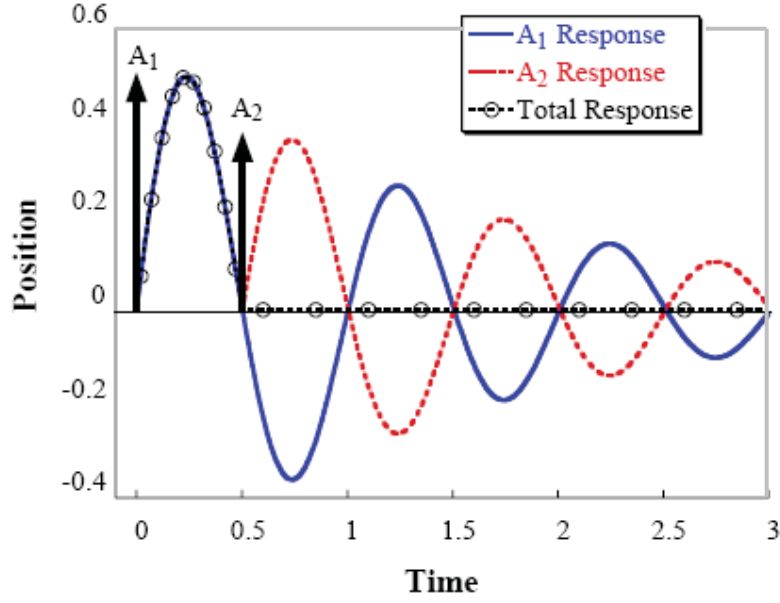
Figure 3.7: Vibration cancellation using two impulses [62]

The negative real part of the eigenvalue λ is the product of the damping ratio and the characteristic frequency. The complex part is the damped frequency $\omega_d = \omega_0 * \sqrt{1 - \xi^2}$, which the impulse response of the system will oscillate with. If this system is now excited by two impulses with a certain time position and height, the oscillation of the response remains zero after the second impulse, which is shown in Figure 3.7 .

In order to find the locations and magnitudes of these impulses, the residual vibration function to an impulse sequence is used. The function (depending on system parameters ξ and ω_0) in equation (3.29) calculates the percentage residual vibration relative to a single unit-magnitude impulse response of the flexible system.

$$V(\omega_0, \xi) = e^{-\xi\omega_0 t_n}\sqrt{C(\omega_0, \xi)^2 + S(\omega_0, \xi)^2} \tag{3.29}$$

$$C(\omega_0, \xi) = \sum_{i=1}^{n} A_i e^{\xi\omega_0 t'_i}cos(\omega_d t_i) \tag{3.30}$$

$$S(\omega_0, \xi) = \sum_{i=1}^{n} A_i e^{\xi\omega_0 t'_i}sin(\omega_d t_i) \tag{3.31}$$

A_i is the magnitude of the impulse at the time location T_i, and n the number of impulses. The total response of the residual vibration function after the last impulse is zero if equations (3.30) and (3.31) are both equal to zero (because they are squared in equation (3.29)). In this

case the amplitude and time location of each impulse can be calculated. To avoid the trivial solution for A_i, and to get normalized results, a third equation

$$\sum_i A_i = 1 \tag{3.32}$$

is added.

Fulfilling these equations, A_i could take very large positive and negative values. For a more suitable solution the magnitudes can be limited to finite values or even to positive values, the following is also required:

$$A_i > 0. \tag{3.33}$$

For an explicit problem with a two-impulse input, there are four unknowns (A_1, A_2, T_1, T_2) and four restrictions to satisfy. The time location of the first impulse can be set to zero, without loss of generality. Setting equations (3.30) and (3.31) respectively to zero (with $T_1 = 0$) resolves to:

$$T_2 = \frac{n\pi}{\omega_d} = \frac{nT_d}{2}, \qquad n = 1, 2, \ldots \tag{3.34}$$

with T_d as the damped period of vibration. That means there are an infinite number of possible solutions for the second time location T_2. Every multiple of the half damped period will do. Normally the vibration should be canceled as soon as possible, hence

$$T_2 = \frac{T_d}{2} \tag{3.35}$$

is the best choice. Using equations (3.32) and (3.35) in (3.30) reveals, after rearranging, the value of A_1 as

$$A_1 = \frac{e^{\frac{\xi\pi}{\sqrt{1-\xi^2}}}}{1 + e^{\frac{\xi\pi}{\sqrt{1-\xi^2}}}}. \tag{3.36}$$

Defining $Q = e^{\frac{-\xi\pi}{\sqrt{1-\xi^2}}}$, the fastest solution for the zero residual vibration response of a single flexible mode system to an impulse sequence is summarized in:

$$\begin{bmatrix} A_i \\ T_i \end{bmatrix} = \begin{bmatrix} \frac{1}{1+Q} & \frac{Q}{1+Q} \\ 0 & 0.5T_d \end{bmatrix}. \tag{3.37}$$

3.2.2 Input shaper in the frequency domain

Input shaper is the method of placing the zeros to cancel system vibration where the unwanted system poles are calculated in the s-plane. An open-loop control of a simple second

order system using frequency-domain input shaper can be demonstrated as in Figure 3.8.
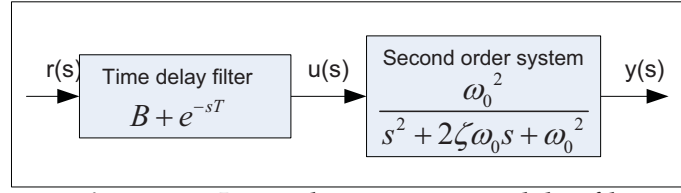
Figure 3.8: Input shaper as a time delay filter

In Figure 3.8, $\frac{\omega_0^2}{s^2+2\zeta\omega_0 s+\omega_0^2}$ is the transfer function of a second order system; $B + e^{-sT}$ is the input shaper, which is explained as time delay filter to remove vibration; $r(s)$ is the input signal; $u(s)$ is the filtered signal; $y(s)$ is the output signal in s-domain.

The zeros produced by the input shaper to cancel unwanted system poles are given by the following equation:

$$B + e^{-sT} = 0. \tag{3.38}$$

In the equation (3.38), B is the amplitude of the proportional signal and T is the delay time of the time-delayed signal, as is represented by the Laplace variable s:

$$s = \sigma + j\omega. \tag{3.39}$$

Replacing equation (3.38) with equation (3.39) and equating the real and imaginary parts to zeros, the following two equations are derived:

$$B + e^{(-\sigma T)}\cos(\omega T) = 0, \tag{3.40}$$

and

$$e^{(-\sigma T)}\sin(\omega T) = 0. \tag{3.41}$$

From equation (3.41), the ω is obtained:

$$\omega = (2n+1)\frac{\pi}{T}, 2n\frac{\pi}{T}. \qquad n = 0, 1, 2, \dots \tag{3.42}$$

Insert equation (3.42) into equation (3.40), the σ is obtained,

$$\sigma = \frac{-ln(\pm B)}{T}, \tag{3.43}$$

45

Therefore, insert equation (3.42) and (3.43) to (3.39), the zeros of the filter are

$$s = \begin{cases} \dfrac{-ln(B) + (2n+1)\pi j}{t} & \omega = (2n+1)\dfrac{\pi}{t} \quad n = 0,1,2,\dots \\[3mm] \dfrac{-ln(-B) + (2n+1)\pi j}{t} & \omega = 2n\dfrac{\pi}{t} \quad n = 0,1,2,\dots \end{cases} \tag{3.44}$$

It is assumed here that B is positive.

To cancel the system poles, the zeros of the input shaper in equation (3.44) should be the same as the poles in equation (3.28). Making the real and imaginary parts of the two equations equal, the parameters of the input shaper B and T can be calculated as

$$T = \frac{\pi}{\omega\sqrt{1-\xi^2}} = T_d/2, \tag{3.45}$$

$$B = e^{\frac{\xi\pi}{\sqrt{1-\xi^2}}}. \tag{3.46}$$

The final value of the single time-delayed controlled system to a unit step input is given by

$$lim_{s\to 0}\frac{1}{s}s\left(\frac{(B+e^{-sT})\omega^2}{s^2 + 2\xi\omega s + \omega^2}\right), \tag{3.47}$$

which equals to

$$B + 1. \tag{3.48}$$

As the input shaper should not change the amplitude of the original signal after shaping, the $B + e^{-sT}$ has to be normalized to be 1 by dividing its magnitude of $B + 1$. Thus, the input shaper is

$$\frac{B + e^{-sT}}{B + 1} \tag{3.49}$$

with $B = e^{\frac{\xi\pi}{\sqrt{1-\xi^2}}}, T = \frac{\pi}{\omega\sqrt{1-\xi^2}} = \frac{1}{2}T_d$, for a second order system.

Equation (3.49) can also be rewritten to

$$\frac{B + e^{-sT}}{B + 1} = A_1 + A_2 e^{-sT} \tag{3.50}$$

with $A_1 = \frac{B}{B+1}$, $A_2 = \frac{1}{B+1}$, and $T = \frac{1}{2}T_d$. This is exactly the same as the input shaper derived from the time domain in equation (3.37).

Here one example of input shaper in frequency domain is given. Assume the second order mechanical system has a natural frequency of 40Hz with a damping ratio of 0.001. From

the above equations, the following values of the input shaper parameters are derived: $A_1 = 0.5008$, $A_2 = 0.4992$ and $T = 0.0125s$. The bode diagram of the second order system (from motor torque to motor velocity) is plotted in Figure 3.9. The pole of the second order system lies in the 40Hz as desired. The bode diagram of input shaper is plotted in Figure 3.10. The input shaper brings series of zeros at 40Hz, 120Hz, ...$(2n + 1) * 40$ Hz. The resultant bode diagram of the second order system with input shaper is shown in Figure 3.11. The pole in Figure 3.9 at 40Hz is already canceled by input shaper. Thus resonance vibration here is eliminated.
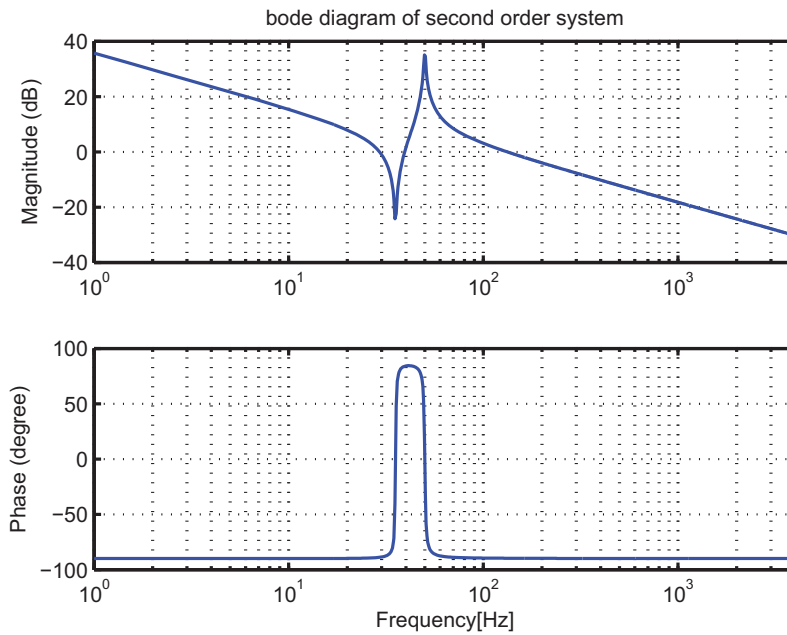
Figure 3.9: Bode diagram of a second order system

3.2.3 Sensitivity of input shaper

The amplitudes and time locations of the impulses of input shaper depend on the system parameters (ω_0 and ξ). If there are estimation errors in these values (and there always are), then the impulse sequence will not result in zero vibration as described above. In fact, for the two-impulse sequence, there can be a lot of vibration for a small modeling error. This lack of robustness was a major problem for the original formulation.

The sensitivity of the input shaper can be visualized by plotting a sensitivity curve that shows the amplitude of residual vibration as a function of the system parameters. The sensitivity curve is a concept/tool introduced along with input shaper by Singer and Seering [59]. It is a plot of the percentage residual vibration of an input shaper as parameters of the system are varied [31]. The vertical axis gives the percentage residual vibration of the
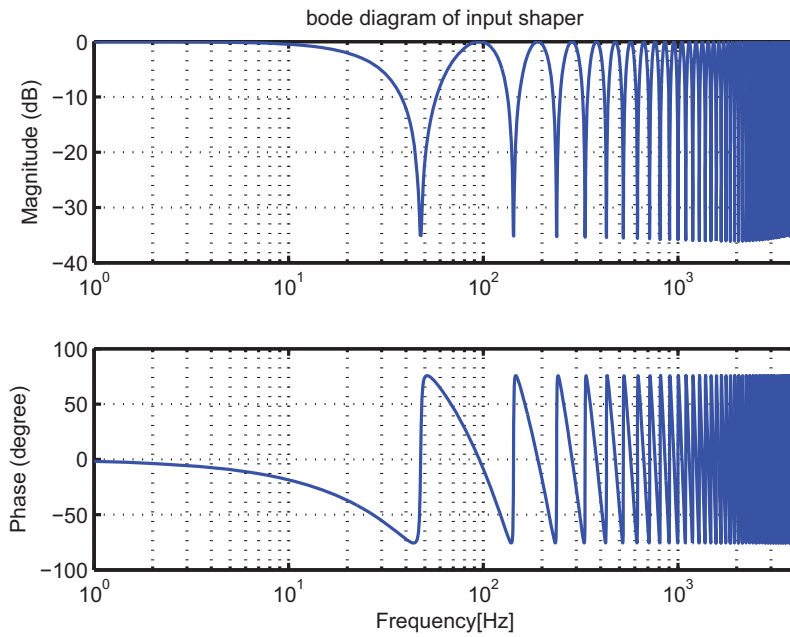
Figure 3.10: Bode diagram of input shaper
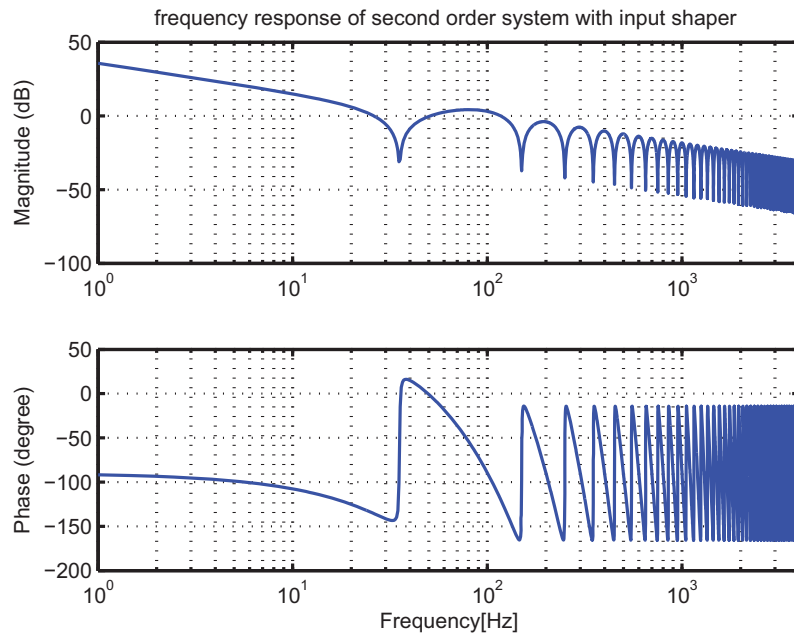
Figure 3.11: Bode diagram of second order system with input shaper

system for a variation in the system's natural frequency. The horizontal axis is the normalized frequency of the modeling frequency to the real natural frequency of the system. The sensitivity of the input shaper is plotted in Figure 3.12. The robustness can be measured quantitatively by measuring the width of the curve at some low level of vibration (for example 5%). This non-dimensional robustness measure is called the shaper's insensitivity.

The input shaper described above is also called Zero Vibration (ZV) shaper. The length of the ZV shaper is one half of the system's damped period. To increase the robustness against parameter uncertainties, Zero Vibration and Derivative (ZVD) shaper adds more constraints. The additional constrains is significantly more robust than the ZV shaper, but at the cost of a shaper length.

Other approaches, for example, Extra Insensitive (EI) shaper, use more constraints to assure robustness over an even bigger range. This Extra Insensitive method has the effect of broadening the frequency sensitivity curve and hence increasing frequency insensitivity. The price for this robust is normally an increased shaper length and four or five impulses instead of three in ZVD and two in ZV.
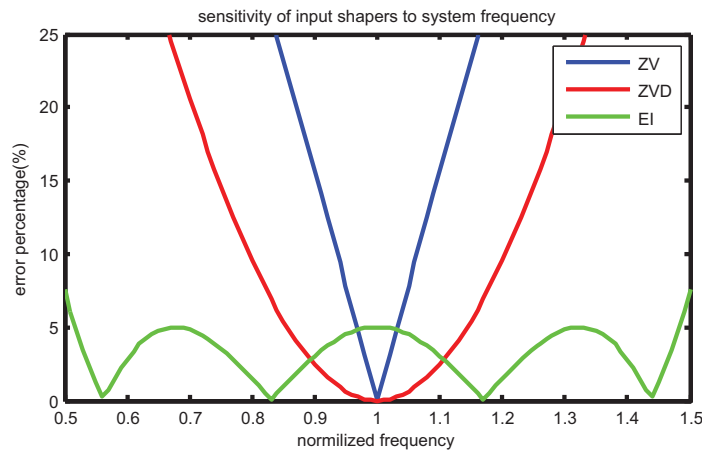
Figure 3.12: Sensitivity of input shapers to frequency estimation error [59]

3.3   Designing Cascade Control Loop with Input Shaper

Comparing the equivalent time of the velocity loop in equation (3.7) with equation (3.21), it is known that the parameters of the PI controller designed with elastic double ratio achieve better dynamic behavior by sacrificing the rise time. In an application where positioning time is very important, the tuning of the PI controller from equation (3.18) and (3.19) may not meet the time requirement. Input shaper, which is very effective in eliminating vibrations, can be applied together with the closed velocity loop to achieve good dynamic behavior

and quick response time. As the input shaper eliminates vibration, the parameters of PI controller in this case can be tuned as in the rigid system, if there is no big disturbance to the mechanical system.

The block diagram of the input shaper together with the closed velocity loop is presented in Figure 3.13. Determination of the parameters of the input shaper is now a problem, as the system's damping ratio and frequency would change with the tuning of the PI controller.
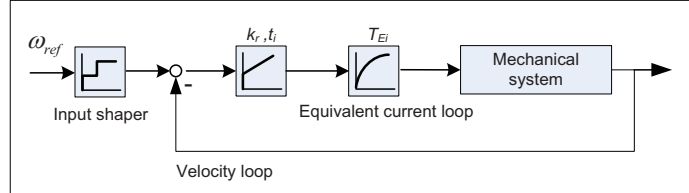
Figure 3.13: Block diagram of velocity control loop with input shaper

3.3.1 Designing Input Shaper for closed velocity loop

The vibrations in the load can come from two sources. One is from the possible vibration of the motor side. The other is from the elastic connection between the motor and the load. The vibration of the motor is normally small. However, the small vibration on the motor side is enlarged by the elastic connection between the motor and the load. Therefore, the vibration of the load is much bigger than the vibration of the motor.

Input shaper for load response

The vibration of the motor can be tuned easily to be very small, however, this small vibration of the motor could bring violent vibration on the load side due to the elastic connection property, especially when there is only small damping. Therefore, elimination of the vibration of the motor is the first step.

In the frequency analysis of the input shaper, it is known that input shaper works by adding zeros to the system to cancel the vibration caused by the system's poles. In the closed velocity loop, the poles of the transfer function of the motor change their position with the tuning of the PI controller. This can be viewed from the root locus plot of the open velocity loop as shown in Figure 3.14.

The transfer function of the open velocity loop, which determines the poles and zeros of the root-locus, is presented in equation (3.51).

$$\frac{\omega_M}{M_M} = \frac{1}{T_{Ei}s + 1} \frac{1}{s(J_M + J_L)} \frac{J_L s^2 + Ds + K}{\frac{J_M J_L}{J_M + J_L}s^2 + Ds + K} \tag{3.51}$$
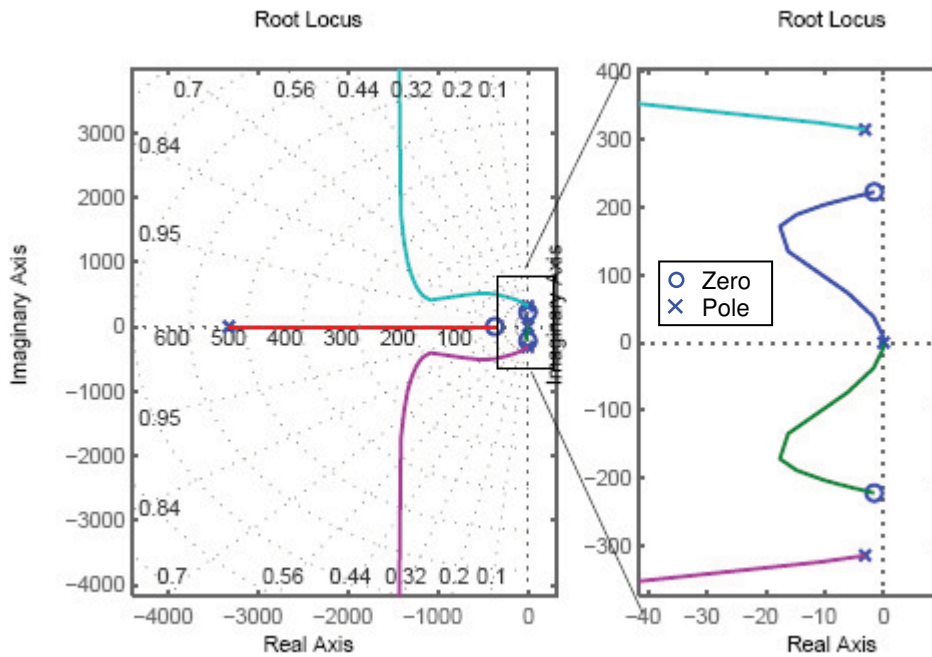
Figure 3.14: Root locus of the open velocity loop

From Figure 3.14, it is known that the two poles move to the position of the two zeros. Those two poles, one of which comes from the PI controller and the other of which comes from the integral of acceleration (torque) to velocity, are located at the origin of the coordinate. These two zeros, which come from the numerator of the equation (3.51), represent the load elastic property of the system. The two poles, which are from the denominator of the equation, are moving toward higher frequency. When the parameters of k_r and t'_i in equation (3.11) are tuned as for a rigid system as in equations (3.5) and (3.6), if there is no disturbance, and/or positioning time is a critical criteria for an elastic system, the poles of the motor can create problems, not seriously to itself, but to the load.

Here an example is given to show the motor response to the tuned k_r and t'_i in an elastic system. The bode diagram, from motor torque to motor velocity, of the closed velocity loop is shown in Figure 3.15. The poles, which originally represented the natural frequency of the system, now moves to the high frequency without causing the vibration problem. The poles which are from the origin of the mechanical system, now causes a vibration problem in the area near the zeros. However, for the motor velocity, as the poles are moving near to the zeros, the effect of the poles are largely canceled by the zeros. This can be seen in Figure 3.16(a). However, in (b) of the same figure, which is the load response, a lot of vibration can be observed.

The high level of vibration in the load is physically caused by the elastic connection. In control terms, compared to the response of the motor, the vibration of the load is due to the
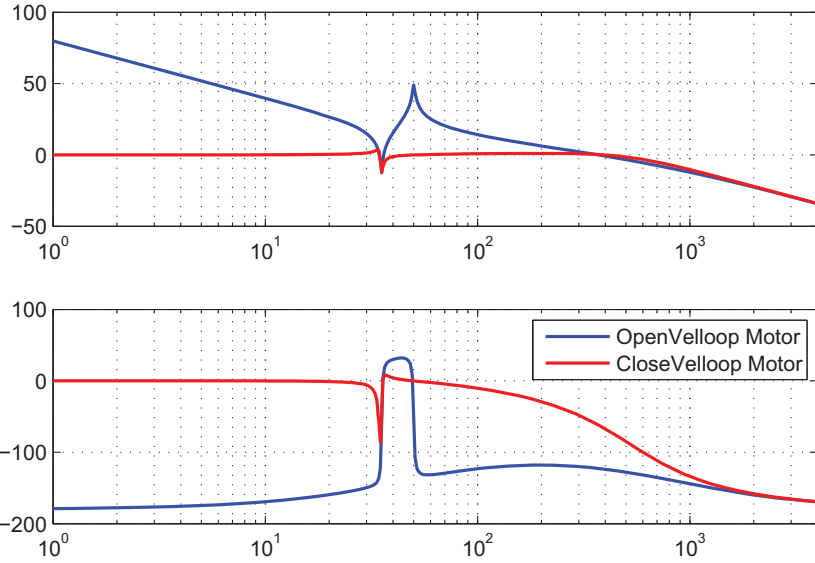
Figure 3.15: Bode diagram - motor torque to motor velocity ($J_M = 0.0013kgm^2$, $J_L = 0.0013kgm^2$, $F_n = 50Hz$, $\xi = 0.01$)

a. Motor response b. Load response
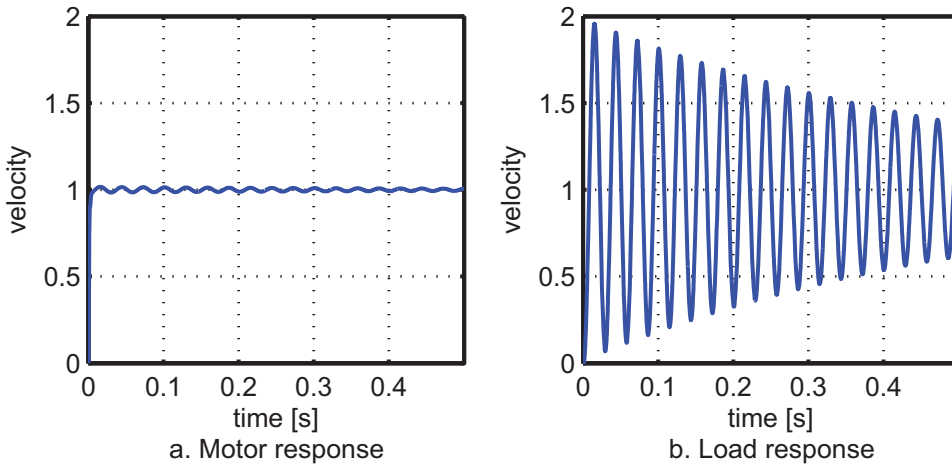
Figure 3.16: Motor and load response with the tuning of PI controller ($J_M = 0.0013kgm^2$, $J_L = 0.0013kgm^2$, $F_n = 50Hz$, $\xi = 0.01$. Controller: $k_r = 3.25Nms/rad$, $t_i = 3.3ms$)

"missing zero" [80] effect. This can be verified in the following equation (3.52) and Figure 3.17. There is only one peak in the close loop for the load velocity as shown in Figure 3.17.

$$\frac{\omega_L}{M_M} = \frac{1}{s(J_M + J_L)} \frac{Ds + K}{\frac{J_M J_L}{J_M + J_L}s^2 + Ds + K}. \tag{3.52}$$

Therefore, adding zeros in the position or near the position of the peak (poles in the transfer function of load), will help to cancel the vibration. When the zeros are added directly in the position of the peak, the vibration of the load will be totally eliminated. But it is difficult to find the position due to the tuning of the PI controller. If the zeros are placed near the
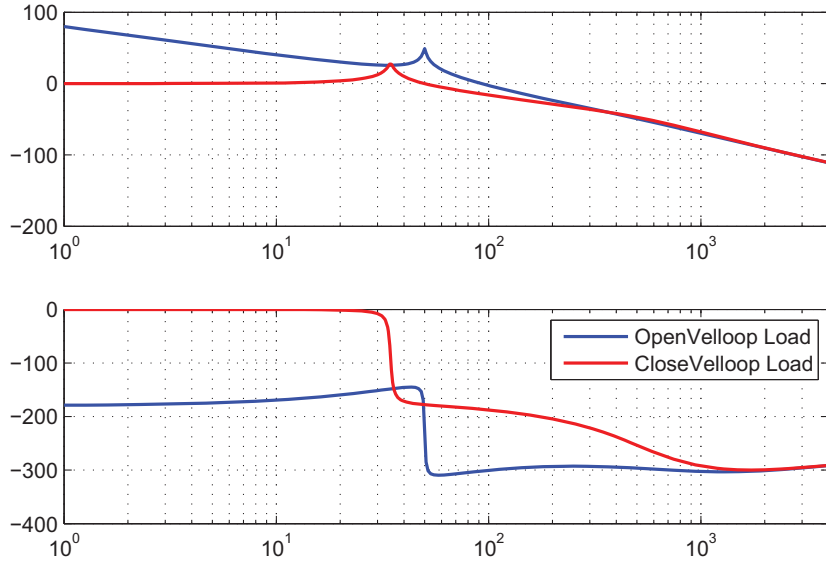
Figure 3.17: Bode diagram - motor torque to load velocity ($J_M = 0.0013kgm^2$, $J_L = 0.0013kgm^2$, $F_n = 50Hz$, $\xi = 0.01$)

position of the peak, for example, the zeros are placed in the position of the zeros in the motor transfer function, then the vibration is greatly reduced. Furthermore, the load will have the same behavior as the motor. Normally adding zeros to the system has to be accompanied by adding poles to the system in order to make the system causal. The added poles can either cause further vibration problems or make the system response slower. But this is not in the application of the input shaper. The input shaper adds zeros to the system without any additional poles. Now the parameters of the input shaper can be determined for an elastic system with closed velocity loop. Although it is difficult to tell the exact position of the frequency after the tuning of the PI parameter, it is known that, after tuning, the system frequency is very near to the mechanical system's frequency at zeros. Therefore, the input shaper can be designed according to the damping ratio and frequency from the zeros in the motor transfer function of the mechanical system in equation(3.51), which are also poles in the load transfer function in equation(3.52). When the ZV input shaper, in the form of $A_1 + A_2 e^{-sT_2}$, is applied, the following parameters are derived as in equation (3.53), according to equation (3.37).

$$
\begin{aligned}
A_1 &= \frac{e^{\frac{\xi_z \pi}{\sqrt{1-\xi_z^2}}}}{1 + e^{\frac{\xi_z \pi}{\sqrt{1-\xi_z^2}}}}, \\
A_2 &= \frac{1}{1 + e^{\frac{\xi_z \pi}{\sqrt{1-\xi_z^2}}}}, \\
T_2 &= \frac{T_z * \sqrt{1 - \xi_z^2}}{2},
\end{aligned}
\tag{3.53}
$$

53

with

ξ_z : the damping ratio of zeros as in Table 3.1 ;

T_z : damped time period of the zeros as in Table 3.1.

Now the description of this effect in the frequency domain is shown in Figure 3.18 and Figure 3.19. Figure 3.18 presents the frequency response of the load in the red curve, and the input shaper in the blue curve. The zero of the input shaper is located near the pole from the load response. Figure 3.19 shows the frequency response of the load after applying the input shaper. Clearly, the zero of the input shaper helps to cancel the pole of the load, resulting in a no vibration behavior for the load.
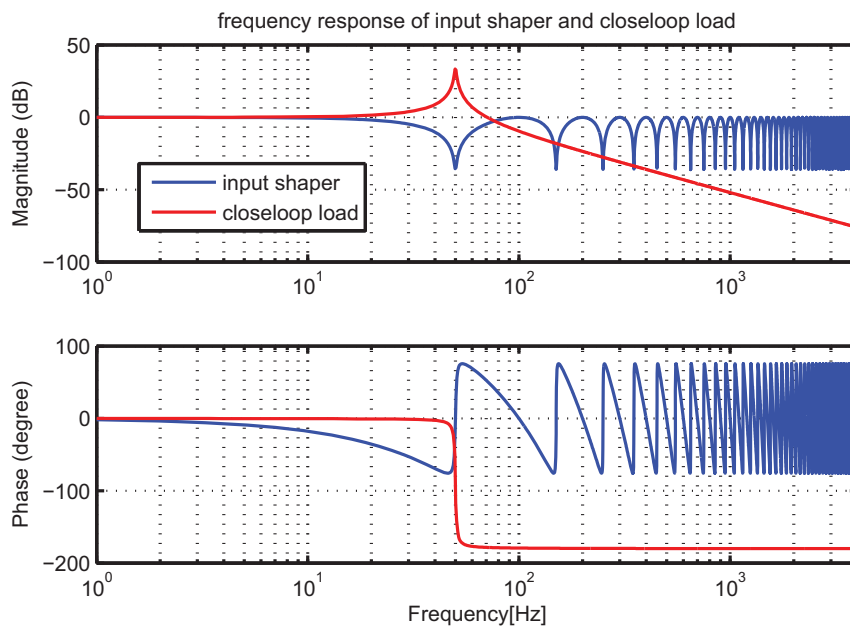
Figure 3.18: Bode diagram - motor torque to load velocity, input shaper ($J_M = 0.0013 kgm^2$, $J_L = 0.0013 kgm^2$, $F_n = 50Hz$, $\xi = 0.01$. Input shaper: $A_1 = 0.5079, A_2 = 0.4921$, $T_2 = 10.5ms$)

Input shaper for motor response

Problems can arise when the estimation of the frequency of the mechanical system is not exact, or the mechanical system changes its frequency in the workspace, or the tuning of the PI controller is not so good in the sense of the motor; in these cases the input shaper cannot compensate all the vibrations. To increase the robustness of the ZV input shaper, the ZVD input shaper can be applied. The ZVD method simply adds two more zeros at the same place as the ZV method. However, it cannot help if the motor is not well tuned. To compensate the vibrations in the motor, another input shaper can be applied. This input
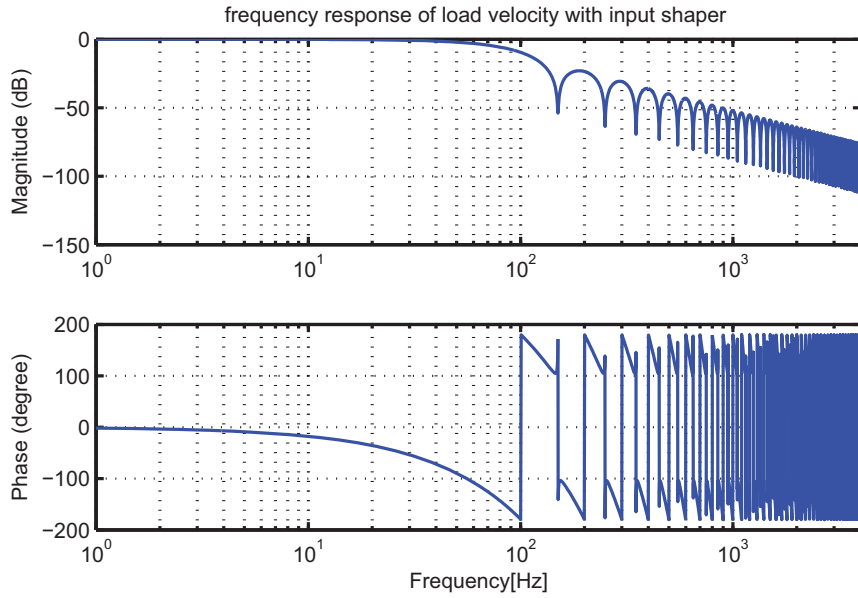
Figure 3.19: Bode diagram of motor torque to load velocity together with input shaper ($J_M = 0.0013 kgm^2$, $J_L = 0.0013 kgm^2$, $F_n = 50Hz$, $\xi = 0.01$. Input shaper: $A_1 = 0.5079$, $A_2 = 0.4921$, $T_2 = 10.5ms$)

shaper is aimed to capture the moving motor poles, which move toward higher frequency as in Figure 3.14. When, due to the tuning of the PI controller, these two poles move quickly to high frequency (or in some situations to the two zeros), then the motor will not have any vibration problems. Only when the two poles do not move far away from their original position, does the vibration of the motor appear. Based on this analysis, the input shaper, which aims to cancel the motor vibration, can be designed to add zeros to the position of the poles in the motor transfer function in equation (3.51). Again, when the input shaper is written in the form of $A_1 + A_2 e^{-sT_2}$, its parameters are derived as in equation (3.54):

$$
\begin{aligned}
A_1 &= \frac{e^{\frac{\xi_n \pi}{\sqrt{1-\xi_n^2}}}}{1 + e^{\frac{\xi_n \pi}{\sqrt{1-\xi_n^2}}}}, \\
A_2 &= \frac{1}{1 + e^{\frac{\xi_n \pi}{\sqrt{1-\xi_n^2}}}}, \\
T_2 &= \frac{T_n * \sqrt{1 - \xi_n^2}}{2},
\end{aligned}
\tag{3.54}
$$

with

ξ_n : the damping ratio in the poles, as in Table 3.1;

T_n : damped time period of the poles, as in Table 3.1.

Input shaper for motor and load response

The total input shaper is then the convolution of the two input shapers above. The input shaper for load vibration due to elastic system in equation (3.53) also helps to reduce the vibration of the motor, and the input shaper for motor vibration, due to the tuning of the PI controller, also helps to reduce the load vibration. The convolution of them also assures the robustness of the input shaper in a bigger frequency range.

Figure 3.20(a) is plotted to demonstrate the effectiveness of the input shaper in equation (3.53) in time domain. It is seen that the vibration of the load is reduced dramatically. The motor response is also better than in Figure 3.16. However, it still vibrates. This is sensed by the slightly vibrating load. Figure 3.20(b) applies the convolved input shaper from equation (3.53) and (3.54). Comparing chart (a) with (b), it is verified that the vibration of the motor is reduced further.
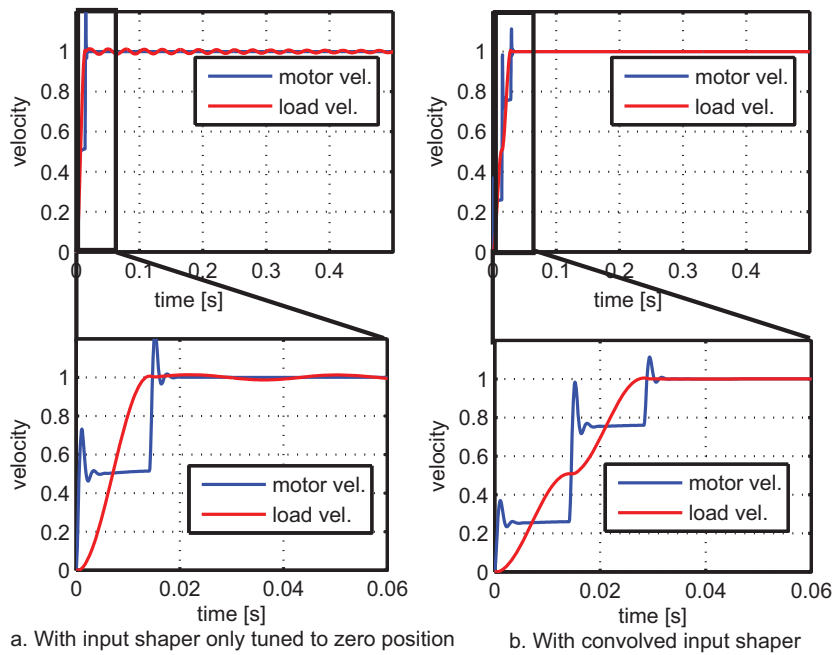
Figure 3.20: Effect of input shaper canceling vibration caused by motor and load ($J_M = 0.0013 kgm^2$, $J_L = 0.0013 kgm^2$, $F_n = 50Hz$, $\xi = 0.01$. Controller: $k_r = 3.25Nms/rad$, $t_i = 3.3ms$)

3.4 Brief Summary of Chapter 3

In this chapter, two methods of eliminating the vibrations from the elastic mechanical system are presented. One way is to tune the PI controller for the elastic mechanical system through

the given simple equations. The other way is to use input shaper in the cascade control loop. The parameters of the PI controller and input shaper are deduced and verified by experiments. Table 3.3 summarizes the parameters of the controller in these two methods.

		elastic double ratio	Rigid double ratio with input shaper
Parameter of velocity loop $(k_r + \frac{1}{st'_i})$	k_r	$k_r = \frac{2\sqrt{2}}{3}\frac{\omega_n^2 J_M}{\omega_z}$	$k_r = \frac{J_M + J_L}{2T_{Ei}}$
	t'_i	$t'_i = \frac{3}{\omega_n^2 J_M}$	$t'_i = \frac{8T_{Ei}^2}{J_M + J_L}$
Parameters of input shaper $(A_1 + A_2 e^{-sT_2})$		—	$A_1 = \frac{1}{1+Q}$ $A_2 = \frac{Q}{1+Q}$ $\omega = \omega_z = \sqrt{\frac{K}{J_L}}$ $\xi = \xi_z = \frac{D}{2}\sqrt{\frac{1}{KJ_L}}$ $Q = e^{\frac{-\xi\pi}{\sqrt{1-\xi^2}}}$ $T_2 = \frac{\pi}{\omega_z}$

Table 3.3: Verifying the parameters of the PI controller

The parameters designed by the elastic double ratio make the system response slower than the rigid double ratio together with an input shaper. This can be seen by comparing the load position response as in Figure 3.21. The rise time for the elastic double ratio is read to be 0.15s from the simulation. The rise time for the rigid double ratio together with an input shaper is read be 0.09s from the simulation.
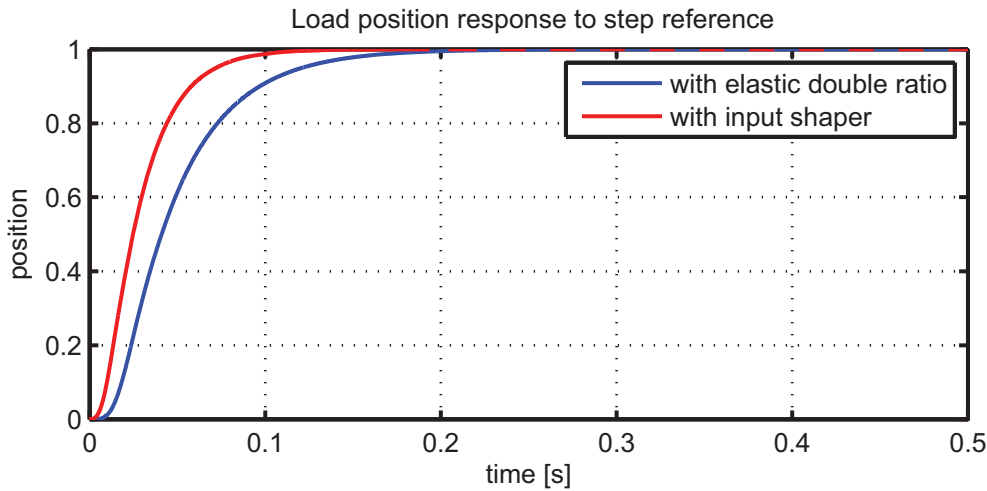
Figure 3.21: Load position response comparison between elastic double ratio controller and controller with input shaper

The application area of these two methods can be summarized as following:

- If the system requires a good compromise between response time and good accuracy, and there is a lot of disturbances to the mechanical system, then tuning the PI controller

according to equation (3.16) and (3.17), and P controller according to equation (3.25) is a better solution.

- When the system requires a very high dynamic, and no or small disturbances exist, then the input shaper can be included in the cascaded control loop. The parameters of the PI controller can be tuned as in rigid systems as in equations (3.5) and (3.6) or equations (3.8) and (3.9). The parameters of the input shaper can be tuned according to equation (3.53).

System Parameters Identification

System modeling and identification plays a central and critical role in the design of control systems. By the physical (theoretical) modeling of dynamic systems, one usually obtains both the structure and the parameters of the mathematical model. The model parameters can generally be calculated, based on physical coefficients or other basic property data of the system. However, some properties may not be completely known and consequently the model structure and parameter uncertainties can be large. Therefore, parameter identification should be employed in addition to physical modeling.

There are two main domains of identification; one is the time domain and the other is frequency domain identification. The classical approach to parameter identification is done in the time domain [36]. It analyzes the free decay of the vibration responses in the time domain. Three groups of methods in the time domain can be classified. The first is the Complex Exponential method [38]. Most time domain parameter identification methods are derived from this method. The second group of methods is the Ibrahim Time Domain method developed in 1977 [22]. It uses the free vibration response of a structure to identify its vibration parameters. The third group of methods is Eigensystem Realization Algorithm (ERA) developed by Juang and Pappa in 1985 [26]. It is one of the most commonly used parameter identification methods. Time domain identification works well in low-order systems, however, it loses its ability when facing high-order systems. Therefore, a number of researchers have started to explore alternative approaches, which are parameter identification in frequency domain [49]. In frequency domain identification, the frequency response of the system is used to estimate the parametric model. The basic idea is to extract frequency response information in the system under consideration. The resulting frequency response information is then used to map in a transfer function model for the system.

A lot of literatures is carrying out parameter identification for two-mass systems [1, 42]. The spring constant, moment of inertia of the masses, and damping constant together with some

non-linear features could be identified for the second order system with more or less effort. In industry, the second order model of the machine tool's axis as in Figure 2.9 is not adequate to represent the feed drive chain. The higher order of the model, as shown in Figure 2.8, is required. However, these identification methods for the low-order system are either not suitable, or too complicated for high order system [19, 50, 69]. Therefore, the objective of this chapter is to derive a simple, effective and generalized method to identify the unknown parameters of a lumped spring-mass system connected in series from frequency response.

The parameters to be identified are the torsional stiffness of the springs and moment of inertia of the masses in the lightly damped drive chain. This parameter identification process is in fact a mapping process, which maps the frequency response of the system to the transfer function of the system as shown in Figure 4.1. The transfer function is derived from the established model structure. The resonance frequencies and anti-resonance frequencies are subtracted from the frequency response of the system. The parameters of the system are obtained by mapping the coefficients of the transfer function and those frequencies. Thus, the process of identification can be divided into three steps.
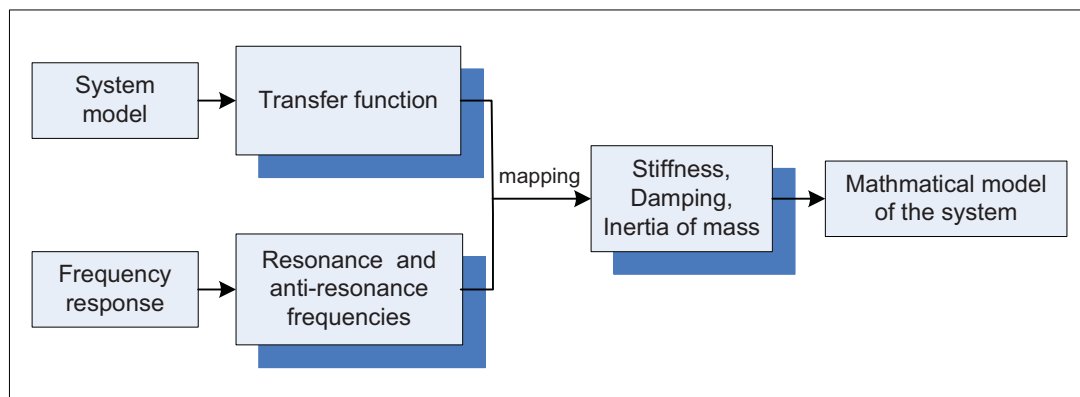
Figure 4.1: Process of parameter identification

- *Step 1*: the general transfer function equation is derived for the n-th order system in terms of the mechanical parameter of the system.

- *Step 2*: the resonance frequencies and anti-resonance frequencies are obtained from the system frequency response.

- *Step 3*: the method of calculating the system parameters from mapping frequency response to transfer function is derived.

The second step, extracting the resonance frequencies and anti-resonance frequencies from the frequency response, can be easily conducted by frequency measurement. It is not discussed in greater detail in this chapter. The first step of deriving a general transfer function

for n-th order system is done in section 4.1, and the third step of parameter mapping is carried out in section 4.2.

4.1 Transfer Function

As discussed in section 2.3, the feed drive system can be modeled as a multiple mass-spring-damper system. Without loss of generality the masses are connected by springs and dampers in series. Assume the system is a $n + 1$ order system consisting of n torsional springs and dampers connecting $n + 1$ masses as shown in Figure 4.2. Only the rotational motion of the masses is considered here.
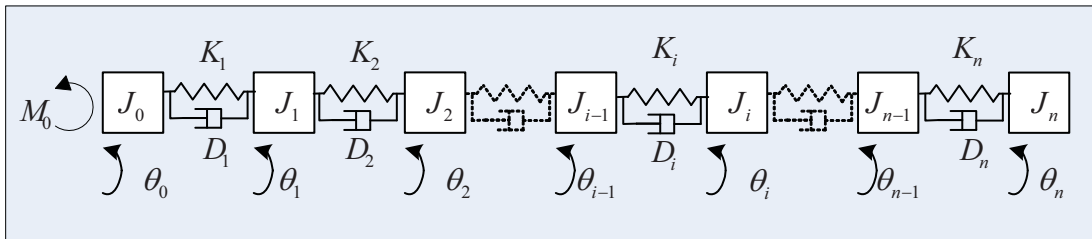
Figure 4.2: Structural model of multi mass-spring-damper system

The mass on the input side has a moment of inertia of J_0, a rotation angle of θ_0 and is driven by an input torque M_0. It is connected to the following mass by means of a spring which has torsional stiffness K_1, and a damper with damping constant D_1. The following mass has a moment of inertia of J_1 and a rotation angle of θ_1. Similarly, the moment of inertia, rotating angle, stiffness and damping constant are defined for further masses, springs and dampers. The block diagram representing the above model is as shown in Figure 4.3.

The transfer function, with the torque M_0 as input and angular velocity $\dot{\theta}_0$ as the output, is of the form,

$$H(s) = \frac{\dot{\theta}_0}{M_0} = \frac{C}{s}\frac{g_n(s)}{f_n(s)},$$
(4.1)

where

$g_n(s)$: the numerator of the transfer function,

$f_n(s)$: the denominator of the transfer function,

C : gain constant.

The above transfer function can be regarded as having two terms: an integral term $\frac{C}{s}$ on the left, which changes the torque input to velocity output, and a ratio term of two polynomials on the right, which determines the dynamic behavior of the system. The denominator of the
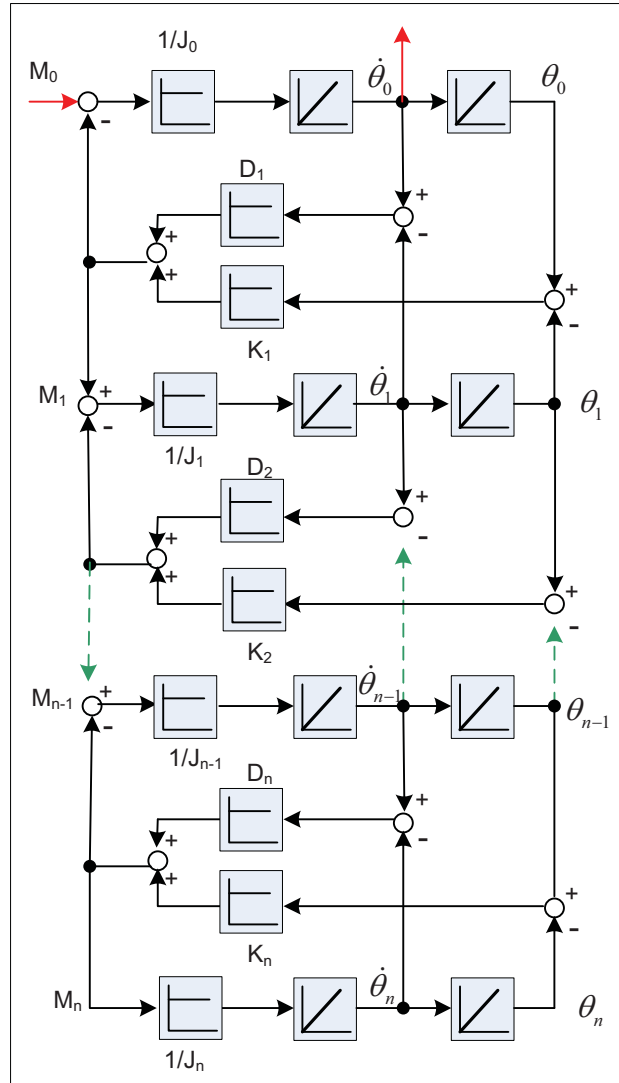
Figure 4.3: Multi mass-spring system model

right term, $f_n(s)$, is normally called the characteristic polynomial. When the characteristic polynomial is equated to zero, it gives the characteristic equation

$$f_n(s) = 0. \tag{4.2}$$

Let M_i be the interacting torque of the ith spring and damper. The equation of the motion of the ith mass is

$$J_i \ddot{\theta}_i(t) = M_i(t) - M_{i+1}(t), \tag{4.3}$$

where $i = 0, \cdots, n$ and $M_0 = M_{n+1} = 0$.

The interacting moment of the ith spring and damper is

$$M_i(t) = K_i \big(\theta_{i-1}(t) - \theta_i(t) \big) + D_i \big(\dot{\theta}_{i-1}(t) - \dot{\theta}_i(t) \big), \tag{4.4}$$

where $i = 1, \cdots, n$.

The transfer function is first derived for values of $n = 1, \cdots, 3$. Then through induction, the transfer function of the high-order system is generalized for any given values of n.

4.1.1   For second order system (n=1)

The structure of the second order system is plotted again in Figure 4.4 here for easy reference and uniform indication.
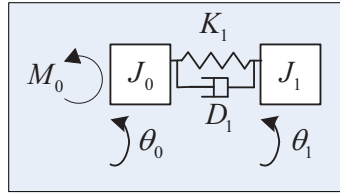
Figure 4.4: Two mass-spring-damper system

From the equations (4.3) and (4.4) and substituting $i = 0$, the equation of motion of the 1st mass is given by

$$J_0 \ddot{\theta}_0(t) + D_1 \left(\dot{\theta}_0(t) - \dot{\theta}_1(t) \right) + K_1 \left(\theta_0(t) - \theta_1(t) \right) = M_0(t). \tag{4.5}$$

From the equations (4.3) and (4.4) and substituting $i = 1$ and $M_2 = 0$, the equation of the 2nd mass is given by

$$J_1 \ddot{\theta}_1(t) + D_1 \left(\dot{\theta}_1(t) - \dot{\theta}_0(t) \right) + K_1 \left(\theta_1(t) - \theta_0(t) \right) = 0. \tag{4.6}$$

The equations (4.5) and (4.6) can be combined to form the motion equation matrix

$$\begin{bmatrix} J_0 & 0 \\ 0 & J_1 \end{bmatrix} \begin{bmatrix} \ddot{\theta}_0 \\ \ddot{\theta}_1 \end{bmatrix} + \begin{bmatrix} D_1 & -D_1 \\ -D_1 & D_1 \end{bmatrix} \begin{bmatrix} \dot{\theta}_0 \\ \dot{\theta}_1 \end{bmatrix} + \begin{bmatrix} K_1 & -K_1 \\ -K_1 & K_1 \end{bmatrix} \begin{bmatrix} \theta_0 \\ \theta_1 \end{bmatrix} = \begin{bmatrix} M_0 \\ 0 \end{bmatrix}. \tag{4.7}$$

The transfer function of such a system with input M_0, and output $\dot{\theta}_0$, is given by

$$\frac{\dot{\theta}_0}{M_0} = \frac{1}{s} \frac{J_1 s^2 + D_1 s + K_1}{J_0 J_1 s^2 + D_1 (J_0 + J_1) s + K_1 (J_0 + J_1)}. \tag{4.8}$$

Dividing the numerator and denominator terms by $J_0 J_1$, the above transfer function is written to

$$\frac{\dot{\theta}_0}{M_0} = \frac{1}{J_0 s} \frac{s^2 + \frac{D_1}{J_1}s + \frac{K_1}{J_1}}{s^2 + (\frac{D_1}{J_0} + \frac{D_1}{J_1})s + (\frac{K_1}{J_0} + \frac{K_1}{J_1})}. \tag{4.9}$$

Let

$$c_i = \frac{K_i}{J_{i-1}}, c_i' = \frac{K_i}{J_i} \quad \text{and} \quad r_i = c_i + c_i', \tag{4.10a}$$

$$d_i = \frac{D_i}{J_{i-1}}, d_i' = \frac{D_i}{J_i} \quad \text{and} \quad m_i = d_i + d_i', \tag{4.10b}$$

setting $i = 1$, and substituting the equations (4.10a) and (4.10b) in equation (4.9),

$$\frac{\dot{\theta}_0}{M_0} = \frac{1}{J_0 s} \frac{s^2 + d_1' s + c_1'}{s^2 + m_1 s + r_1}. \tag{4.11}$$

the characteristic polynomial and the numerator are

$$f_1(s) = s^2 + m_1 s + r_1, \tag{4.12a}$$

$$g_1(s) = s^2 + d_1' s + c_1'. \tag{4.12b}$$

4.1.2 For third order system (n=2)

The model of the third order system is plotted in Figure 4.5.
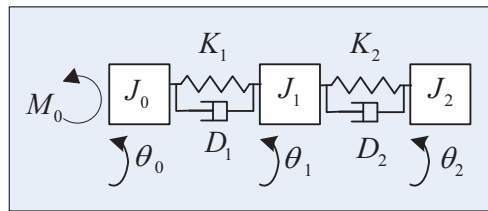
Figure 4.5: Three mass-spring-damper system

The equation of motion of the 1st mass is the same as equation (4.5). From equations (4.3) and (4.4) and substituting $i = 1$, the equation of motion of the 2nd mass is given by

$$J_1 \ddot{\theta}_1(t) + D_1(\dot{\theta}_1(t) - \dot{\theta}_0(t)) + D_2(\dot{\theta}_1(t) - \dot{\theta}_2(t)) + \\ + K_1(\theta_1(t) - \theta_0(t)) + K_2(\theta_1(t) - \theta_2(t)) = 0. \tag{4.13}$$

From the equations (4.3) and (4.4) and substituting $i = 2$ and $M_3 = 0$, the equation of motion of 3rd mass is given by

$$J_2\ddot{\theta}_2(t) + D_2(\dot{\theta}_2(t) - \dot{\theta}_1(t)) + K_2(\theta_2(t) - \theta_1(t)) = 0. \tag{4.14}$$

The equations (4.5), (4.13) and (4.14) can be combined to form the motion equation matrix of the third order system

$$
\begin{bmatrix} J_0 & 0 & 0 \\ 0 & J_1 & 0 \\ 0 & 0 & J_2 \end{bmatrix} \begin{bmatrix} \ddot{\theta}_0 \\ \ddot{\theta}_1 \\ \ddot{\theta}_2 \end{bmatrix} + \begin{bmatrix} D_1 & -D_1 & 0 \\ -D_1 & D_1+D_2 & -D_2 \\ 0 & -D_2 & D_2 \end{bmatrix} \begin{bmatrix} \dot{\theta}_0 \\ \dot{\theta}_1 \\ \dot{\theta}_2 \end{bmatrix} +
$$
$$
+ \begin{bmatrix} K_1 & -K_1 & 0 \\ -K_1 & K_1+K_2 & -K_2 \\ 0 & -K_2 & K_2 \end{bmatrix} \begin{bmatrix} \theta_0 \\ \theta_1 \\ \theta_2 \end{bmatrix} = \begin{bmatrix} M_0 \\ 0 \\ 0 \end{bmatrix}. \tag{4.15}
$$

The transfer function of such a system with input M_0, and output $\dot{\theta}_0$, is given by

$$\frac{\dot{\theta}_0}{M_0} = \frac{1}{s} \frac{J_1 J_2 s^4 + (J_1 D_2 + J_2 D_1 + J_2 D_2) s^3 +}{J_0 J_1 J_2 s^4 + (J_0 J_2 D_1 + J_1 J_2 D_1 + J_0 J_1 D_2 + J_0 J_2 D_2) s^3 +}$$
$$\frac{+(D_1 D_2 + J_1 K_2 + J_2 K_1 + J_2 K_2) s^2 +}{+(D_1 D_2 J_0 + D_1 D_2 J_1 + D_1 D_2 J_2 + J_0 J_2 K_1 + J_1 J_2 K_1 + J_0 J_1 K_2 + J_0 J_2 K_2) s^2 +}$$
$$\frac{+(K_1 D_2 + K_2 D_1) s + K_1 K_2}{+(J_0 K_1 D_2 + J_0 K_2 D_1 + J_1 K_2 D_1 + J_2 K_1 D_2 + J_2 K_2 D_1) s + (J_0 K_1 K_2 + J_1 K_1 K_2 + J_2 K_1 K_2)}.$$
$$\tag{4.16}$$

Dividing the numerator and denominator terms by $J_0 J_1 J_2$, and substituting (3.11a) and (3.11b) in the equation, the transfer function of equation (4.16) is rewritten to

$$\frac{\dot{\theta}_0}{M_0} = \frac{1}{J_0 s} \frac{(s^2 + d_1' s + c_1')(s^2 + m_2 s + r_2) - (d_2 s + c_2)(d_1' s + c_1')}{(s^2 + m_1 s + r_1)(s^2 + m_2 s + r_2) - (d_2 s + c_2)(d_1' s + c_1')}. \tag{4.17}$$

From equations (4.12a) and (4.17), the characteristic polynomial is as shown in equation (4.18a). From equations (4.12b) and (4.17), the numerator is shown in equation (4.18b).

$$f_2(s) = (s^2 + m_2 s + r_2) f_1(s) - (d_2 s + c_2)(d_1' s + c_1'), \tag{4.18a}$$

$$g_2(s) = (s^2 + m_2 s + r_2) g_1(s) - (d_2 s + c_2)(d_1' s + c_1'). \tag{4.18b}$$

4.1.3 For fourth order system (n=3)

The model of the third order system is shown in Figure 4.6.
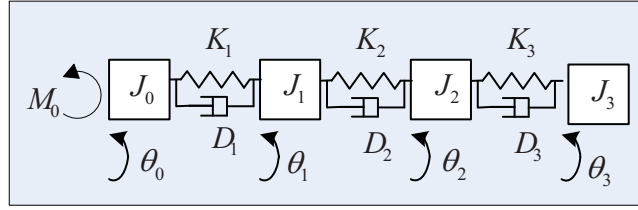
Figure 4.6: Four mass-spring-damper system

The equation of motion of the 1st mass and 2nd mass are the same as equation (4.5) and (4.13) respectively. From equations (4.3) and (4.4) and substituting $i = 2$, the equation of motion of the 3rd mass is given by

$$
\begin{aligned}
J_2\ddot{\theta}_2(t) + D_2(\dot{\theta}_2(t) - \dot{\theta}_1(t)) + D_3(\dot{\theta}_2(t) - \dot{\theta}_3(t)) + \\
+ K_2(\theta_2(t) - \theta_1(t)) + K_3(\theta_2(t) - \theta_3(t)) = 0.
\end{aligned}
\tag{4.19}
$$

From equations (4.3) and (4.4) and substituting $i = 3$ and $D_4 = 0$, the equation of motion of the 4th mass is given by

$$
J_3\ddot{\theta}_3(t) + D_3(\dot{\theta}_3(t) - \dot{\theta}_2(t)) + K_3(\theta_3(t) - \theta_2(t)) = 0.
\tag{4.20}
$$

The equations (4.5), (4.13), (4.19), (4.20) can be combined to form

$$
\begin{bmatrix} J_0 & 0 & 0 & 0 \\ 0 & J_1 & 0 & 0 \\ 0 & 0 & J_2 & 0 \\ 0 & 0 & 0 & J_3 \end{bmatrix}
\begin{bmatrix} \ddot{\theta}_0 \\ \ddot{\theta}_1 \\ \ddot{\theta}_2 \\ \ddot{\theta}_3 \end{bmatrix}
+
\begin{bmatrix} D_1 & -D_1 & 0 & 0 \\ -D_1 & D_1+D_2 & -D_2 & 0 \\ 0 & -D_2 & D_2+D_3 & -D_3 \\ 0 & 0 & -D_3 & D_3 \end{bmatrix}
\begin{bmatrix} \dot{\theta}_0 \\ \dot{\theta}_1 \\ \dot{\theta}_2 \\ \dot{\theta}_3 \end{bmatrix}
+
$$

$$
+
\begin{bmatrix} K_1 & -K_1 & 0 & 0 \\ -K_1 & K_1+K_2 & -K_2 & 0 \\ 0 & -K_2 & K_2+K_3 & -K_3 \\ 0 & 0 & -K_3 & K_3 \end{bmatrix}
\begin{bmatrix} \theta_0 \\ \theta_1 \\ \theta_2 \\ \theta_3 \end{bmatrix}
=
\begin{bmatrix} M_0 \\ 0 \\ 0 \\ 0 \end{bmatrix}.
\tag{4.21}
$$

Dividing the numerator and denominator terms by $J_0J_1J_2J_3$ of the transfer function determined by equation (4.21), and substituting (3.11a) and (3.11b), the transfer function of such a system with input M_0, and output $\dot{\theta}_0$, is given by

$$\frac{\dot{\theta}_0}{M_0} = \frac{1}{J_0 s} \frac{\begin{aligned}&(s^2 + m_3 s + r_3)((s^2 + d'_1 s + c'_1)(s^2 + m_2 s + r_2) - (d_2 s + c_2)(d'_1 s + c'_1)) + \\ &-(d_3 s + c_3)(d'_2 s + c'_2)(s^2 + d'_1 s + c'_1)\end{aligned}}{\begin{aligned}&(s^2 + m_3 s + r_3)((s^2 + m_1 s + r_1)(s^2 + m_2 s + r_2) - (d_2 s + c_2)(d'_1 s + c'_1)) + \\ &-(d_3 s + c_3)(d'_2 s + c'_2)(s^2 + m_1 s + r_1)\end{aligned}}. \tag{4.22}$$

From equations (4.12a), (4.18a), (4.22), the characteristic polynomial is calculated as in equation (4.23a). From (4.12b) and (4.18b) and (4.22), the numerator is shown in equation (4.23b).

$$f_3(s) = (s^2 + m_3 s + r_3) f_2(s) - (d_3 s + c_3)(d'_2 s + c'_2) f_1(s), \tag{4.23a}$$

$$g_3(s) = (s^2 + m_3 s + r_3) g_2(s) - (d_3 s + c_3)(d'_3 s + c'_2) g_1(s). \tag{4.23b}$$

4.1.4 For n^{th} order system

For different values of n, the transfer function follows a systematic pattern. The characteristic polynomial can thus be generalized for $n > 1$ as in equation (4.24a). The numerator can be generalized for $n > 1$ as in equation (4.24b):

$$f_n(s) = (s^2 + m_n s + r_n) f_{n-1}(s) - (d_n s + c_n)(d'_{n-1} s + c'_{n-1}) f_{n-2}(s), \tag{4.24a}$$

$$g_n(s) = (s^2 + m_n s + r_n) g_{n-1}(s) - (d_n s + c_n)(d'_{n-1} s + c'_{n-1}) g_{n-2}(s). \tag{4.24b}$$

where

$$f_0(s) = 1,$$
$$f_1(s) = s^2 + m_1 s + r_1 s,$$
$$g_0(s) = 1,$$
$$g_1(s) = s^2 + d'_1 s + c'_1.$$

From equations (4.11), (4.17), (4.22), it is also known that there is a constant

$$C = \frac{1}{J_0} \tag{4.25}$$

in the equations.

Equations (4.24a), (4.24b), (4.25) are combined to form the general equation of the transfer function as shown in equation (4.1). Now equation (4.1) has the form of

$$
\begin{aligned}
H(s) &= \frac{\dot{\theta}_0}{M_0} = \frac{C}{s} \frac{g_n(s)}{f_n(s)} \\
&= \frac{1}{J_0 s} \frac{(s^2 + m_n s + r_n) g_{n-1}(s) - (d_n s + c_n)(d'_{n-1}s + c'_{n-1})g_{n-2}(s)}{(s^2 + m_n s + r_n) f_{n-1}(s) - (d_n s + c_n)(d'_{n-1}s + c'_{n-1})f_{n-2}(s)},
\end{aligned}
\tag{4.26}
$$

where

$$
\begin{aligned}
&n > 1, \\
&f_0(s) = 1, \\
&f_1(s) = s^2 + m_1 s + r_1 s, \\
&g_0(s) = 1, \\
&g_1(s) = s^2 + d'_1 s + c'_1.
\end{aligned}
$$

The above equation (4.26) is the general transfer function of any order of the system of masses connected in series by dampers and springs.

For no damping systems, as $D_i = 0 (i = 1, \cdots, n)$, therefore $d_i = 0 (i = 1, \cdots, n)$, equations (4.24a) and (4.24b) can be simplified to:

$$
f_n(s) = (s^2 + r_n)f_{n-1}(s) - c_n c'_{n-1} f_{n-2}(s),
\tag{4.27a}
$$

$$
g_n(s) = (s^2 + r_n)g_{n-1}(s) - c_n c'_{n-1} g_{n-2}(s),
\tag{4.27b}
$$

where

$$
\begin{aligned}
&n > 1, \\
&f_0(s) = 1, \\
&f_1(s) = s^2 + r_1, \\
&g_0(s) = 1, \\
&g_1(s) = s^2 + c'_1.
\end{aligned}
$$

4.2 Parameter Identification in Frequency Domain

The parameters of the system without damping of any order will be identified in this section. The parameters to be identified are $J_1, J_2, \cdots, J_n$ and $K_1, K_2, \cdots, K_n$ $(D_1, D_2, \cdots, D_n = 0$, for no damping system). J_0, the inertia of motor, is normally well known for a feed drive system.

As when c_i and c_i' in equation (4.27a) and (4.27b) are known, the unknown parameters of the system can be solved easily as shown in Figure 4.7. Therefore, the parameter identification of the mechanical system is in fact the identification process of c_i and c_i'.
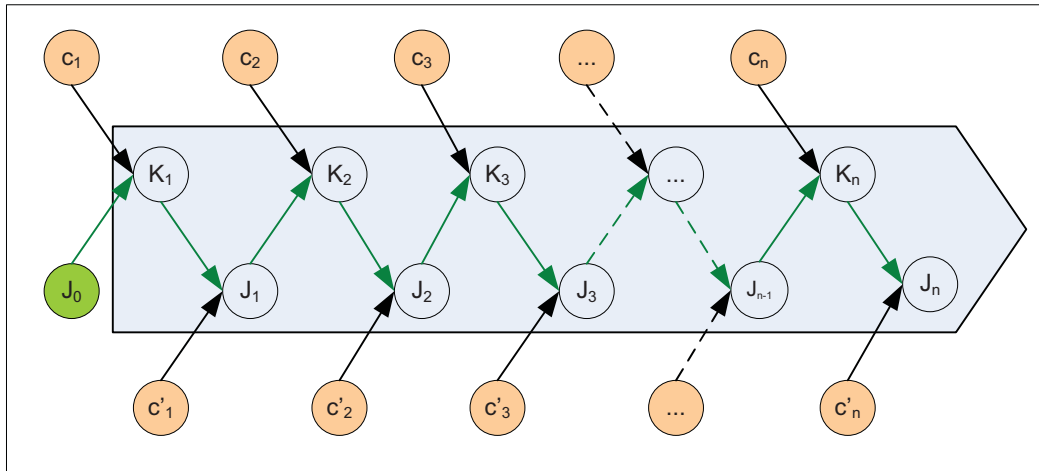
Figure 4.7: String knot relationship among the parameters

In Figure 4.7, K_1 is first calculated from c_1 and J_0, through the relationship $c_i = \frac{K_i}{J_{i-1}}$ in equation (4.10a). Then J_1 can be calculated from c_1' and the already known K_1 through $c_i' = \frac{K_i}{J_i}$ as in equation (4.10a). Further, K_2 is calculated from c_2 and J_1, J_2 is calculated from c_2' and K_2, until K_n and J_n are calculated. This is a process of trying to untie a string with a lot of knots. The knots are $c_1, c_2, \cdots, c_n$ and $c_1', c_2', \cdots, c_n'$. When those knots are known, it is very easy to untie the string from the start point of J_0, and to unveil $J_1, J_2, \cdots, J_n$ and $K_1, K_2, \cdots, K_n$.

Therefore, the method to calculate c_i and c_i' should be first derived here. This is done by mapping the transfer function and the frequency response as stated before. From frequency measurement all characteristic frequencies, corresponding to the poles p and zeros z in the transfer function of the system, can be found using the Bode diagram.

As for the mechanical system without damping the resonance frequency equals to the eigen-frequency of the system, the measured resonance frequency and anti-resonance frequency are directly the imagery part of the system poles and zeros (for a system without damping, the real parts of the poles and zeros of the system are zero). When damping of the mechanical system is small, the resonance frequency is approximately equal to the eigenfrequency of the system. E.g. with 0.1 damping ratio, the eigenfrequency is only 1% less than the characteristic frequency; the resonance freqency is only 0.1% less than the eigenfrequency.

The denominator and numerator terms of the transfer function of the system are calculated from these poles and zeros. The mapping of the transfer function derived from the n-th order system in section 4.1 and from the poles and zeros from frequency measurement can then

be processed. The coefficients of these denominator and numerator terms of the transfer function determined by poles and zeros are represented by the letters 'a' and 'b' respectively. In the following derivations, 'x' terms have been introduced to identify the general pattern of the steps being followed.

The mapping process is first done for $n = 1, \cdots, 3$ as has been done in deriving the transfer function from model. General mapping is then deduced based on induction theory.

4.2.1 For second order system (n=1)

For $n = 1$, the pole and zero are p_1 and z_1 respectively. The denominator and numerator of the transfer function determined by frequency response are written to

$$f_1(s) = s^2 + p_1^2 = s^2 + {}^1a_1, \tag{4.28a}$$
$$g_1(s) = s^2 + z_1^2 = s^2 + {}^1b_1. \tag{4.28b}$$

With $n = 1$, from equations (4.27a) and (4.27b), it is known that the denominator and numerator of the transfer function are

$$f_1(s) = s^2 + r_1, \tag{4.29a}$$
$$g_1(s) = s^2 + c_1'. \tag{4.29b}$$

Mapping equations (4.28a) and (4.29a), as well as equations (4.28b) and (4.29b), the relationships between the coefficients of the transfer functions expressed by different methods are

$$^1a_1 = r_1, \tag{4.30a}$$
$$^1b_1 = c_1'. \tag{4.30b}$$

From equations (4.10a), (4.30a) and (4.30b), the c_1 and c_1' are

$$c_1 = {}^1a_1 - {}^1b_1, \tag{4.31a}$$
$$c_1' = {}^1b_1. \tag{4.31b}$$

4.2.2 For third order system (n=2)

For $n = 2$, the poles and zeros are (p_1, p_2) and (z_1, z_2) respectively. The denominator and numerator of the transfer function determined by frequency response are written to

$$f_2(s) = (s^2 + p_1^2)(s^2 + p_2^2) = s^4 + {}^2a_1 s^2 + {}^2a_2, \tag{4.32a}$$

$$g_2(s) = (s^2 + z_1^2)(s^2 + z_2^2) = s^4 + {}^2b_1 s^2 + {}^2b_2. \tag{4.32b}$$

With $n = 2$, from equations (4.27a) and (4.27b), the denominator and numerator of the transfer function are

$$f_2(s) = (s^2 + r_2)(s^2 + r_1) - c_1' c_2 = s^4 + (r_1 + r_2)s^2 + (r_1 r_2 - c_1' c_2), \tag{4.33a}$$

$$g_2(s) = (s^2 + r_2)(s^2 + c_1') - c_1' c_2 = s^4 + (c_1' + r_2)s^2 + (r_1 r_2 - c_1' c_2). \tag{4.33b}$$

Mapping equations (4.32a) and (4.33a), as well as equations (4.32b) and (4.33b), the relationships between the coefficients of the transfer functions expressed by different methods are

$$^2a_1 = r_1 + r_2, \tag{4.34a}$$

$$^2b_1 = c_1' + r_2, \tag{4.34b}$$

$$^2a_2 = r_1 r_2 - c_1' c_2, \tag{4.34c}$$

$$^2b_2 = c_1' r_2 - c_1' c_2. \tag{4.34d}$$

From equations (4.10a), (4.34a) and (4.34b), c_1 is

$$^2a_1 - {}^2b_1 = r_1 - c_1' = c_1, \tag{4.35a}$$

$$c_1 = {}^2a_1 - {}^2b_1. \tag{4.35b}$$

From equations (4.10a), (4.34c) and (4.34d), the following relationship exists:

$$^2a_2 - {}^2b_2 = r_1 r_2 - c_1' r_2 = r_2 c_1. \tag{4.36}$$

Let $x_{11} = \frac{{}^2a_2 - {}^2b_2}{c_1}$, and combine this with equation (4.36), x_{11} is rewritten to

$$x_{11} = r_2. \tag{4.37}$$

From equations (4.34b) and (4.37), c_1' is calculated as

$$c_1' = {}^2b_1 - x_{11}. \tag{4.38}$$

From equations (4.10a) and (4.34d), ${}^2b_2$ is rewritten to

$$^2b_2 = c_1'r_2 - c_1'c_2 = c_1'c_2', \tag{4.39}$$

Let $x_{11}' = \frac{{}^2b_2}{c_1'}$, combine this with equation (4.39), x_{11}' is

$$x_{11}' = c_2'. \tag{4.40}$$

From equations (4.10a), (4.37) and (4.40), the following equation is obtained:

$$c_2 = x_{11} - x_{11}'. \tag{4.41}$$

From equations (4.35), (4.38), (4.40) and (4.41), together with the definition of x_{11} and x_{11}', c_1, c_1', c_2 and c_2' are summarized as

$$
\begin{aligned}
c_1 &= {}^2a_1 - {}^2b_1, \quad x_{11} = \frac{{}^2a_2 - {}^2b_2}{c_1}, \\
c_1' &= {}^2b_1 - x_{11}, \quad x_{11}' = \frac{{}^2b_2}{c_1'}, \\
c_2' &= x_{11}', \\
c_2 &= x_{11} - x_{11}'.
\end{aligned}
\tag{4.42}
$$

4.2.3 For fourth order system (n=3)

For $n = 3$, the poles and zeros are (p_1, p_2, p_3) and (z_1, z_2, z_3) respectively. The denominator and numerator of the transfer function determined by frequency response are written to

$$f_3(s) = \prod_{i=1}^{3}(s^2 + p_i^2) = s^6 + {}^3a_1 s^4 + {}^3a_2 s^2 + {}^3a_3, \tag{4.43a}$$

$$g_3(s) = \prod_{i=1}^{3}(s^2 + z_i^2) = s^6 + {}^3b_1 s^4 + {}^3b_2 s^2 + {}^3b_3. \tag{4.43b}$$

From equations (4.29a), (4.32a) and (4.27a), the denominator is known as in following equation (4.44a). From equations (4.29b), (4.32b) and (4.27b), the numerator of the transfer function is determined as in following equation (4.44b):

$$f_3(s) = (s^2 + r_3)(s^2 + {}^2a_1 s^2 + {}^2a_2) - c_2' c_3(s^2 + r_1),$$
$$= s^6 + ({}^2a_1 + r_3)s^4 + ({}^2a_1 r_3 + {}^2a_2 - c_2' c_3)s^2 + ({}^2a_2 r_3 - r_1 c_2' c_3), \tag{4.44a}$$
$$g_3(s) = (s^2 + r_3)(s^2 + {}^2b_1 s^2 + {}^2b_2) - c_2' c_3(s^2 + c_1'),$$
$$= s^6 + ({}^2b_1 + r_3)s^4 + ({}^2b_1 r_3 + {}^2b_2 - c_2' c_3)s^2 + ({}^2b_2 r_3 c_1' c_2' c_3). \tag{4.44b}$$

Mapping equations (4.43a) and (4.44a), as well as equations (4.43b) and (4.44b), the relationships between the coefficients of the transfer functions expressed by different methods are

$$ {}^3a_1 = {}^2a_1 + r_3, \tag{4.45a}$$
$$ {}^3b_1 = {}^2b_1 + r_3, \tag{4.45b}$$
$$ {}^3a_2 = {}^2a_1 r_3 + {}^2a_2 - c_2' c_3, \tag{4.45c}$$
$$ {}^3b_2 = {}^2b_1 r_3 + {}^2b_2 - c_2' c_3, \tag{4.45d}$$
$$ {}^3a_3 = {}^2a_2 r_3 - r_1 c_2' c_3, \tag{4.45e}$$
$$ {}^3b_3 = {}^2b_2 r_3 - c_1' c_2' c_3. \tag{4.45f}$$

From equations (4.35), (4.45a) and (4.45b), c_1 is calculated as

$$ {}^3a_1 - {}^3b_1 = {}^2a_1 - {}^2b_1 = c_1, \tag{4.46a}$$
$$ c_1 = {}^3a_1 - {}^3b_1. \tag{4.46b}$$

From equations (4.34b) and (4.45b), the following relationship exists:

$$ {}^3b_1 = {}^2b_1 + r_3 = c' + r_2 + r_3. \tag{4.47}$$

From equations (4.35), (4.36), (4.45c) and (4.45d), the following equation can be obtained:

$$ {}^3a_2 - {}^3b_2 = ({}^2a_1 - {}^2b_1)r_3 + ({}^2a_2 - {}^2b_2) = c_1(r_2 + r_3). \tag{4.48}$$

Let $x_{11} = \frac{{}^3a_2 - {}^3b_2}{c_1}$, and combine this with equation (4.48), x_{11} can also be rewritten to

$$ x_{11} = r_2 + r_3. \tag{4.49}$$

From equations (4.47) and (4.49), c_1' can be calculated as

$$c_1' = {}^3b_1 - x_{11}. \tag{4.50}$$

From equations (4.34b), (4.34d) and (4.45d), the following relationship exists:

$$\begin{aligned}
{}^3b_2 &= {}^2b_1r_3 + {}^2b_2 - c_2'c_3 = (c_1' + r_2)r_3 + c_1'r_2 - c_1'c_2 - c_2'c_3 \\
&= c_1'r_3 + r_2r_3 + c_1'c_2' - c_2'c_3.
\end{aligned} \tag{4.51}$$

From equations (4.10), (4.36), (4.45e), and (4.45f), the following equation can be obtained:

$$\begin{aligned}
{}^3a_3 - {}^3b_3 &= ({}^2a_3 - {}^2b_3)r_3 - (r_1 - c_1')c_2'c_3 = c_1r_2r_3 - c_1c_2'c_3 \\
&= c_1(r_3r_2 - c_2'c_3).
\end{aligned} \tag{4.52}$$

Let $x_{12} = \frac{{}^3a_3 - {}^3b_3}{c_1}$, and combine this with equation (4.52), x_{12} can also be written to,

$$x_{12} = r_2r_3 - c_2'c_3. \tag{4.53}$$

From equations (4.51) and (4.53), the following equation can be derived:

$$^3b_2 - x_{12} = c_1'(c_2' + r_3). \tag{4.54}$$

Let $x_{11}' = \frac{{}^3b_2 - x_{12}}{c_1'}$, and combine this with equation (4.54), x_{11}' can also be written to

$$x_{11}' = r_3 + c_2'. \tag{4.55}$$

From equations (4.10a), (4.49), and (4.55), c_2 can now be calculated using the following equation:

$$c_2 = x_{11} - x_{11}'. \tag{4.56}$$

From equations (4.10a), (4.39), and (4.45f), the following equation can be obtained:

$$^3b_3 = {}^2b_2r_3 - c_1'c_2'c_3 = c_1'c_2'r_3 - c_1'c_2'c_3 = c_1'c_2'c_3'. \tag{4.57}$$

Let $x_{12}' = \frac{{}^3b_3}{c_1'}$, combine this with equation (4.57), x_{12}' can also be written to

$$x_{12}' = c_2'c_3'. \tag{4.58}$$

74

From (4.10a), (4.53), and (4.58), the following equation can be obtained:

$$x_{12} - x'_{12} = r_2 r_3 - c'_2 c_3 - c'_2 c'_3 = c_2 r_3,$$ (4.59)

Let $x_{21} = \frac{x_{12} - x'_{12}}{c_2}$, combine this with equation (4.59), x_{21} can also be written to

$$x_{21} = r_3.$$ (4.60)

From equations (4.55) and (4.60), c'_2 can be calculated as

$$c'_2 = x'_{11} - x_{21},$$ (4.61)

Let $x'_{21} = \frac{x'_{12}}{c'_2}$, combine this with equation (4.58), x'_{21} can also be written to

$$x'_{21} = c'_3,$$ (4.62)

From equations (4.10a), (4.60) and (4.62), c_3 is calculated as

$$c_3 = x_{21} - x'_{21}.$$ (4.63)

From equations (4.46b), (4.50), (4.56), (4.61), (4.62) and (4.63), together with the definition of $x_{11}, x'_{11}, x_{12}, x'_{12}, x_{21}$ and $x'_{21}, c_1, c'_1, c_2, c'_2, c_3$ and c'_3 are summarized as

$$
\begin{aligned}
c_1 &= {}^3a_1 - {}^3b_1, & x_{11} &= \frac{{}^3a_2 - {}^3b_2}{c_1}, \\
c'_1 &= {}^3b_1 - x_{11}, & x_{12} &= \frac{{}^3a_3 - {}^3b_3}{c_1}, & x'_{11} &= \frac{{}^3b_2 - x_{12}}{c'_1}, \\
c_2 &= x_{11} - x'_{11}, & x'_{12} &= \frac{{}^3b_3}{c'_1}, & x_{21} &= \frac{x_{12} - x'_{12}}{c_2}, \\
c'_2 &= x'_{11} - x_{21}, & x'_{21} &= \frac{x'_{12}}{c'_2}, \\
c'_3 &= x'_{21}, \\
c_3 &= x_{21} - x'_{21}.
\end{aligned}
$$ (4.64)

The deduction process of $c_1, c'_1, c_2, c'_2, c_3, c'_3, c_4$ and c'_4 for fifth order system (n=4) is presented in Appendix A.2.

4.2.4   For $(n+1)^{th}$ order system

From equation (4.31) for $n = 1$, equation (4.42) for $n = 2$, and equation (4.64) for $n = 3$, the c and x for n are deduced as

$$c_1 = {}^n a_1 - {}^n b_1, \quad x_{11} = \frac{{}^n a_2 - {}^n b_2}{c_1},$$

$$c_1' = {}^n b_2 - x_{11}, \quad x_{12} = \frac{{}^n a_2 - {}^n b_2}{c_1}, \quad x_{11}' = \frac{{}^n b_2 - x_{12}}{c_1'}$$

$$c_2 = x_{11} - x_{11}', \quad x_{13} = \frac{{}^n a_4 - {}^n b_4}{c_1}, \quad x_{12}' = \frac{{}^n b_3 - x_{13}}{c_1'}, \quad x_{21} = \frac{x_{12} - x_{12}'}{c_2},$$

$$c_2' = x_{11}' - x_{21}, \quad x_{14} = \frac{{}^n a_5 - {}^n b_5}{c_1}, \quad x_{13}' = \frac{{}^n b_4}{c_1'}, \quad x_{22} = \frac{x_{13} - x_{13}'}{c_2}, \quad x_{21}' = \frac{x_{12}' - x_{22}}{c_2'},$$

$$\vdots \quad \vdots$$

$$c_i = x_{(i-1)1} - x_{(i-1)1}', \quad x_{1(2i-1)} = \frac{{}^n a_{2i} - {}^n b_{2i}}{c_1}, \quad \cdots \quad x_{i1} = \frac{x_{(i-1)2} - x_{(i-1)2}'}{c_i},$$

$$c_i' = x_{(i-1)1}' - x_{i1}, \quad x_{1(2i)} = \frac{{}^n a_{2i+1} - {}^n b_{2i+1}}{c_1}, \quad \cdots \quad x_{i1}' = \frac{x_{(i-1)2}' - x_{i2}'}{c_i'},$$

$$\vdots \quad \vdots$$

$$c_{n-1} = x_{(n-2)1} - x_{(n-2)1}', \quad x_{(n-2)2} = \frac{x_{1(n-1)}'}{c_{n-2}'}, \frac{x_{(n-2)2} - x_{(n-2)2}'}{c_{n-1}},$$

$$c_{n-1}' = x_{(n-2)1}' - x_{(n-1)1}, \quad x_{(n-1)1}' = \frac{x_{(n-2)2}}{c_{n-1}'},$$

$$c_n' = x_{(n-1)1}',$$

$$c_n = x_{n-1} - x_{(n-1)1}'$$

$$\tag{4.65}$$

The left superscript index n in the a, b item in the above equation indicates that the system is an $(n+1)^{th}$ order system. The left superscript index is introduced in the process of calculating the higher order transfer function from the lower order system's transfer function. As now all a, b items in equations (4.31),(4.42),(4.64),(A.33) and (4.65) are coefficients of the same order of the system, the left superscript index $1, 2, \cdots, n$ is no more needed. Therefore, in the following equations, the left superscript index will be deleted.

The aim of this parameter identification method is first to get the c in the form of the coefficients determined by the poles and zeros of the system. From equation (4.65), it is known that the intermediate value x should be first calculated. From equation (4.65), the equations for calculating x and x' are generalized as

$$
x : \begin{cases}
x_{1j} = \dfrac{a_{(j+1)} - b_{(j+1)}}{a_1 - b_1}, & j = 1, \cdots, (n-1) \\[3mm]
x'_{1j} = \dfrac{b_{(j+1)} - x_{1(j+1)}}{b_1 - x_{11}}, & j = 1, \cdots, (n-1), x_{1n} = 0 \\[3mm]
x_{ij} = \dfrac{x_{(i-1)(j+1)} - x'_{(i-1)(j+1)}}{x_{(i-1)1} - x'_{(i-1)1}}, & i = 2, \cdots, (n-1), j = 1, \cdots, (n-1) \\[3mm]
x'_{ij} = \dfrac{x'_{(i-1)(j+1)} - x_{i(j+1)}}{x'_{(i-1)1} - x_{(i-1)1}}. & i = 2, \cdots, (n-1), j = 1, \cdots, (n-1), x_{i(n+1-i)} = 0
\end{cases}
\tag{4.66}
$$

The c_i and c'_i are generalized as

$$
c : \begin{cases}
c_1 = a_1 - b_1 \\[2mm]
c'_1 = b_1 - x_{11} \\[2mm]
c_i = x_{(i-1)1} - x'_{(i-1)1} & i = 2, \cdots, n \\[2mm]
c'_i = x'_{(i-1)1} - x_{i1} & i = 2, \cdots, n.
\end{cases}
\tag{4.67}
$$

For implementation, all the terms of a, b, x and x' are summarized into a $(2n+1) \times (2n+1)$ matrix as given in table 4.1.

	1	2	3	4	5	6	⋯	n	n+1	n+2	n+3	⋯	2n−2	2n−1	2n	2n+1
1	a_1	a_2	a_3	a_4	a_5	a_6	⋯	a_n								
2		b_1	b_2	b_3	b_4	b_5	⋯	b_{n-1}	b_n							
3			x_{11}	x_{12}	x_{13}	x_{14}	⋯	$x_{1(n-2)}$	$x_{1(n-1)}$	0						
4				x'_{11}	x'_{12}	x'_{13}	⋯	$x'_{1(n-3)}$	$x'_{1(n-2)}$	$x'_{1(n-1)}$						
5					x_{21}	x_{22}	⋯	$x_{2(n-4)}$	$x_{2(n-2)}$	$x_{2(n-2)}$	0					
6						x'_{21}	⋯	$x'_{2(n-5)}$	$x'_{2(n-4)}$	$x'_{2(n-3)}$	$x'_{2(n-2)}$					
7								$x_{3(n-6)}$	$x_{3(n-5)}$	$x_{3(n-4)}$	$x_{3(n-3)}$	⋯				
						⋯		⋯					⋯	0, $x'_{(n-3)3}$, $x_{(n-2)2}$	0		
2n−2														$x'_{(n-2)1}$	$x'_{(n-2)2}$		
2n−1															$x_{(n-1)1}$	0	
2n																$x'_{(n-1)1}$	
2n+1																	0

Table 4.1: Matrix of c, c', x, x'

The column 1 to n in the first row of the matrix consists of coefficients of the denominator of the transfer function. The column 2 to n+1 in the second row consists of coefficients of the numerator of the transfer function. The column $(2i + 1)$ to $(2i + n)$ in row $(2i + 1)$ consists of $x_{ij}, i = 1 \cdots (n - 1), j = 1 \cdots (n - 1)$. The column $(2i + 2)$ to $(2i + n + 2)$ in row $(2i + 2)$ consists of $x'_{ij}, i = 1 \cdots (n - 1), j = 1 \cdots (n - 1)$. The elements in the matrix are summarized as following:

$$element(i, j) : \begin{cases} element(1, j) = a_j, & j = 1 \cdots n \\ element(2, j + 1) = b_j, & j = 1 \cdots n \\ element(2i + 1, 2i + j) = x_{ij}, & i, j = 1 \cdots (n - 1) \\ element(2i + 1, 2i + n) = 0, & i = 1 \cdots n, \\ element(2i + 2, 2i + 1 + j) = x'_{ij}. & i, j = 1 \cdots n - 1 \end{cases} \quad (4.68)$$

From equations (4.66) and (4.68), the x and x' can be calculated from the elements in table 4.1 as

$$x_{ij} = \frac{element(2i - 1, 2i + j - 1) - element(2i, 2i + j)}{element(2i - 1, 2i - 1) - element(2i, 2i)}, \quad (4.69a)$$

$$x'_{ij} = \frac{element(2i, 2i + j) - element(2i + 1, 2i + j + 1)}{element(2i, 2i) - element(2i + 1, 2i + 1)}, \quad (4.69b)$$

where $i, j = 1 \cdots, n - 1$.

From equations (4.67) and (4.68), the general equation for c_i and c'_i is

$$c_i = element(2i - 1, 2i - 1) - element(2i, 2i), \quad (4.70a)$$

$$c'_i = element(2i, 2i) - element(2i + 1, 2i + 1), \quad (4.70b)$$

where $i = 1, \cdots, n$.

Now, the values of c_i, c'_i for any order of the system are known. J_0 is already known. The stiffness of each spring as well as the moment of inertia of each mass can be calculated using the relationships shown in Figure 4.7 and the following equations:

$$K_i = c_i J_{i-1}, \quad (4.71a)$$

$$J_i = \frac{K_i}{c'_i}, \quad (4.71b)$$

where $i = 1, \cdots, n$.

The seemingly complicated parameter identification process is now ended with a very simple process and calculations as shown in Figure 4.8. Inputs to the calculation process are

the poles and zeros (resonance frequency and anti-resonance frequency) of the system and motor inertia. The matrix is formatted by equations (4.68) and equation (4.69). c and c' are calculated from elements in matrix according to equation (4.70). The required J and K are solved through equations in (4.71).
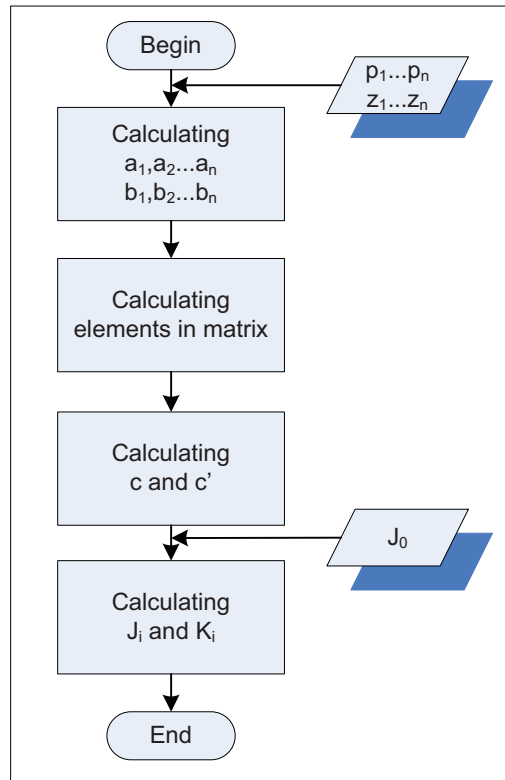
Figure 4.8: Flow chart of identification process

4.2.5 Results and simulations

The processes and equations for identifying the system parameters are described in the above section. These equations are well suited for computational purposes for any order of the system. These derivations are deduced from the general pattern followed by the lower order undamped systems. This identification process is also suitable for slightly damped system (e.g, damping ratio < 0.1). The reason is that, for slightly damped system the characteristic and natural frequency are very near. This will be verified by the following simulation result.

The simulation is done with a 10th order slightly damped system ($n = 9$). The moment of inertia of the motor is $0.01 kgm^2$. Damping is set to $0.01 Nm \cdot s/rad$ for all springs. Other parameters are defined in the table 4.2 where the unit of K_i is Nm/rad and the unit of J_i is kgm^2. The sampling process is done at the sampling rate of 8 kHz.

Fig 4.9 shows the bode plot of the system. The poles and zeros of the system extracted from the frequency response are as follows:
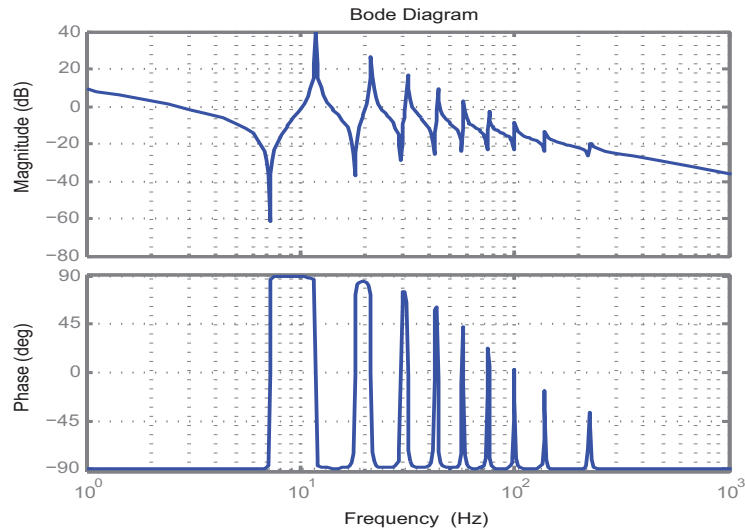
Figure 4.9: Frequency response of the simulated system

$$p_1 = 11.8Hz, \qquad z_1 = 7.2Hz,$$

$$p_2 = 21.3Hz, \qquad z_2 = 17.9Hz,$$

$$p_3 = 31.8Hz, \qquad z_3 = 29.4Hz,$$

$$p_4 = 43.8Hz, \qquad z_4 = 42.1Hz,$$

$$p_5 = 58.1Hz, \qquad z_5 = 56.8Hz,$$

$$p_6 = 75.9Hz, \qquad z_6 = 74.8Hz,$$

$$p_7 = 100.2Hz, \qquad z_7 = 99.1Hz,$$

$$p_8 = 138.7Hz, \qquad z_8 = 137.5Hz,$$

$$p_9 = 225.5Hz, \qquad z_9 = 223.6Hz.$$

Then through equation (4.68) to (4.71), the systems parameters can be identified as in table 4.2.

Comparing the identified values to the initial values, it can be seen that the identification process works almost perfectly. To see the difference more easily, the absolute values of errors computed by equation (4.72) are placed in table 4.2 as well. The biggest error of the spring constant occurs at the first spring with 0.05% error. The biggest error of the inertia value occurs at the last mass with 0.033%.

Parameters		Original values		Identified values		Errors	
Inertia	Stiffness	Inertia	Stiffness	Inertia	Stiffness	Inertia	Stiffness
(kgm^2)	(Nm/rad)	(kgm^2)	(Nm/rad)	(kgm^2)	(Nm/rad)	$(\%)$	$(\%)$
J_1	K_1	0.001	900	0.001	900.4547	0	0.05
J_2	K_2	0.002	800	0.002	800.0269	0	0.003
J_3	K_3	0.003	700	0.003	700.0029	0	0.0004
J_4	K_4	0.004	600	0.004	599.9953	0	0.0008
J_5	K_5	0.005	500	0.005	499.9836	0	0.003
J_6	K_6	0.006	400	0.006001	399.9711	0.017	0.007
J_7	K_7	0.007	300	0.007001	299.9603	0.014	0.013
J_8	K_8	0.008	200	0.008002	199.9534	0.025	0.023
J_9	K_9	0.009	100	0.008997	99.9521	0.033	0.04

Table 4.2: Original and identified parameters of the simulated system

$$Error = \left| \frac{Identified \quad values - Original \quad values}{Original \quad values} \right| * 100\% \tag{4.72}$$

The above identification algorithm is originally deduced for no damping system. It is also suitable for system with low damping. For a system with big damping this identification algorithm is not applicable. New method should be found for system with big damping.

Trajectory Analysis and Trajectory Redesign through Wavelet Synthesis

The trajectory from its time optimal plan is designed to drive the mechanical system at its full capacity at each point of time of at least one axis. However, the designed trajectory may bring violent vibrations due to the mechanical properties of the axes mechanism. There are not always vibrations along the whole trajectory, mostly only in the area where resonance frequency in one of the corresponding axis exists. Therefore, determining where the vibrations will happen and how intense the vibrations will be along the trajectory is very important for taking further steps to intentionally reduce the vibration in the trajectory design phase. To reduce the vibration level that is invoked by the resonance frequency, the trajectory has to be redesigned or modified so that there is no frequency excitation near the resonance frequency of that axis in axial setpoints.

To find out where a specified frequency in a motion profile occurs, time-frequency localization analysis is needed. The time-frequency tool has to be carefully chosen to get a quick and precise result. The objective of this analysis is to determine, for a given signal, how much energy has been located at a particular time and a given frequency. Important for the trajectory analysis of an axis is to determine how many amplitude errors this trajectory will bring to the axis due to the excitation of the axis. This amplitude error can then be checked to see if it is within the error tolerance set by the user. When the error is outside the tolerance, redesigning has to be commenced. Otherwise, it means that the designed trajectory is not the source of the possible vibration problem of that axis. Therefore the aim of this chapter is to make sure that the setpoints of all axes will not invoke resonance vibrations to the corresponding axis mechanism. To achieve this aim, three steps are necessary:

> **Step 1:** find out a suitable method/tool for the time-frequency analysis. This will
> be done in section 5.1. Section 5.1 introduces the existing possible methods of

time-frequency analysis first. Then Wavelet Transform (WT) method, to be exact, the continuous complex Morlet wavelet, is chosen as a suitable tool for the task of this work.

Step 2: find out the vibration level due to the setpoints and the resonance frequency of the mechanical system of the corresponding axis. This is to be conducted in section 5.2. The trajectory is studied with the help of Wavelet Synthesis to find out the vibration level due to the resonance frequency.

Step 3: redesign the trajectory to reduce the level of vibrations caused by the setpoints of each axis. Section 5.3 describes this process.

5.1 Time Frequency Analysis

One of the basic tools in signal frequency analysis is the Fourier Transform (FT) or its modified version Fast Fourier Transform (FFT) [14]. The frequency spectrum of the signal can be obtained from the output of FT, but with no time information. A typical output of a FT analysis of a signal is shown in Figure 5.1(b). The original time domain signal is in Figure 5.1(a). From Figure 5.1(b), it is very clear that in the signal, the following frequencies appear: 20Hz, 50Hz, and 80Hz. Although it can be known from the FT analysis that the signal has a certain frequency content with certain energy, but it is not possible to know at which time interval(s) this frequency content occurs in the signal. To obtain both frequency and time information from the signal, time-frequency analysis method is required. The most common time-frequency analysis methods are Short Time Fourier Transform (STFT) [2][9] and Wavelet Transform (WT) [12].

(a) Time domain signal   (b) Signal in Frequency domain
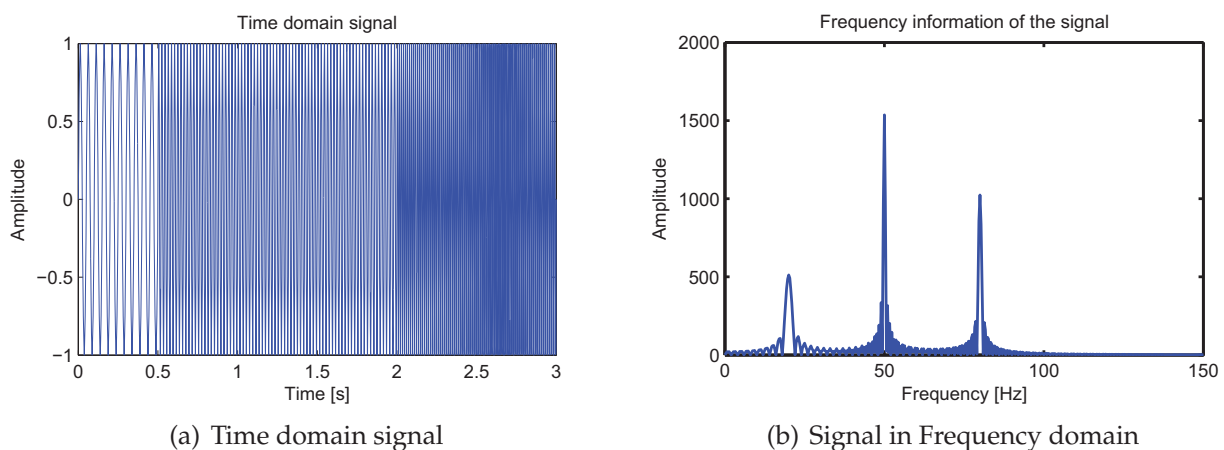
Figure 5.1: Frequency Information from Fourier Transform

5.1.1 Short Time Fourier Transform

As stated before, FT is not suitable for time-frequency analysis. But if the whole signal is separated into small enough segments, and these segments of the signal can be assumed to be stationary, then the FT method can be applied to analyze the signal within the segment. For the stationary purpose of the segment signal, a window function should be chosen. Thus as the window moves along the signal, the FT is carried out in the windowed signal to obtain the frequency information. Concurrently, the time information can be obtained from the window position. By doing so, the time axis is added to the coordinate besides the frequency axis in analyzing the signal. The process of the short time windowed Fourier Transform is known as Short Time Fourier Transform (STFT) [41]. As a result, in STFT, the frequency information is obtained from the Fourier transform of the windowed signal, and the time information is obtained from the position of the sliding window. Figure 5.2 shows the moving window along the signal process as explained above. The time-frequency information of the signal is plotted in Figure 5.3(b) for the same signal as in Figure 5.1(b). From Figure 5.3(b), it is known that there are 3 main frequencies existing in the signal. The frequency 20Hz appears between 0s and 0.5s. The frequency 50Hz appears between 0.5s and 2s, and the frequency 80Hz appears between time 2s and 3s.
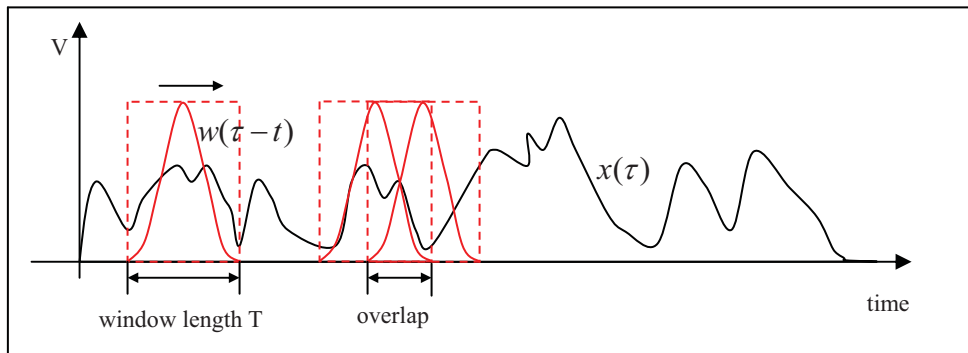
Figure 5.2: Principle of Short Time Fourier Transform

Mathematically, the STFT can be expressed by the following equation[10]:

$$STFT(t, f) = \int_{-\infty}^{\infty} x(\tau) \cdot w^*(\tau - t) \cdot e^{-j2\pi f \tau} d\tau, \tag{5.1}$$

where

$x(\tau)$: the signal itself,

$w(\tau - t)$: the window function,

$*$: conjugate complex.

(a) Time domain signal (b) Signal in time and frequency domain
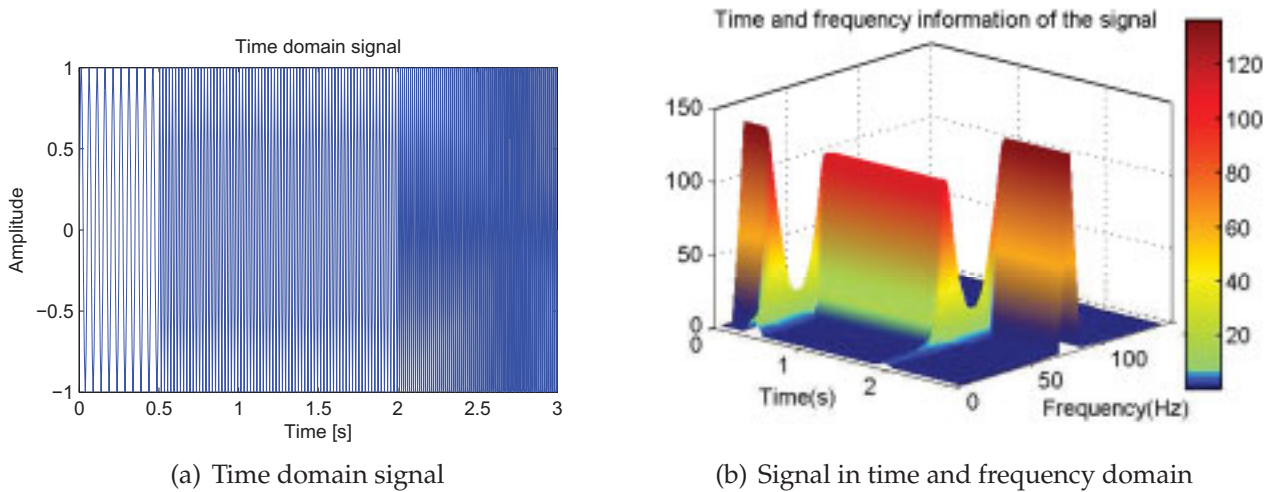
Figure 5.3: Time and frequency information from Short Time Fourier Transform

Clearly equation (5.1) depicts that the STFT of the signal is nothing but the Fouier Transform of the signal multiplied by a window function.

To perform STFT, three elements must be first determined: the type of window, the window length, and the overlap of the windows [24].

The window type $w(t)$ directly affects the trade-off between frequency resolution and side-lobe attenuation. There are some common window functions, like rectangular window, Hanning window, hamming window, blackman window and others. Different windows have different properties. The window that can best fit the needs of application has to be chosen. The rectangular window function has high side lobes, therefore it is normally not recommended. The Hanning window and Hamming window function have better frequency resolution and moderate side lobes rejection. These two windows would be suitable for frequency analysis in trajectory signal. The Blackman window function has a good side lobe attenuation and a moderately frequency resolution. It is a good general purpose window.

Besides the type of window, the window length is also an important variable for determining the time and frequency resolution performance. The smaller the window width, the more sharp the time determination is or, in other words, the better the time resolution. Wider window means more "vague" time information or, in other words, worse time resolution. The frequency resolution is also determined according to the window width. This shows how sharply the frequency can be determined. The wider the window is, the higher the frequency resolution, and vice versa. As a general property of all time-frequency analysis techniques, it is not possible to get both best time resolution and best frequency resolution. So there is always a trade-off between them, and the window width should be adjusted to

fit the requirements of the application. This trade-off is expressed mathematically by the uncertainty principle, and this principle applies for all time-frequency analysis techniques.

In addition, to increase time resolution, and to avoid missing the frequency component on the boundary of the window, the overlap of the windows should be used as shown in Figure 5.2. An overlap is defined as the percentage of the common length of two neighboring windows to the window's length. Without overlap, the time resolution is totally defined by the length of the window. By using the overlap of the window, the time resolution could be improved to some extent. Especially for low frequencies in the signal, using a big overlap can help to improve the time resolution.

The application of the STFT mentioned above has the same window length and window overlap for all the frequencies. The STFT is thus classified as a fixed or single resolution method for time-frequency analysis. In real application, the frequency resolution is not so important for high frequency contents as for low frequency contents in the signal. On the contrary, the good time resolution for high frequency is more important than it is for low frequency. Optimizing the STFT can require some effort. In many instances, a multi-resolution analysis is simpler and more practical to use and more robust.

5.1.2 Multi-resolution Short Time Fourier Transform

Multi-resolution STFT provides a better resolution solution than the STFT [77]. It changes the window length according to different frequencies. For high frequency, the window length is set to a small value, for a low frequency, the window length is set to a high value to get the full information of this frequency. This leads to good time resolution and poor frequency resolution at high frequency and good frequency resolution and poor time resolution at low frequency.

Multi-resolution STFT is still STFT, and the three elements: window type, window length, and overlap need to be determined. The window type remains the same, but the window length and overlap can be changed to reach the multi-resolution requirements. The width of the window should be short in order to get good time resolution, but should not be so short as could not detect the specified frequency. According to the Nyquist-Shannon sampling theorem , the window length of the frequency F can be specified to

$$N = (2 \sim 3) * \frac{t}{t_s} = (2 \sim 3) * \frac{F_s}{F},$$ (5.2)

where

N : the window length,

t : the period of the specified frequency F,

t_s : the sampling time of the signal,

F_s : the sampling frequency of the signal.

The time resolution is totally dependent on the window length if the window slides along the signal without any overlap. The overlap here is defined as the percentage of the window length in multi-resolution STFT. Therefore it is a relative overlap. In STFT the length of overlap is fixed.

Multi-resolution short time Fourier transform is still a pseudo time-frequency analysis. It has three shortcomings. The first shortcoming is that it is not possible to achieve a very fine time localization, as after a certain narrowing of the window, the information for the spectrum becomes meaningless and shows no relation to the spectrum of the original signal. Secondly, in STFT and multi-resolution STFT, the properties of the signal are scrambled with the properties of the window function, which is the means of chopping up the signal. Thirdly, when doing windowed FT, the specified frequency, resonance frequency in this work, may not appear in the frequency component of FT analysis. In order to get the information of the specified frequency, interpolation is needed after getting the Fourier transformation of the windowed signal. This could again cause the problem of leakage.

Although the time and frequency resolution problems are results of a universally valid physical phenomenon (Heisenberg's uncertainty principle) and exist regardless of the transform used, it is possible to analyze any signal by using a better approach called Wavelet Transform (WT).

5.1.3   Wavelet Transform

Wavelet Transform (WT) can be considered as another important tool to perform the time-frequency localization to overcome the resolution problem in STFT and multi-resolution STFT. Wavelet Transform is done in a similar way to the STFT analysis, in the sense that the signal is multiplied with a function, similar to the window function in the STFT, and the transform is computed separately for different segments of the time-domain signal. Wavelet Transform can be continuous or discrete. Continuous Wavelet Transform (CWT) is adopted for harmonic analysis because of its ability to preserve phase information [25, 72].

Mathematically, the Continuous Wavelet Transform(CWT) can be expressed by [40]:

$$CWT(a,b) = \int_{-\infty}^{\infty} x(t)\psi_{a,b}^{*}(t)dt, \tag{5.3a}$$

$$\psi_{a,b}(t) = \frac{1}{\sqrt{a}}\psi\left(\frac{t-b}{a}\right), \tag{5.3b}$$

where

- $*$: conjugate complex ,
- a : scale factor,
- b : translation factor,
- $x(t)$: signal to be analyzed,
- $\psi_{a,b}$: mother wavelet.

The variables a and b, scale (related to frequency) and translation (related to time), are the new dimensions after the wavelet transform. The set of wavelets are generated from a single basic wavelet, the so-called mother wavelet, by scaling and translation as shown in equation (5.3). The factor $\frac{1}{\sqrt{a}}$ in equation (5.3) is for energy normalization across different scales.

Equation (5.3) shows how a function $x(t)$ is decomposed into a set of basis functions $\psi_{a,b}(t)$, named wavelets. A wavelet is a waveform of effectively limited duration that has an average value of zero, while the sine waves, which are the basis of Fourier analysis, do not have limited duration – they extend from minus to plus infinity. And where sinusoids are smooth and predictable, wavelets tend to be irregular and asymmetric. In the time domain the wavelet has two main features [70]:

- it has a small concentrated burst of finite energy; and

- it exhibits some oscillation in time.

The first feature makes the wavelet "little" in the sense that it is well localized in time, whereas the second feature makes it "wavy" and hence a wavelet. As the wavelet has some oscillating nature, then the result of convolving it with a signal will be high if both have the same frequency and are in phase, and low value if:

- both have the same frequency and are out of phase, or

- they have different frequencies and are in/out of phase.

To compensate the low value when the both signals have the same frequency and are out of phase, a complex wavelet can be applied. When the absolute value of the calculation of the Wavelet Transform is used as the result for the WT, then the problem of the low values in the situation of same frequency but out of phase is overcome.

As the wavelet and the signal become similar in terms of frequency, the amplitude value of the WT becomes higher. Therefore the WT can capture an image of the frequency content that is near to the center frequency of the wavelet. The wavelet is translated along the time axis to scan the whole signal, and the value of the WT is plotted instantly at each time. The WT checks the existence of frequency content that is close to what is known as "wavelet center frequency". To check other ranges of frequencies, the center frequency of the wavelet should be changed. This is done by stretching (or shrinking) the wavelet by a scaling factor called "scale". By such scaling, another wavelet is obtained, similar to the mother wavelet but with another center frequency, which is called, in this case, scaled frequency corresponding to the scale used. The more stretched the wavelet is, the smaller its scaled frequency.

The relation between the scale and the scaled frequency is given as:

$$F_a = \frac{F_c}{a \cdot t_s},$$

(5.4)

where

F_a : scaled frequency (in Hz, the frequency to be tested) ,

F_c : wavelet center frequency (for the mother wavelet, dimensionless),

t_s : sampling period (in seconds).

Note that the scale factor a is nondimensional and is the ratio of the size of the scaled wavelet to the size of the mother wavelet.

In other words, the Wavelet Transform is using the scaled wavelet moving along the signal to see the similarity between the wavelet and the signal. The similarity is in the sense of similar frequency content. The calculated WT coefficients refer to the closeness of the signal to the wavelet at the current scale. The scale of the wavelet changes continuously, and the scaled wavelet moves along the signal continuously too. Thus better resolution results can be obtained from the WT than from multi-resolution STFT. Of course, the time-frequency resolution of the WT has to obey the uncertainty theorem too.

It worth noting that as the scaled frequency increases, the wavelet becomes more shrunken and this means better time resolution. This is a main difference between STFT and WT. In STFT, the time resolution is constant and depends on the width of the window. In WT,

however, the time resolution adapts to frequencies. This property is very important as will be shown later in the section about generalization principles.

Time-Frequency window

As mentioned above, the relation between the time resolution and the frequency resolution is governed by the uncertainty principle. The combination between the time window and the frequency window is known as the time-frequency window. By plotting the time window width and the frequency window width at its corresponding scaled frequency on the time-frequency plane, a rectangle is obtained. The area of this rectangle is always the same, governed by Heisenberg box. The Heisenberg box for any frequency at any time is limited by

$$\delta_\omega \delta_t \geq \frac{1}{2},$$ (5.5)

where

δ_ω : the frequency resolution,

δ_t : the time resolution.

The mathematical expression of the time-frequency window is as follows [40]

$$\left[b + a \cdot t^* - a \cdot \frac{\Delta_t}{2}, b + a \cdot t^* + a \cdot \frac{\Delta_t}{2} \right] \times \left[\frac{\omega^*}{a} - \frac{\Delta_\omega}{2a}, \frac{\omega^*}{a} - \frac{\Delta_\omega}{2a} \right],$$ (5.6)

where

t^* and ω^* : the center time and center frequency for the mother wavelet,

Δ_t and Δ_ω : the time and frequency resolution for the mother wavelet.

It is worth noting, that the area of the rectangular time-frequency windows is always given by $\Delta_t \Delta_\omega$ for any frequency contents and any time location; and thus it is independent of the parameters a and b, and it is determined only by the wavelet used. The frequency resolution of a scaled frequency content in a signal is given by the expression $\delta_\omega = \frac{\Delta_\omega}{a}$; the time resolution is given by the expression $\delta_t = \Delta_t a$.

The relation between time and frequency windows can be shown in Figure 5.4. This is the graphical representation of the trade-off between time resolution and frequency resolution. It also shows how the widths of the frequency and the time windows change with the scaled frequency. The figure shows the rectangular time-frequency window at different scales (or

pseudo-frequencies). It can be seen from the figure that at the higher scaled frequency (corresponding to a_2 in the figure) the width of the frequency window is big. This means bad frequency resolution. On the other hand the width of the time window is small, which means good time resolution. The opposite is true for low frequencies. It can also be seen from the figure that the time shift, b, has no effect on the dimensions of the time-frequency window. It can also be seen that the area of the rectangle is always the same.
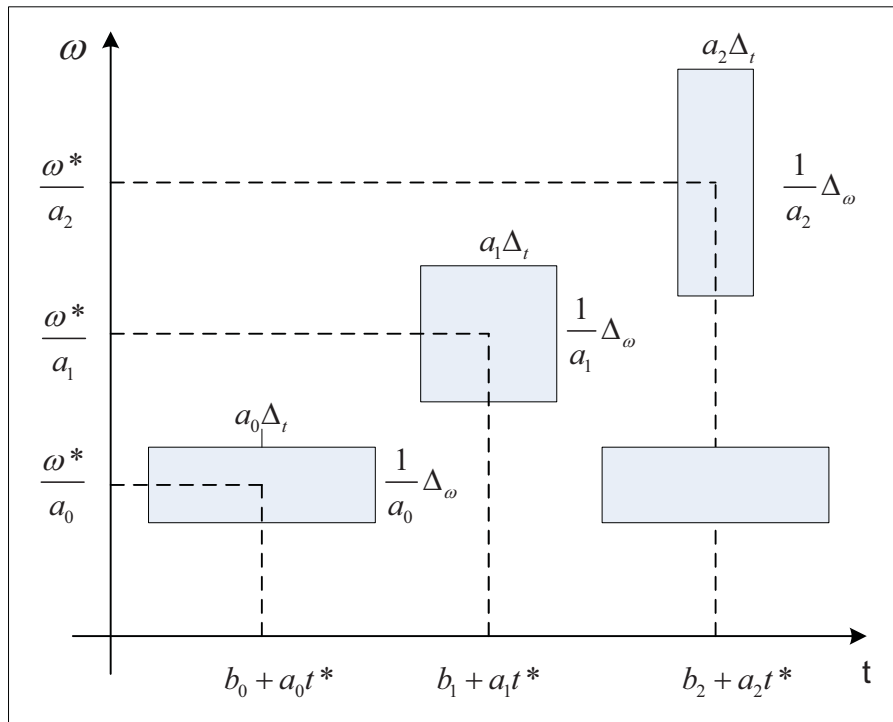
Figure 5.4: Time-frequency windows in wavelet transform [40]

The Complex Morlet Wavelet

What remains an opened issue is the choice of the mother wavelet function. Many wavelet families exist in the area of wavelet analysis, such as Haar wavelet, Mexican-Hat wavelet, Morlet wavelet and others. In choosing the wavelet function, there are several factors which should be considered [71].

1. Orthogonal or nonorthogonal. Orthogonal wavelet analysis is useful for signal processing as it gives the most compact representation of the signal. Unfortunately it is not suitable for time series analysis, as an aperiodic shift in the time series produces a different wavelet spectrum. Conversely, a nonorthogonal analysis is useful for time series analysis, where smooth, continuous variations in wavelet amplitude are expected.

2. Complex or real. A complex wavelet function will return information about both amplitude and phase and is better adapted for capturing oscillatory behavior. Especially

when the wavelet with the signal both have a similar frequency but are out of phase, the complex wavelet function is useful. A real wavelet function returns only a single component and can be used to isolate peaks or discontinuities.

3. Shape. The wavelet function should reflect the type of features present in the time series. For time series with sharp jumps or steps, one would choose a boxcar-like function such as Haar, while for smoothly varying time series one would choose a smooth function such as Morlet.

Before the wavelet function is chosen, the aim of the time-frequency analysis will be stressed here. The aim of the time-frequency analysis in this work is to find out specified frequencies along the time of the trajectory.

- The trajectory data to be analysed are time series signals. Therefore the chosen wavelet should have the nonorthognal property.

- The oscillatory behavor in the trajectory is to be detected. The chosen wavelet should then be complex.

- The trajecotry is jerk-limited, the time series of the velocity trajectory is therefore smoothly varying with time series. The chosen wavelet should have smooth shape.

Complex Morlet wavelet is nonorthognal, complex and have a damped cosine shape. Therefore the complex Morlet wavelet is choosen for the analysis of the trajectory data in this work as it fulfills the above three factors. More over, the Morlet wavelet is characterized by the smallest achievable time-frequency window [18]. A complex Morlet wavelet can easily be visualized as a wave because of it's oscillatory nature and has a neat closed form expression. The mathematical function for a complex Morlet mother wavelet in the time domain is as follows [70]

$$w(t) = \frac{1}{\sqrt{\pi \cdot F_b}} \cdot e^{j2\pi F_c t - (\frac{t^2}{F_b})}, \tag{5.7}$$

where

F_b : the dimensionless bandwidth indication,

F_c : the wavelet dimensionless center frequency ,

t : the nondimensional time parameter.

The bandwidth indication F_b can be referred to as the spectral equivalent of damping.

Accordingly, the mathematical expression of a Morlet mother wavelet in frequency domain is,

$$w(f) = e^{-\pi^2 F_b (f - F_c)^2}, \tag{5.8}$$

with the same meaning of F_b and F_c as in equation (5.7). f is the nondimensional frequency parameter.

In fact, there are other ways to express the Morlet wavelet. These are basically all the same, but they differ in the names of the parameters. The above mentioned form, which is adopted as the meaning of the parameters, is easy to understand and to control. For example, by increasing the bandwidth indication F_b, the frequency resolution is increased and the time resolution is decreased.

Figure 5.5(a) shows the plot of a complex Morlet mother wavelet with a nondimensional center frequency of 1 and a nondimensional bandwidth indication of 1. The Morlet wavelet looks like a sine wave but has a concentrated burst around $t = 0$. The wavelet fades away quickly as time increases. For higher bandwidths the wavelet fades away more slowly than the wavelet in the figure. This implies better frequency resolution, and worse time resolution. The opposite is true for lower bandwidths. The complex Morlet wavelet, as its name implies, consists of a real part and an imaginary part. In the figure the real part is in blue and the imaginary part is in red. The imaginary part is phase-shifted from the real part by $\pi/2$. The corresponding base wave in frequency domain is presented in Figure 5.5(b).
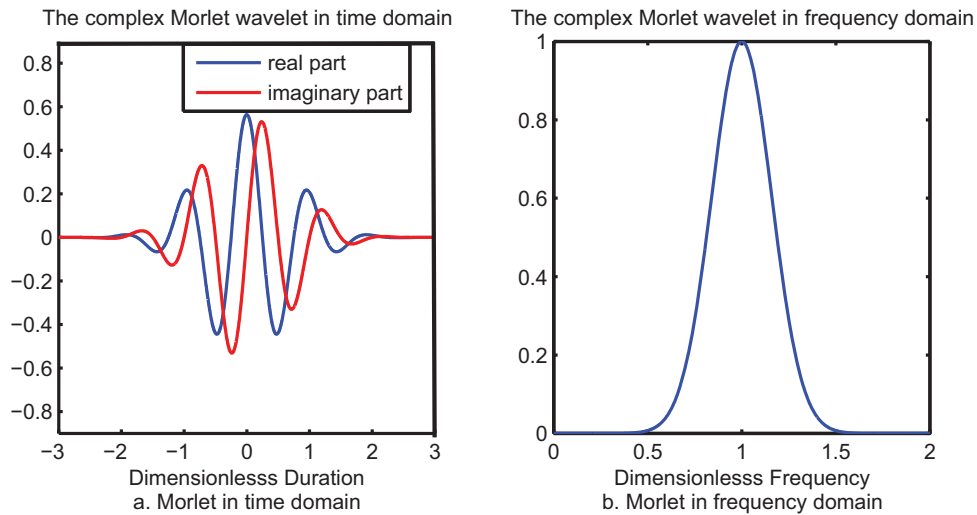

Figure 5.5: Complex Morlet wavelet

The frequency resolution and time resolution mentioned for the complex Morlet mother wavelet are:

$$\Delta_\omega = \frac{1}{\sqrt{F_b}}, \tag{5.9}$$

$$\Delta_t = \frac{\sqrt{F_b}}{2}. \tag{5.10}$$

For a dilated complex Morlet wavelet, the corresponding frequency and time resolution are,

$$\delta_\omega = \frac{1}{a\sqrt{F_b}}, \tag{5.11}$$

$$\delta_t = \frac{a\sqrt{F_b}}{2}. \tag{5.12}$$

5.1.4 Comparison

As discussed before, the STFT represents a less inaccurate and less efficient method of time-frequency localization, as it imposes a window on to the analysis. In addition, several window lengths must usually be analyzed to determine the most appropriate choice. Multi-resolution STFT solves the resolution problem of STFT by changing the window length automatically according to the different frequencies. Wavelet transform is such a solution that would solve the time-frequency problem better than STFT in most cases. Like multi-resolution STFT, WT is designed to give good time resolution at high frequencies and good frequency resolution at low frequencies. However, WT is different from multi-resolution STFT in three aspects:

- time in WT is the real time localization, while in STFT, it is localization of the position of window. Therefore, the time information from WT is more accurate than from STFT;

- no interpolation for a specified frequency is needed in WT, as each frequency component can be found by a corresponding scale. In this sense, the frequency information from the WT is more accurate than from the STFT which may have to use interpolation for the specified frequency;

- no determination of the optimal window length and overlap of windows is needed.

Wavelet Transform is therefore determined for a time-frequency analysis of a real velocity signal due to its good performance of time and frequency resolution. Further, Complex Morlet Wavelet is the most suitable wavelet for this work, due to its phase information and the wavy shape of the wavelet. Thus, it is possible to find out the time location where the resonance frequency of the system exists. This time period is dangerous because resonance vibration would happen.

95

5.2 Predicting Vibraton Level Along Time

Two definitions need to be clarified first:

- **amplitude error**. Amplitude error in this work is defined as the amplitude increase or reduction of the response amplitude compared with command amplitude at the specified frequency along time. No phase information is included in the amplitude error.

- **following error**. Following error is defined as the difference between the response signal and command signal. Following error includes the amplitude error and phase information. However, it is difficult to separate the amplitude error and phase information from the following error.

When the command signal contains frequencies that are equal or close to the resonance frequency of the machine axis, the resonance vibration problem may occur in that machine axis. By applying Wavelet Transform to analyze the trajectory command, it is possible to find out when this resonance vibration could happen and how big it is. However, whether the resonance vibration will happen, or how large the vibration will be, remains unknown. If the command signal is a pure sinusoidal signal, the output amplitude can easily be calculated and predicted by using Fourier Transform. For an arbitrary trajectory which is not sinusoidal and not periodic, the task of output response estimation cannot be performed by Fourier Transform. Markert [39] introduced an analytical approach to solve the problem of a system output estimation for a second order mechanical system during the ramp up or ramp down. The ramping process is a very special case, and although it seems to be an easy case, the analytical approach of the system output is highly sophisticated.

Convolving the trajectory signal with the impulse response of the mechanical system is another approach. The response of the mechanical system to the trajectory signal can be calculated, and the following error can be obtained by getting the difference between the response signal and the input signal. In fact, however, the following error is not of interest, the amplitude error is more important, as the resonance vibration level can be read directly from the amplitude error. This cannot be done by impulse convolution. Moreover, the impulse response of a poorly damped mechanical system takes very long time to settle down. Thus, it leads to a calculation time and poor time resolution in the response output for poorly damped system. Hence, detecting and estimating the possible vibration level caused by the resonance frequency in an arbitrary command signal poses a problem. Wavelet synthesis, as

will be presented in this section, provides a quick and accurate way to calculate amplitude error, which is required in the next step of trajectory redesign.

In the following explanation, it is important to know that impulse convolution calculates following error, and the wavelet methods calculates amplitude error.

5.2.1 Second order system response

This work deals with systems whose response can be approximated by the response of a second order system at least for some bandwidth. In machine tools it is nearly impossible to find a pure second order system, but many mass-spring-damper systems can be reasonably approximated by a second order system.

The transfer function that represents a second order system can take many forms depending on the setup of the physical components of the system, and on the input and output considered. The transfer function of the second order system considered here is expressed by the following equation:

$$G(s) = \frac{\omega_0^2}{s^2 + 2\xi\omega_0 s + \omega_0^2}, \tag{5.13}$$

where

ω_0 : characteristic frequency of the system,

ξ: damping ratio.

The amplitude of the frequency response of such system is given as the modulus of $G(j\omega)$, which is throughout this work is simply named as G. This represents the steady state response for sinusoidal input of frequency ω. Substituting for $\frac{\omega}{\omega_0}$ by frequency ratio r, the value of G in this case is calculated from the following relation:

$$G = \frac{1}{\sqrt{(1 - r^2)^2 + (2\xi r)^2}}. \tag{5.14}$$

Although only this frequency response function is considered, the principles adopted in this work are also applicable to other types of second order systems.

It should be noted here that the only variables that determine the amplitude of response are the damping ratio ξ, and the frequency ratio r. This property is very important, because it means that any two systems having the same damping ratio will have the same G if the frequency ratio r is considered without decoupling ω and ω_0, even if the characteristic frequencies ω_0 of the two systems are different. By plotting G versus ω for two different

systems with same damping ratio and different natural frequencies such that $\omega_{02} > \omega_{01}$, the frequency response curve of the second system will be exactly similar to that of the first system, but stretched along the ω axis by the ratio $\frac{\omega_{02}}{\omega_{01}}$.

The G curve (which is also known as the Bode magnitude plot) for a system with different damping ratio is given in the following Figure 5.6. Usually in a Bode plot the amplitude is plotted in decibels and the frequency is plotted on logarithmic scale. Here both are plotted in absolute scale, because this will help in illustrating the next steps.
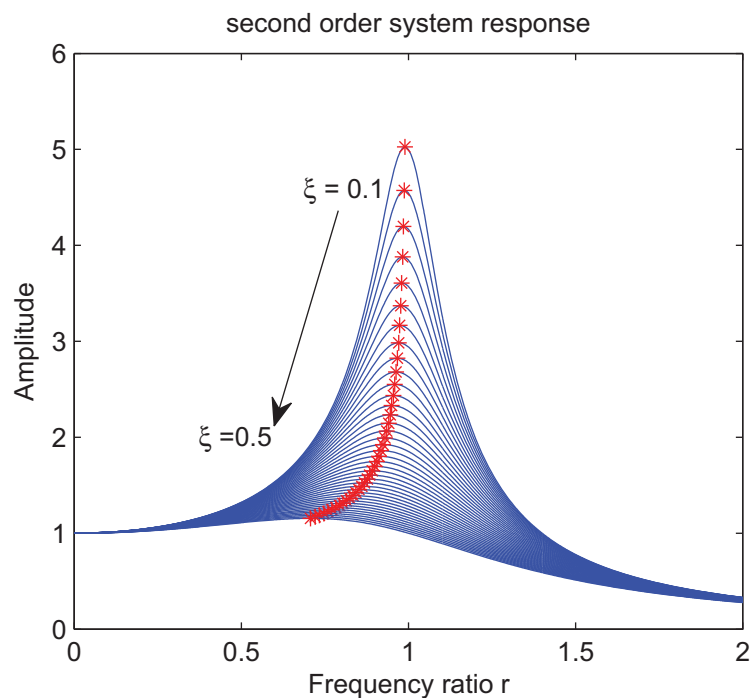

Figure 5.6: Frequency response of second order system with different damping ratio

From Figure 5.6, it is known that if the damping ratio and characteristic frequency of the system are known, the response amplitude of the system to a specified frequency can also be obtained. Resonance frequency is the frequency at which a system tends to oscillate at maximum amplitude. For an undamped system, resonance frequency is equal to the characteristic frequency and natural frequency of the system. For a damped system, the resonance frequency is not equal to the characteristic frequency and natural frequency system, especially when the damping ratio is big. Figure 5.6 also tells the fact that with a bigger damping ratio, the difference between the resonance frequency and the characteristic frequency of the system is greater.

The maximum G at resonance frequency and the corresponding frequency ratio r for a certain damping ratio ζ can be found out by setting $\frac{dG}{dr} = 0$,

$$\frac{dG}{dr} = \frac{2r(1 - 2\xi^2 - r^2)}{((1 - r^2)^2 + (2r\xi)^2)^{\frac{3}{2}}} = 0. \tag{5.15}$$

So when $r = 0$ or $r = \sqrt{1 - 2\xi^2}$, G can have the maximum value. As $r > 0$, therefore, when

$$r = \sqrt{1 - 2\xi^2}, \tag{5.16}$$

G has the maximum value of

$$G_{max} = \frac{1}{2\xi\sqrt{1 - \xi^2}}. \tag{5.17}$$

The equation G expresses amplitude amplification. The increment of the amplitude can be expressed by the following equation (5.18), assuming an input or command signal with an amplitude of 1:

$$E = G - 1. \tag{5.18}$$

5.2.2 Amplitude error calculation of the response of a second-order system by Wavelet Synthesis

As described in section 5.1, Wavelet Transform, to be exact, the complex Morlet wavelet, can be used to detect the resonance frequency in the command signal. However, the coefficients that are calculated from Wavelet Transform only tells the similarity between the resonance frequency and the central frequency of the wavelet. To evaluate the vibration level this resonance frequency creates, the coefficients from the Wavelet Transform have to be related to the amplitude response of the mechanical system, as will be shown in the following. Besides, one wavelet curve cannot totally reconstruct the system response in frequency domain, more wavelet curves are needed. In general, there are three steps for doing so [18],

> *Step 1:* Determination of the time-frequency components of the given input signal (analysis).
>
> *Step 2:* Modification of the coefficients (extraction),
>
> *Step 3:* Construction of the output signal (synthesis).

The first step is the general time-frequency analysis. As in this work, the natural frequency of the mechanical system is already known and is to be located in the signal, therefore, the time-frequency analysis for a wide range of frequencies is not needed. The frequency

location is mainly focused on the natural frequency and frequencies lower than it. This process is combined in this work in step 3. However, when only the time and frequency information in the signal are required, step 1 is needed, and the further two steps can be neglected.

The second step is to extract or modify the wavelet coefficient to make the amplitude of wavelet analysis represent the system response. This is an important step in getting meaningful results.

The third step is a process of synthesis, which is to construct the output of the system response using two or more wavelet curves.

Step two and step three, which include step one for a signal frequency time location, are described in the following section 5.2.2 and section 5.2.2 separately.

Fitting system response curve and complex Morlet wavelet in frequency domain curve

The frequency domain complex Morlet Wavelet in equation (5.8) is written here again for convenience:

$$w(f) = e^{-\pi^2 F_b (f - F_c)^2}. \tag{5.19}$$

The Morlet Wavelet in frequency domain in equation (5.19) can be explained as following: when frequency f approaches the central frequency F_c, the wave reaches its highest point of value 1. This corresponds to the maximal frequency response of the system when the frequency ratio is approaching $\sqrt{1 - 2\xi^2}$. The width of the wave in frequency domain depends on the parameter F_b. The bigger the F_b is, the narrower the wave is. This corresponds to the damping ratio ξ in the system frequency response. The smaller the damping ratio is, the sharper the response of the system is. Therefore, the Wavelet in frequency domain resembles the frequency response of the mechanical system in the following way:

- central frequency F_c ↔ normalized resonance frequency $\sqrt{1 - 2\xi^2}$;

- frequency variable f ↔ frequency ratio r;

- band width F_b ↔ damping ratio ξ;

- amplitude of wavelet in frequency domain ↔ amplitude of frequency response.

Accordingly, to fit these two curves in the wavelet curve, the following parameters have to be determined:

- the center frequency F_c in the mother wavelet, corresponding to the generalized resonance frequency of the mechanical system;

- scaling factor a, corresponding to the natural frequency of the mechanical system;

- the bandwidth indication F_b in the mother wavelet, corresponding to the bandwidth or shape of the second order system.

- the maximum amplitude of the wavelet curve, corresponding to the maximum response of the mechanical system;

Determination of F_c

In the frequency domain of the wavelet, as in equation (5.19), F_c is where the maximum amplitude occurs. In the response of the second order system, the maximum amplitude happens when $r = \sqrt{1 - 2\xi^2}$, as in equation (5.16). Therefore,

$$F_c = \sqrt{1 - 2\xi^2}. \tag{5.20}$$

Determination of scaling factor a

The scaling factor corresponding to the frequency to be tested (the system's characteristic frequency) can be deduced from equation (5.4):

$$a = \frac{F_c F_s}{F_a}, \tag{5.21}$$

with

F_c: central frequency of mother wavelet,
F_s: sampling frequency of signal,
$F_a = F_0$, and F_0 is the characteristic frequency of the mechanical system.

Determination of F_b

The bandwidth of the scaled wavelet must be similar to the bandwidth of the second order system. Here the bandwidth is defined as the frequency interval around the central frequency in wavelet or resonance frequency in second order system where the energy has faded to one half of the maximal value; this corresponds to a variation in the relative amplitude of a value of $\frac{1}{\sqrt{2}}$ and of the level by $-3dB$, always with respect to the maximal value at the point of central frequency or resonance frequency.

The bandwidth of the wavelet curve can be adjusted by adjusting F_b. Let the mother wavelet curve and the generalized second order system have the same bandwidth at the relative amplitude of a value of $\frac{1}{\sqrt{2}}$ respectively

$$w(f) = \frac{\sqrt{2}}{2}. \tag{5.22}$$

Combining equation (5.19) and equation (5.22) gives

$$f = F_c \pm \frac{1}{\pi\sqrt{F_b}}\sqrt{|\, ln(\frac{\sqrt{2}}{2})\,|}. \tag{5.23}$$

Based on equation (5.23), the bandwidth of the scaled wavelet is,

$$WT_{Bandwidth} = \frac{2}{\pi\sqrt{F_b}}\sqrt{|\, ln(\frac{\sqrt{2}}{2})\,|}. \tag{5.24}$$

The bandwidth of the generalized second order system can be determined from the following equation:

$$\frac{1}{(1-r^2)^2 + (2\xi r)^2} = \frac{1}{2\xi\sqrt{1-\xi^2}}\frac{\sqrt{2}}{2}. \tag{5.25}$$

Solving the above equation, the bandwidth of the second order system can be approximated to be

$$SOS_{Bandwidth} \approx \frac{\sqrt{\xi\sqrt{1-\xi^2}}}{2\sqrt{2}}. \tag{5.26}$$

Making the bandwidth in wavelet and the bandwidth in second order system to be equal gives

$$F_b = \frac{16\,|\, ln(\sqrt{2})\,|}{\xi\pi^2\sqrt{1-\xi^2}}. \tag{5.27}$$

From the above F_b, it is found out that

$$F_b \approx \frac{1}{2\xi} \tag{5.28}$$

can approximate the F_b in equation (5.27).

The error from the approximation in equation (5.26) and (5.28) can be plotted out in the following Figure 5.7.

The Figure 5.7 explains the width difference between the wavelet in frequency domain and the system response at the -3dB, when $F_b = \frac{1}{2\xi}$ is used. For example, when the damping
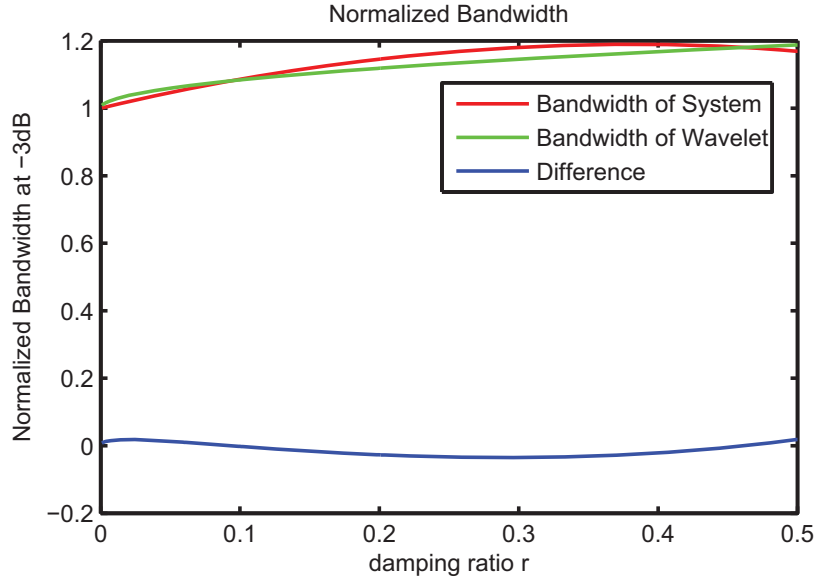
Figure 5.7: Bandwidth difference between system and Wavelet

ratio is 0.2, the width of the wavelet is about 0.0269 narrower than the system frequency response.

Fitting the maximum amplitude

There are two steps in fitting the maximum amplitude of the scaled wavelet and the second order system. First of all, the maximum amplitude of the wavelet base curve and the frequency response curve of the second order system need to fit. This can be assured simply by multiplying the maximum amplitude of the system frequency response with the equation of the wavelet in frequency domain, as the maximum amplitude of wavelet in frequency domain is 1. The maximum amplitude of the system frequency response can be calculated by equation (5.18) and equation (5.17) as in the following equation:

$$E_{max} = G_{max} - 1 = \frac{1}{2\xi\sqrt{1-\xi^2}} - 1. \tag{5.29}$$

The mother wavelet in frequency domain as in equation (5.19) should therefore be modified to:

$$w(f) = E_{max} * w(f) = (\frac{1}{2\xi\sqrt{1-\xi^2}} - 1) * e^{-\pi^2 F_b(f-F_c)^2}. \tag{5.30}$$

Secondly, the energy normalization factor $\frac{1}{\sqrt{a}}$ added to the scaled wavelet as in equation (5.3) for widely accepted wavelet function, has to be compensated. Here the factor $\sqrt{a}$ is applied to cancel this normalization effect. Therefore, the following factor has to be multiplied to the scaled wavelet in order to get rid of the normalization effect:

$$\sqrt{a} = \sqrt{\frac{F_s\sqrt{1-2\xi^2}}{F_0}}. \tag{5.31}$$

Thus, the scale factor to be multiplied by the detecting frequency is

$$c = (\frac{1}{2\xi\sqrt{1-\xi^2}} - 1)(\sqrt{\frac{F_s\sqrt{1-2\xi^2}}{F_0}}). \tag{5.32}$$

Finally, the wavelet in frequency domain is

$$w(f) = c * e^{-F_b\pi^2(f-F_c)^2}, \tag{5.33}$$

with $c = (\frac{1}{2\xi\sqrt{1-\xi^2}} - 1)(\sqrt{\frac{F_s\sqrt{1-2\xi^2}}{F_0}})$, $F_b = \frac{1}{2\xi}$ and $F_c = \sqrt{1-2\xi^2}$.

Synthesis

The wavelet in equation (5.33) can only stand for the area that is near the resonance frequency. To make the wavelet better interpret the frequency response of the system, more wavelets can be applied by also computing F_c, F_b and the E_{max} factor, as in the following equation(5.34):

$$E(t) = \sum_i^N CWT(signal(t), F_{ni}, wavelet_i) * c_i \tag{5.34}$$

N is the number of wavelets needed to fit the curve. Normally, $N \leq 4$.

This synthesis process can be visualized from Figure 5.8. In Figure 5.8(a), the wavelet curve (red) is compared with the curve of the system response (blue). It is seen that the wavelet curve and the system response curve are similar in the area of the resonance frequency. But they have differences when the frequency ratio is small. Therefore, a second wavelet curve is added in the low frequency ratio range. The second wavelet curve is shown in (b) in green. The synthesis curve of the first wavelet and second wavelet is plotted in (c) in red. There are still some differences between the synthesis curve and the system response curve. Therefore, a third wavelet curve, as shown in (d) in green, is calculated. Now, the finally synthesis wavelet curve to represent the system response is presented in (e) in red. Of course there are still small differences between the synthesis wavelet curve and system response curve, but they are not important. The reasons are: first, they are located in a very low frequency ratio range; and second, they contribute a very small value in amplitude detection, especially in a low damping system.
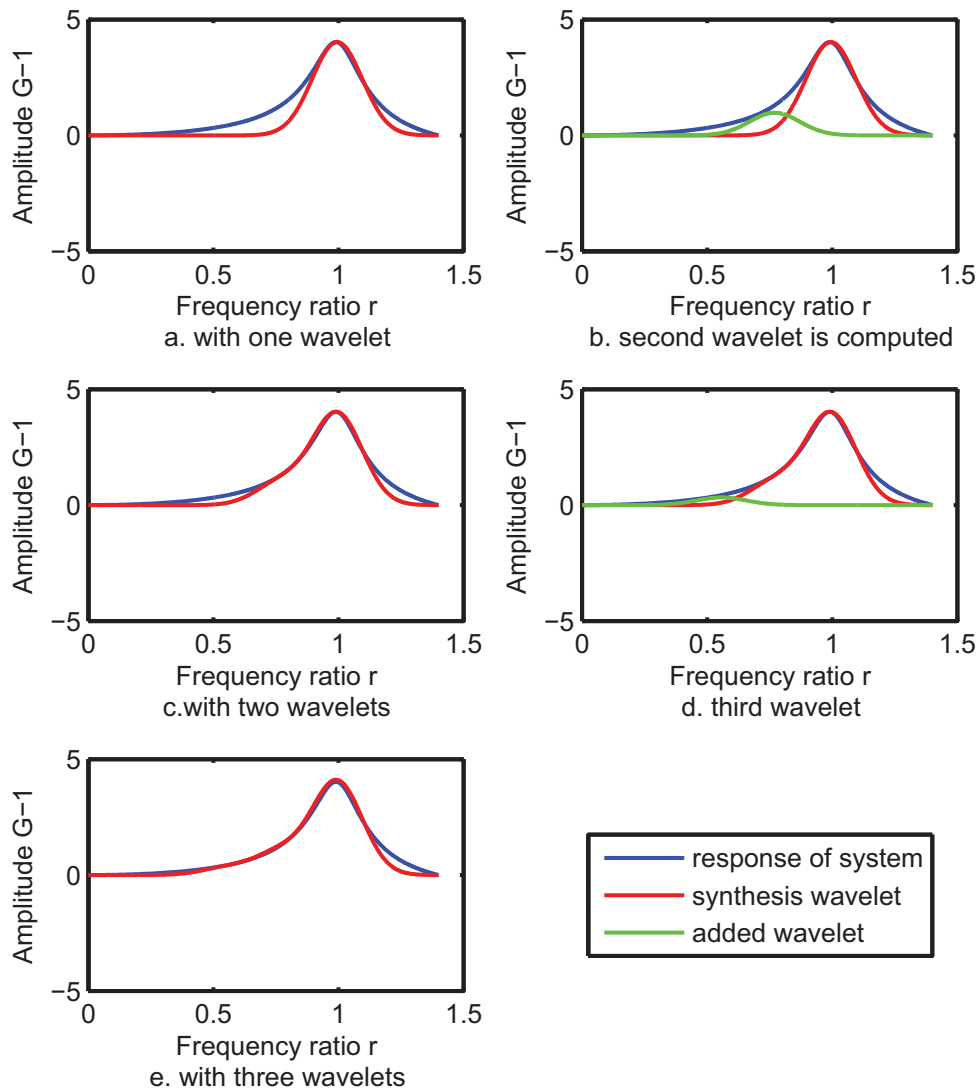
Figure 5.8: Influence of more wavelets on the frequency response

Equation (5.34) yields the estimated error as a function of time. The results of the estimated errors can be further used to identify the time intervals in which the error exceeds a specified acceptable limit so that some corrective action can be taken.

Two examples of detecting response by impulse convolution and synthesis wavelets

The second order system with a damping ratio ξ of 0.1 and a natural frequency of $\omega_0 = 50rad/s$ is taken as the closed velocity loop in this section. Two test signals are given to prove the amplitude error calculation methods. The two test signals are:

- chirp signal,

- a real velocity profile from time-optimal trajectory planning.

The wavelet synthesis method is more practical than the impulse convolution method in detecting the response in the following aspects:

- The impulse convolution method provides following errors of the response, while the wavelet synthesis method generates an approximation of the amplitude error in envelope. Wavelet synthesis is more suitable in application, as it is more easy to tell from the wavelet synthesis methods how much amplitude error from vibration will be caused by the resonance frequency.

- Impulse convolution takes a much longer time to get the response, especially when the mechanical system is poorly damped or the input signal is long. The time for impulse convolution increases exponentially to the length of the input signal. The time for wavelet synthesis increases only linearly.

The comparison of the two methods is confirmed by the two signals in the following simulation.

Chirp signal

The chirp signal has an amplitude of 1, with an initial frequency of $0.016rad/s$ and final frequency of $54rad/s$ in 20 seconds. The sampling frequency of the chirp signal is set to $F_s = 2000Hz$. The frequency $50rad/s$ is the characteristic frequency of the mechanical system.

Figure 5.9 presents the initial chirp velocity in the blue curve and the response velocity of the second order system in the red curve. The response velocity is obtained by convolving the input signal with the impulse response of the mechanical system. It is seen that the response velocity has a peak when the chirp frequency passes through the resonance frequency of the second order system. It is worth noting that the maximum amplitude of the response in this figure can be read out to be 5. Then the maximum amplitude error, without considering the phase difference, should be 4. But the following error, due to the phase difference between the response signal and command signal, is bigger than 4, as will be shown next.

The following error in the velocity signal can be calculated by the difference between the response signal and input signal. They are plotted in Figure 5.10 in red curves for the impulse convolution method. Note that the maximum following error here is 5.17. This effect is caused by the phase difference between the response and the input signal.
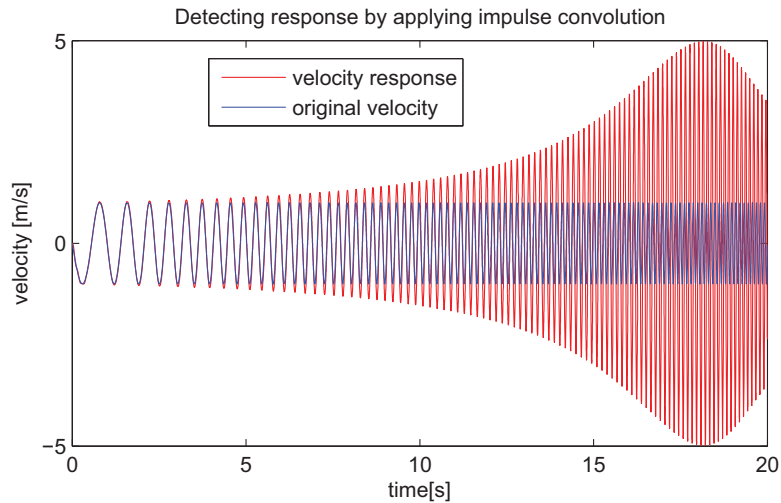
Figure 5.9: System velocity response to chirp signal

Amplitude error is then calculated by the synthesis wavelets. The result is plotted in the black curve in Figure 5.10. Normally the calculated amplitude error is bigger than 0, but for the convenience of comparing, it is plotted as envelope. Note that the maximum amplitude error is 4. The maximum amplitude error appears a littler earlier than the maximum following error, as the amplitude error through wavelet synthesis tells exact the time position of the resonance frequency, the following error reveals the response which includes the phase information.
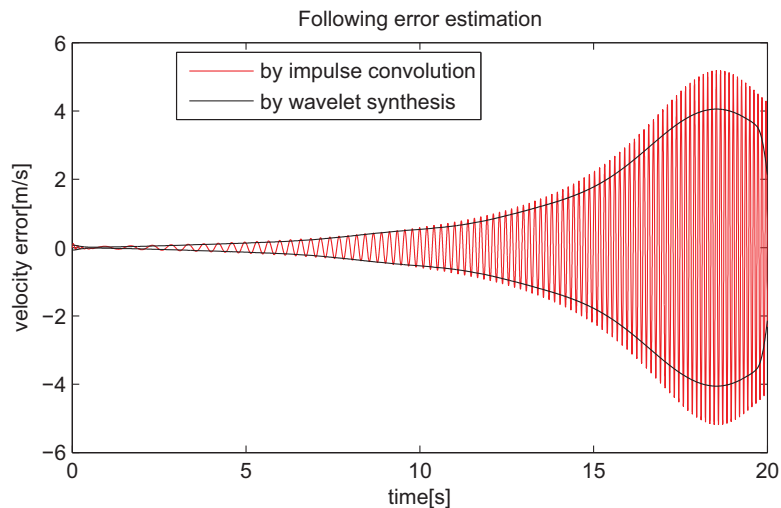

Figure 5.10: Following error by impulse convolution and amplitude error by wavelet synthesis

From the above simulation and calculation, it is known that the synthesis wavelets provide good time location of the resonance frequency of the system, and give a good estimation of the amplitude error of response. This is actually what is needed for the next step.

It is also worth noting that in this case the calculation time of the impulse convolution is twice as long as the calculation time of the synthesis wavelets. If the test signal is longer,

the calculation time of the impulse convolution method increases exponentially, while the calculation time of the wavelet synthesis increases linearly.

A real velocity profile from time-optimal trajectory planning

The velocity signal in this example is obtained from a time-optimal trajectory plan, and is plotted in the blue curve in Figure 5.11. The calculated response by the impulse convolution is shown in Figure 5.11 with a red curve.
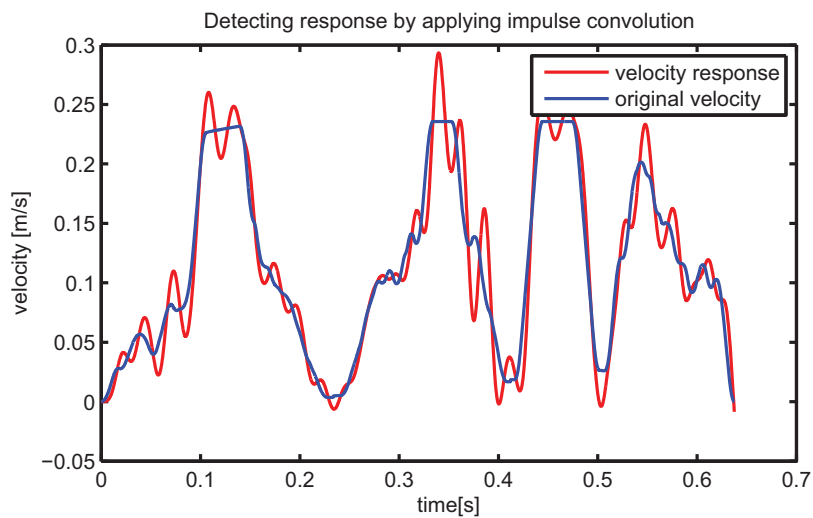

Figure 5.11: System velocity response to real velocity signal

The corresponding following error of the response of the real velocity signal is calculated by the difference between the response signal and input signal and plotted in Figure 5.12 with a red curve.

Synthesis wavelets are now applied to generate the amplitude error envelope. The result is plotted with the black curve in the same figure.

In Figure 5.12 the same two effects as in Figure 5.11 can be observed. First, the following error amplitude calculated by impulse convolution is bigger than the amplitude error envelope by wavelet synthesis. Second, the maximum amplitude error by wavelet synthesis appears earlier than the maximum following error by impulse convolution. The reason for this two effects is the same as in chirp signal: in impulse convolution, there is a phase difference between the response and original signal. Hence, the following error amplitude by the impulse convolution method illustrates not exactly the amplitude enlargement of the system and also not exactly the moment when the resonance frequency appears in the signal.
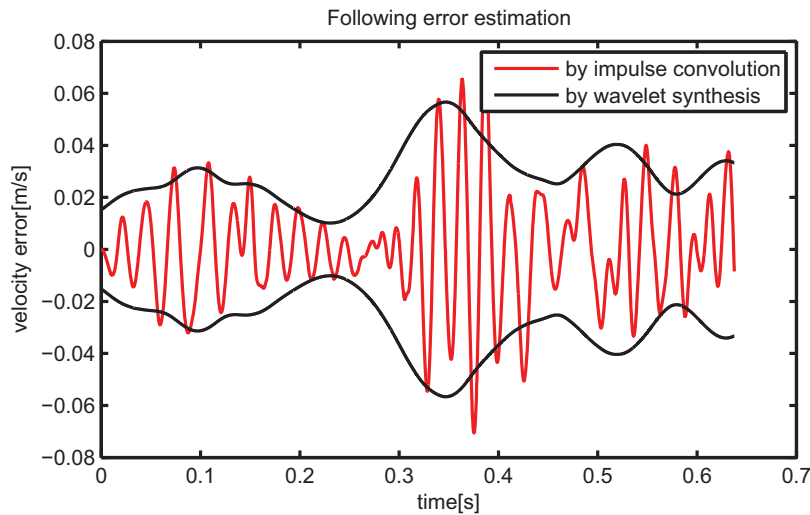
108

Figure 5.12: Following error by impulse convolution and amplitude error envelope by wavelet synthesis

5.2.3 Summary of amplitude error calculation by Wavelet Synthesis

The above algorithm is to find a way to calculate the error between input amplitude and output amplitude in the mechanical transfer element between drive and tool in machine tools. Wavelet analysis is used as a time-frequency analysis tool to calculate the frequency response of second order systems. The input signal is analyzed by the synthesis wavelets in the way introduced in section 5.2.2, such that the amplitude of the error between input and output signals is estimated. Simulation results show that the proposed algorithm yields good results in estimating the amplitude error levels, and in the time location of the resonance frequency of the mechanical system, of the response of machine tools with flexible structures. It is difficult to use wavelet analysis (or any other time-frequency analysis) in the normal way (i.e. analyzing the whole spectrum of the signal in time and frequency) because of the uncertainty principle which puts limitations on both the time and frequency resolutions. Analyzing the full spectrum, besides being time consuming, cannot give a correct calculation of the system response because of the associated uncertainties. Therefore the proposed synthesis algorithm can give better means of analysis because it does not aim to carry out a full spectrum analysis, but rather focus on the frequency that causes problem to the mechanical system.

In order to improve the proposed algorithm and to use it correctly, its application limitations are discussed below.

- Response cancellation effect: the system response usually has an oscillatory nature. In case of an input signal of compound frequency content, at one point in time, the system response due to a certain frequency content in the input can be positive, while the

system response due to another frequency content (or due to a certain lag) is negative, so both responses cancel each other out (for example, the application of input shaping). This cannot be sensed by the algorithm because it calculates only the absolute value of the amplitude of the error of response.

- Limited frequency range: the algorithm can estimate the response error for a frequency range only a little above the characteristic frequency of the system. At higher frequencies the error is large. In some applications this can be acceptable, while in others maybe not. It is worth noting that at high frequencies the value of G becomes less than 1 which means that (G-1) is less than zero. This cannot be estimated by the algorithm, because the value of the Wavelet Transform cannot go below zero.

- Time-frequency analysis: when the frequency and time information are needed in a signal, full spectrum analysis by wavelet transform can be conducted. When the response of the system (with a natural frequency) to the input signal is needed, synthesis wavelets are required. And normally, one wavelet is enough to detect the resonance response.

5.3 Resonance Frequency Reduced Trajectory

The resonance frequency of the mechanical system in the axial trajectory comes from the trajectory design process. In the trajectory design process, time optimization under the restriction of the machine tool capacity is the main aim. No attention is paid to the possibility of resonance vibration that the trajectory could bring, which makes the time optimal trajectory no longer time optimal in the respect of response.

Now that the area on the trajectory where the resonance vibration could happen can be found, the next step is to find a solution to reduce the vibration. To reduce resonance vibration, the most effective way, when no mechanical change is possible, is to get rid of the resonance frequency that exists in the axial trajectory. This can be done by reducing or increasing the limitation of the jerk in the trajectory design phase, which is to be described next.

5.3.1 Reduction of vibration in axis motion

When the limitations (velocity, acceleration, jerk) of a path for a trajectory plan are changed, the resultant trajectory includes different frequency contents as before. Changing the limi-

tation of the jerk is the most efficient way to change the frequency contents in the trajectory, as at the most moments, the axis jerk reaches its maximum in time optimal trajectory plan. To change the frequency contents in the trajectory, the jerk limitation can either be increased or lowered. However, increasing the jerk limitation can cause the machine tool to overrun its capability. Hence, lowering the path jerk limitation in the problematic areas of the path is the solution. Besides the vibration caused by the resonance phenomenon, there are also vibrations due to the rapid change of the acceleration in soft control as described in section 2.1.2.

The movement law in 2.3 with controlled jerk in soft control is defined as,

$$
\dddot{s}(t) = \begin{cases}
\hat{J}t, & 0 \leq t < t_1 \\
\hat{a}, & t_1 \leq t < t_2 \\
\hat{a} - \hat{J}t, & t_2 \leq t < t_3 \\
0, & t_3 \leq t < t_4 \\
-\hat{J}t, & t_4 \leq t < t_5 \\
-\hat{a}, & t_5 \leq t < t_6 \\
-\hat{a} + \hat{J}t, & t_6 \leq t < t_7 \\
0. & t_3 \leq t
\end{cases}
\tag{5.35}
$$

with

$\hat{J}$: maximum jerk,

$\hat{a}$: maximum acceleration

When it is applied to the second-order mechanical system, maximum dynamic vibration error is mainly related to each uniformly accelerated phase due to the jerk value and constant jerk time, which is the phase before the constant acceleration phase. From the first constant acceleration phase of the movement law in the above equation, the expression of the dynamic vibration error can be resolved as in the following equation (5.36) [5][4]:

$$
E_{vib}(t) = \frac{\hat{J}}{\omega_0^3} \left[-sin(\frac{\hat{a}\omega_0}{\hat{J}})cos(\omega_0\bar{t}) - (cos(\frac{\hat{a}\omega_0}{\hat{J}}) - 1)sin(\omega_0\bar{t}) \right],
\tag{5.36}
$$

with

$\bar{t} = t - \frac{\hat{a}}{\hat{J}}$,

ω_0 : characteristic frequency,

Equation (5.36) demonstrates the nonlinear influence of the jerk value on the oscillatory amplitude. Lowering the jerk would minimize the vibration amplitudes of the system with the minimum sacrifice of speed. When the maximum jerk value $\hat{J}$ is correctly tuned, the frequency in the axial trajectory that is near or equals to the axial resonance frequency can be changed, therefore, motion errors in the axial movements are considerably reduced. However only reducing the jerk on the individual axis is not helpful, as the path parameters are considered in the trajectory planning phase. When the path jerk limitation is reduced, in the new calculated trajectory, the axis velocity, acceleration and jerk are also changed. Of course there are also cases where path jerk and/or path acceleration are zero, for example in a circle with constant path velocity, both path jerk and acceleration are zero. In such cases, path acceleration or path velocity has to be reduced.

5.3.2 Process of Redesign

The trajectory designed through the time optimal trajectory planning algorithm is parametrized with the curve parameter 's', which is named as the s-domain trajectory or path trajectory. The path trajectory has to be transfered to axial trajectories for each axis according to equation (2.2) in the time domain for further use. The resulting trajectory for each axis is named the time domain trajectory or axial trajectory. The process of trajectory designing from the capacity of the machine tools for a given path is described in section 2.1.2. It can be summarized as in the following Figure 5.13.
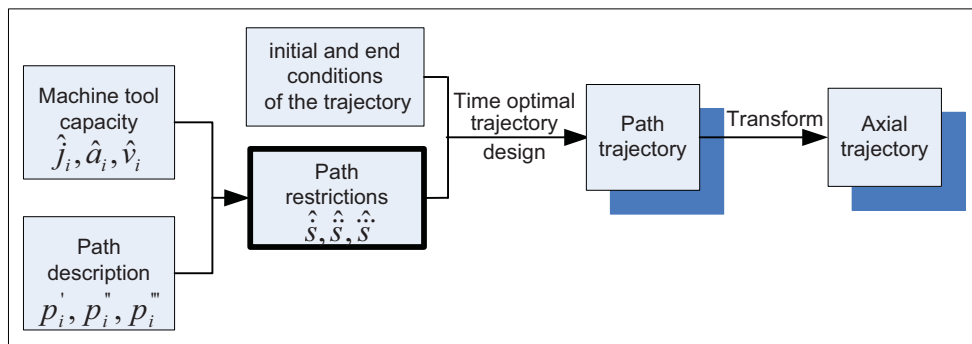

Figure 5.13: Process of trajectory design

Resonance vibration can happen on each axis of the machine tool. The axial trajectories of the machine tool are not the same. Normally, the resonance frequency of the machine tool axes are not the same either. Therefore, vibration analysis has to be done for each axis for its own resonance frequency. Thus, for the axial trajectory of each axis, the area where the resonance frequency exists can be found out through the Wavelet Transform as explained

in section 5.2. When the problematic areas in each axial trajectory are found, it is now possible to get rid of the excitation of the axis. However, in order to keep the path which is determined by the axial trajectories the same as before, it is necessary to change all the axial trajectories accordingly. Hence, modifications have to be carried out in the path trajectory, so that the axis trajectory of each axis can still keep the path. Thus, finding out the problematic area in the path trajectory from all the axial trajectories is unavoidable. This process can be explained more clearly by Figure 5.14. Then lowering the path jerk limitation in that problematic area and redesigning the path trajectory is the only way to lower the vibration in this situation. As already explained, redesigning the trajectory separately for only one axis in time domain is not possible, when a contour must be followed.
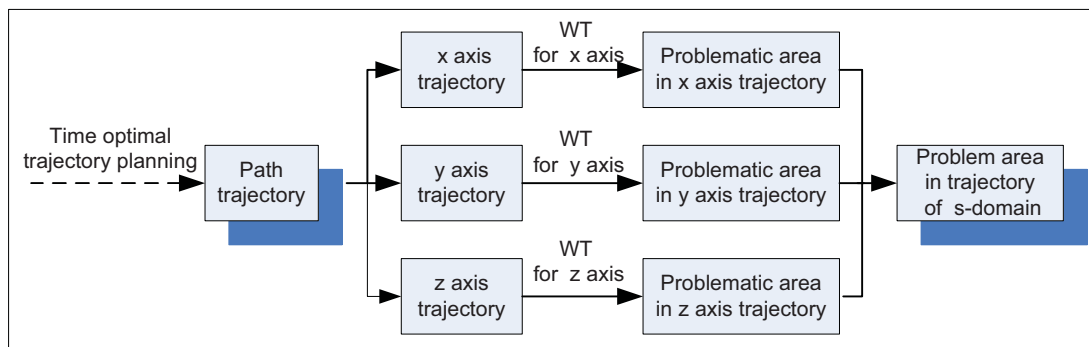

Figure 5.14: Find problematic area path trajectory

The redesigning process, shown in Figure 5.15, involves the same time optimization process as shown in Figure 5.13. Besides the time optimization process, the wavelet synthesis analysis of the resonance frequency in each axis is added to make sure that the designed trajectory will not create violent vibrations for that axis. For example, if there are violent vibrations in a machine tool axis, areas of the existence of resonance frequency are to be found. The corresponding path jerk is lowered, and the redesigning process of the time optimal plan is repeated.

Lowering the jerk limitation in the problematic areas is simple. However, how much the jerk should be lowered is unknown. The influence of lowering the path jerk on the frequency contents in the axial trajectory cannot be quantified. Therefore, it is not feasible to fix the reduction amount of the path jerk. An iterative process is required to decide whether the jerk should be further lowered or not, based on the wavelet synthesis of the vibration caused by resonance frequency contents in the axial trajectory. For each iterative process, the amount of reduction of jerk can be set to within 10% of the last jerk value, depending on the user.

One criterion for stopping the iterative process is the wavelet synthesis of the vibration within given limitation. The limitation can be set by the user according to the separate

application. Lowering down the jerk also means that the trajectory will have a longer time. It is not recommended to lower the jerk to a very low value, for example to the 50% of the orignal jerk limitation. Therefore, another criterion for stopping the iterative process is to set the maximum number of the iterative process. If the program is stopped by the second criterion, the vibration in axial trajectory may still appear, because of the frequency near the resonance frequency of that axis. In this case, further reduction of the acceleration or velocity limitation can be conducted. This is the same process as in lowering the jerk limitation, and will not be described here.

The above described iterative redesign process of the trajectory is shown in Figure 5.15.
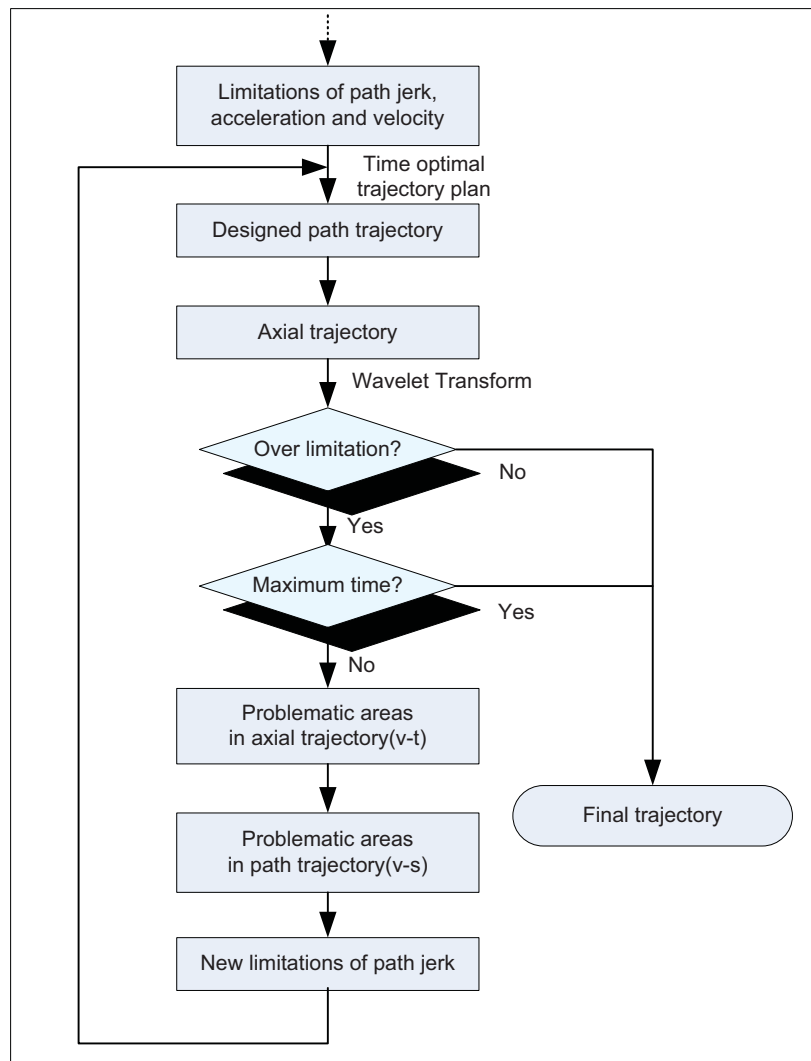

Figure 5.15: Redesign process of the trajectory to get rid of resonance frequency

5.4 Simulation Results

In this section, some simulation results are provided to verify the method presented above. The simulations are trajectories for a three-axis machine tool along a described path. The velocity trajectories of the x, y and z axes are shown in Figure 5.16. The final time of those velocity trajectories is $t_0 = 0.6382s$. The eigenfrequency of the x and y axes is 32Hz each, of z axis 50Hz. The damping ratio of each axis is 0.1.
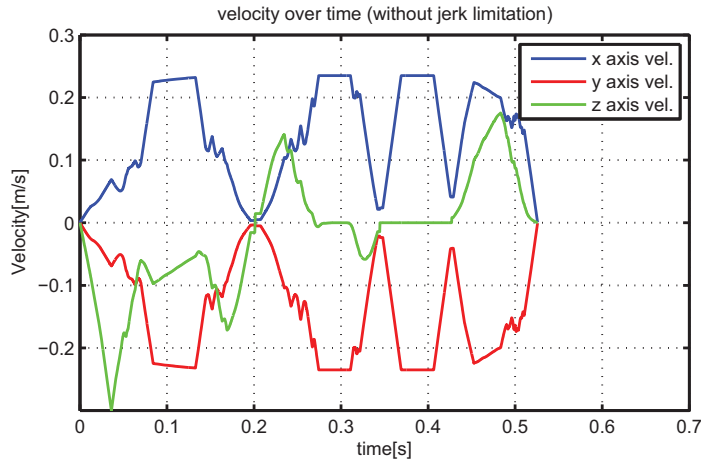
(a) Trajectories without jerk limitation
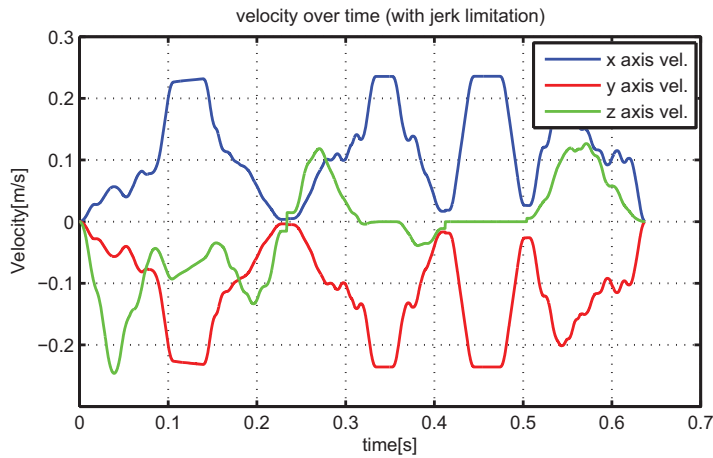
(b) Trajectories with jerk limitation

Figure 5.16: Axial velocity trajectories of a path

Figure 5.16(a) are velocity trajectories designed by brisk control prociple. The velocity trajectories in Figure 5.16(b) are designed according to the soft control principle, which is the jerk limited time optimal trajectory plan theory described in section 2.1.2. The soft control trajectories take longer time (0.11s in this case). Compared with the trajectories designed under the brisk control principle, the vibrations of the machine tool axes are already reduced with the soft control principle. However, in some areas of the trajectories some violent vibrations

can still happen, due to the reasons of resonance phenomenon or excessive jerk. In the blue curve of Figure 5.17(a), vibrations (amplitude error between original input and response) are estimated, according to the wavelet synthesis method developed in section 5.2, of the axis x and y with the designed trajectory along the mechanical axes. Similarly, the blue curve in (b) represents the vibrations from the z velocity trajectory along the z axis. In the application, if only $\Delta v = 0.04m/s$ for the vibration amplitude errors of each axis is allowed, the trajectories must be redesigned. The redesign process is done as given in section 5.3. The red curves in the (a) and (b) of Figure 5.17 are the vibration amplitude errors of the new velocity trajectories. Both of them are below the requirement of $0.04m/s$. The new trajectories now take $t_1 = 0.6720s$, that means plus 5.3%.
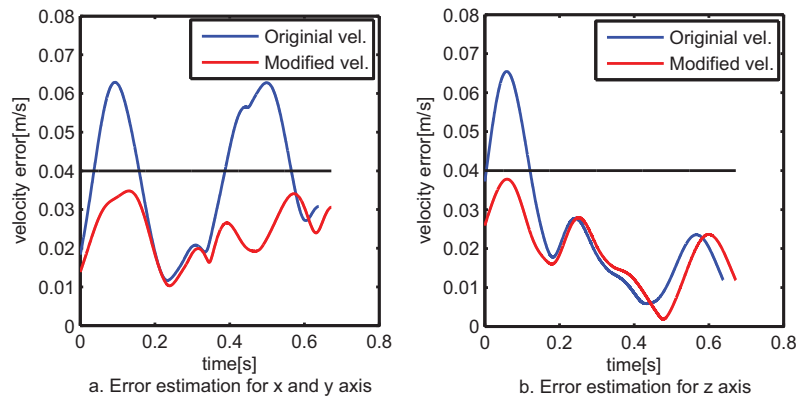

a. Error estimation for x and y axis   b. Error estimation for z axis

Figure 5.17: Estimated vibration amplitude error

Figure 5.18 shows the responses of the x and y axes to the original velocity and to the redesigned velocity (x and y axes have same trajectory and same eigenfrequency). In Figure 5.18(a), the blue curve is the original x axis velocity, the red curve is the corresponding response velocity to the original velocity. In Figure 5.18(b), the blue curve is the redesigned x axis velocity, and the corresponding response is the red curve. Clearly, the response to the redesigned velocity is better than to the original velocity, as the vibration amplitude error is lowered down to be within $0.04m/s$. In Figure 5.19, the responses to the original and redesigned velocity of z axis are plotted. Again, the blue curve in Figure 5.19(a) is the original velocity for the z axis. The red curve in Figure 5.19(a) is the response to it. In Figure 5.19(b), the blue curve is the redesigned velocity of z axis, and the red one is the response to the redesigned velocity.

The time increment from the original trajectory($t_0 = 0.6382$) to the redesigned trajectory ($t_1 = 0.6720s$) is 5.3%, but the reduction of the vibration is obvious. If the same time length of the redesigned trajectory is equally distributed to the original velocity, the reduction of the vibration is not visible.
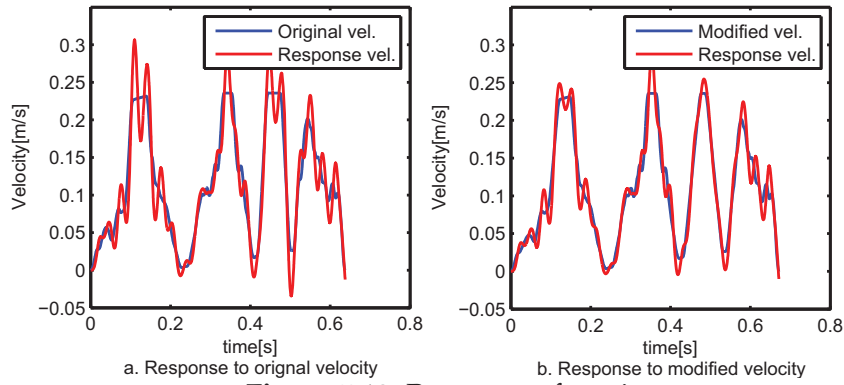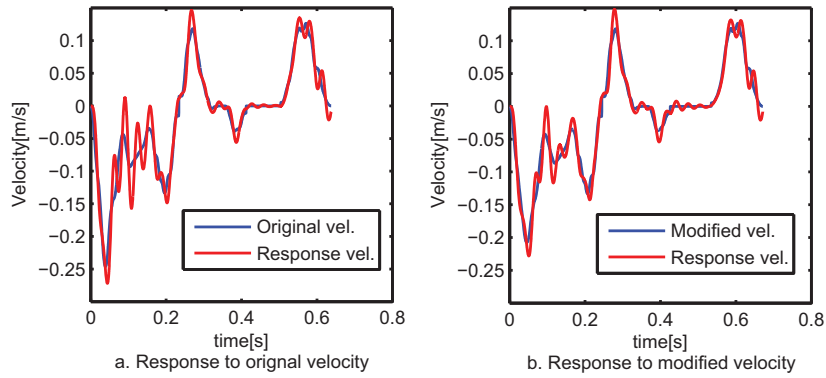
Figure 5.18: Response of x axis

Figure 5.19: Response of z axis

Now, if the application requires that only $\Delta v = 0.02 m/s$ should be allowed, a new velocity trajectory plan has to be redesigned. Figure 5.20 shows the vibration amplitude error through the wavelet synthesis method again. The blue curves in both (a) and (b) are the same as in Figure 5.17. The red curves are the redesigned trajectory response error according to the limitation of $0.02 m/s$. The time for the new trajectory is now $t_2 = 0.779s$ instead of the original $t_0 = 0.6382s$, plus 22%.
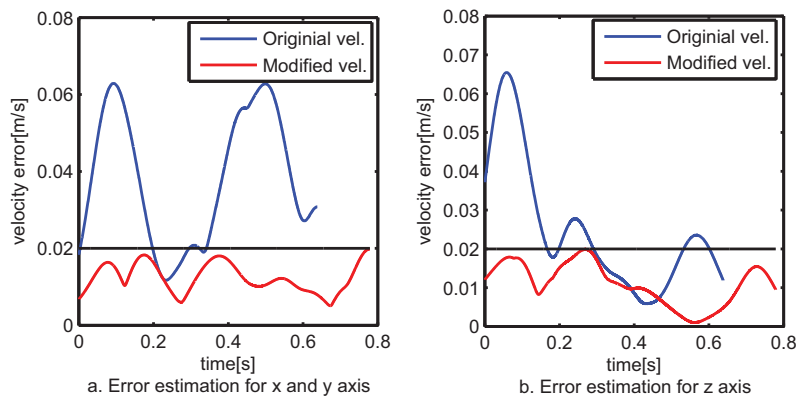
Figure 5.20: Estimated vibration amplitude error

The response of the newly redesigned trajectory of x axis velocity is shown in Figure 5.21(b). In Figure 5.21(b), the blue curve is the redesigned trajectory and the red one is the response. Compared with Figure 5.21(a), which is the same as Figure 5.18(a), the vibration of the redesigned trajectory is greatly reduced. The same conclusion can also be drawn for the trajectory of the z axis in Figure 5.22.

a. Response to orignal velocity   b. Response to modified velocity

Figure 5.21: Response of x axis

a. Response to orignal velocity   b. Response to modified velocity

Figure 5.22: Response of z axis

Examples and Experiments
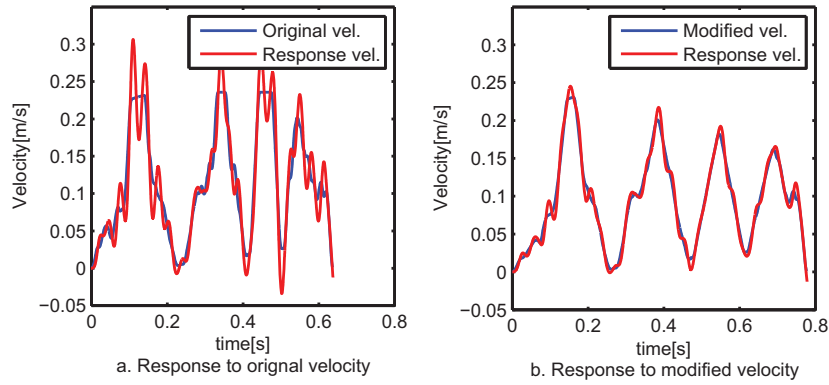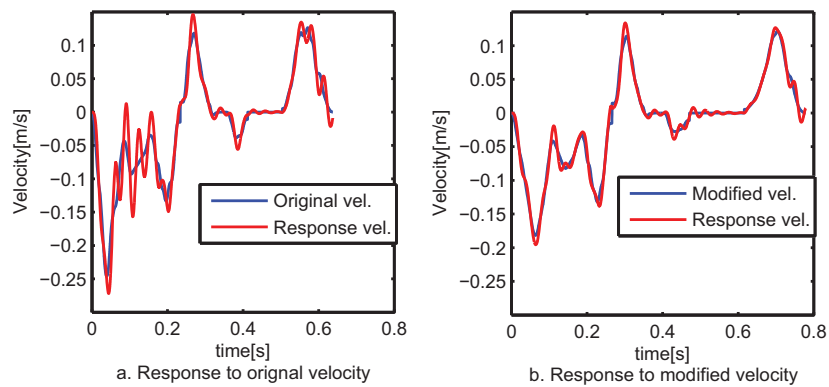
In this chapter, the work in chapter 3 and chapter 5 will be tested by the test rig that is described in section 2.3.1. As the test rig can be modeled as a second order system, the theory in chapter 4 is not needed here.

From Figure 2.13, it is known that the pole of the mechanical system is $F_n = 50Hz$, and the zero of the mechanical system is $F_z = 35Hz$. The inertia of the load is the same as the motor, $J_M = J_L = 0.0013kgm^2$, from the motor data sheet. Thus, the spring constant can be calculated to be $K = 66Nm/rad$ (see also Appendix A.1).

The experiments are made for the trajectories which are already mentioned in chapter 5. The unit of velocity trajectory in chapter 5 is m/s. In the experiment, the unit of velocity is min^{-1}. The value in the experiment is $1000*$ the value in Figure 5.18(a).

- trajectory 1: from time optimal trajectory plan as in Figure 5.18(a);

- trajectory 2: redesigned trajectory after wavelet analysis as in Figure 5.18(b). The load response of the redesigned trajectory should not exceed $0.04 * 1000 = 40min^{-1}$;

- trajectory 3: redesigned trajectory after wavelet analysis as in Figure 5.21(b). The load response of the redesigned trajectory should not exceed $0.02 * 1000 = 20min^{-1}$.

These three trajectories are the velocity setpoints to four control strategies:

- strategy 1: PI controller is tuned as if the system is a rigid system. The equation (3.5) and (3.6) are applied. Resultant parameter: $k_r = 3.25Nm \cdot s/rad$ and $t_i = 3.3ms$.

- strategy 2: PI controller is automatically tuned by Siemens firmware. The parameters of the controller are: $k_r = 1.149Nm \cdot s/rad$ and $t_i = 16.3ms$.

- strategy 3: PI controller is tuned according to the elastic double ratio method; the equation (3.16) and (3.17) are applied. Resultant parameter: $k_r = 0.553Nm \cdot s/rad$ and $t_i = 12.7ms$;

- strategy 4: PI controller is tuned as if the system is a rigid system, and an input shaper is added. The parameters of PI controller are the same as in strategy 1, the parameters of input shaper are: $A_1 = 0.5056$, $A_2 = 0.4944$, $T_1 = 0$, $T_2 = 14.1ms$.

The motor velocity and load velocity will be obtained from the sensor attached to them. In the following plots, the motor velocities are curves in blue, and the load velocities are curves in red. The following errors between the load velocity and motor velocity are plotted in Appendix A.3.

Trajectory 1: time optimal trajectory

The velocity setpoints for the test rig is the original output from time optimal trajectory plan. The response of the motor and load to this command under different control strategy is plotted out in Figure 6.1. In Figure 6.1(a), the PI controller parameters are tuned as if the mechanical system is a rigid one. It is seen that there are a lot of vibrations on the load response. In Figure 6.1(b), the PI controller parameters are tuned by the Siemens Firmware automatically. The vibrations of the load are reduced a lot. In Figure 6.1(c), the PI controller parameters are tuned through the elastic double ratio. The vibrations are reduced further compared with (b). Then in Figure 6.1(d), the input shaper is added, and the PI controller is tuned the same as in (a). Although there are still vibrations, it can be seen that the further improvement is obvious.

Trajectory 2: redesigned trajectory with following error restriction of $40min^{-1}$

The setpoints in this test is the redesigned trajectory after the wavelet analysis in chapter 5. The requirement of the redesigned trajectory through the wavelet analysis is that the following error should not be over $40min^{-1}$. The response of the load and motor to this trajectory are presented in Figure 6.2. In Figure 6.2(a), the PI controller parameters are tuned the same as in Figure 6.1(a), as if the mechanical system is a rigid one. Comparing Figure 6.2(a) with Figure 6.1(a), the maximum vibration level is already reduced. In Figure 6.2(b), the PI controller parameters are tuned by the Siemens firmware automatically. The vibrations of the load are reduced. In Figure 6.2(c), the PI controller parameters are tuned through the elastic double ratio. The vibrations are reduced further compared with (b). Then in Figure 6.2(d), the input shaper is added, and the PI controller is tuned the same as in (a). Only small vibrations can still be identified.

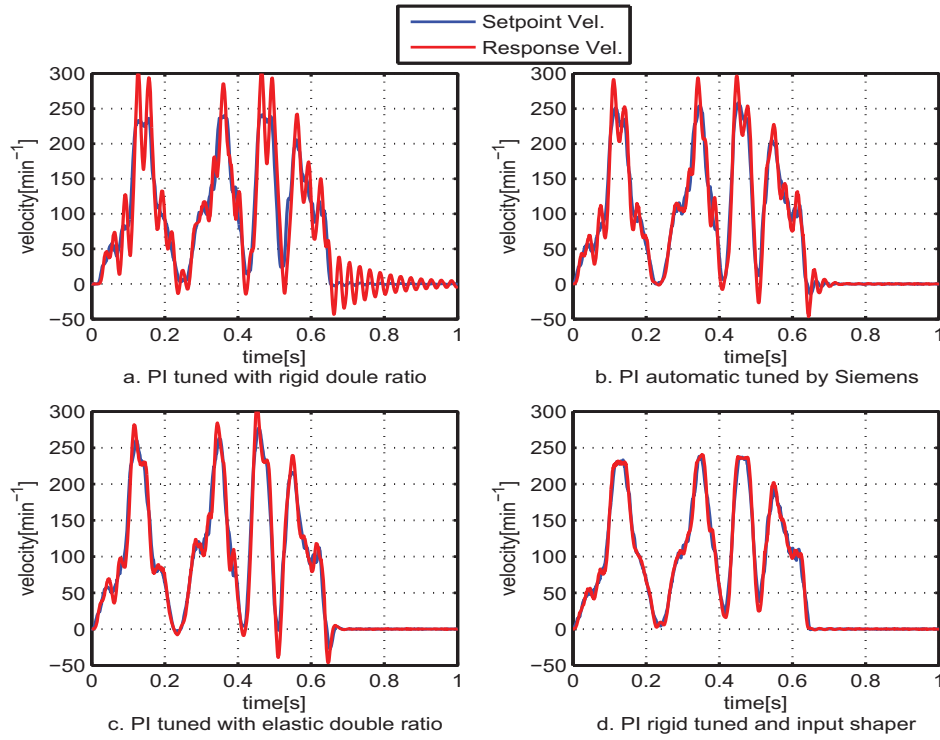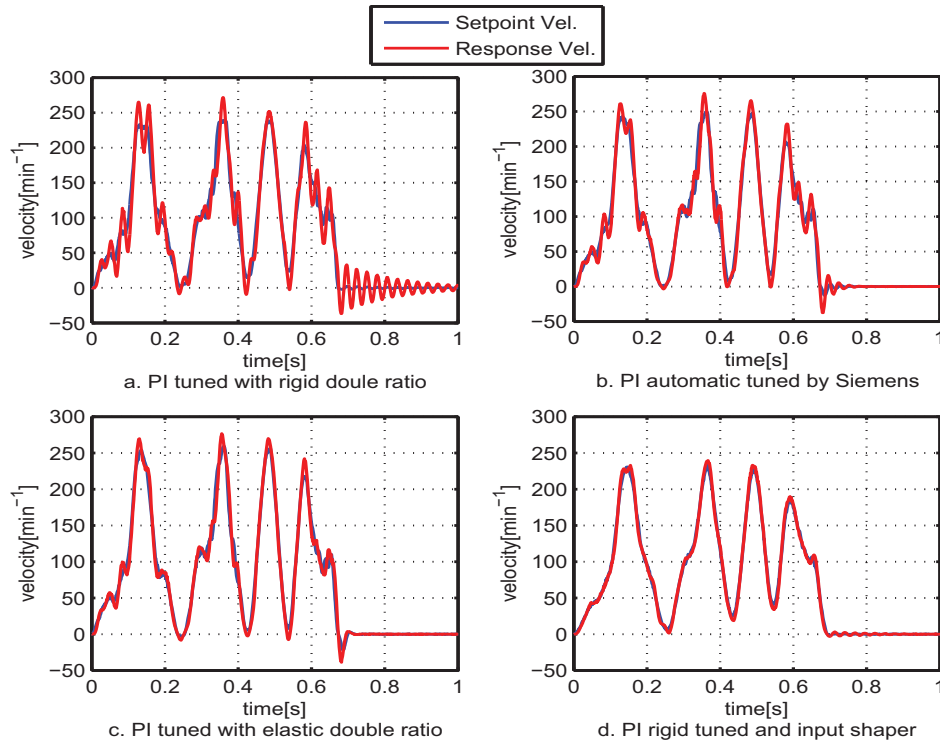**Figure 6.1:** Time optimal trajectory

Figure 6.2: Redesigned trajectory with maximum $40min^{-1}$ following error restriction

Trajectory 3: redesigned trajectory with following error restriction of $20min^{-1}$

The setpoints in this experiment is the second redesigned trajectory after the wavelet analysis in chapter 4. The restriction of the redesigned trajectory through the wavelet analysis

is that the following error should not exceed $20min^{-1}$. The response of the load and motor to this trajectory is presented in Figure 6.3. In Figure 6.3(a), the PI controller parameters are tuned the same as in Figure 6.3(a), as if the mechanical system is a rigid one. Comparing Figure 6.3(a) with Figure 6.1(a) and Figure 6.2(a), the maximum vibration level is reduced further. In Figure 6.3(b), the PI controller parameters are tuned by the Siemens Firmware automatically. The vibrations of the load are reduced compared with (a). In Figure 6.3(c), the PI controller parameters are tuned through the elastic double ratio. The vibrations are reduced further compared with (b). Then in Figure 6.3(d), the input shaper is added, and the PI controller is tuned the same as in (a). Almost no vibrations can be identified.
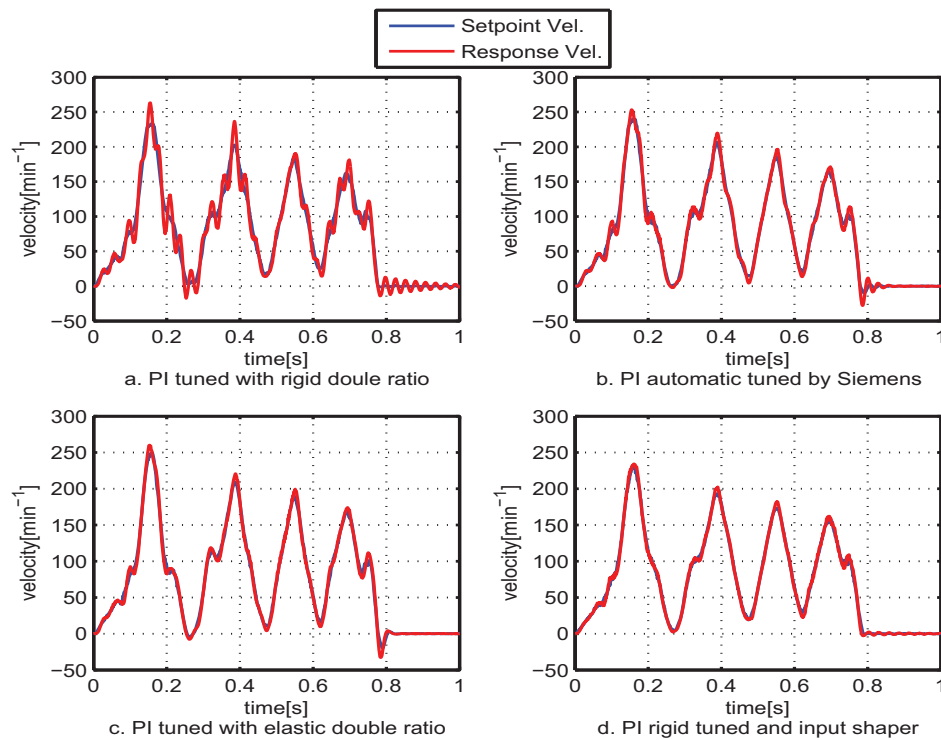
Figure 6.3: Redesigned trajectory with maximum $20min^{-1}$ following error restriction

The load velocity following errors of the three trajectories in Figure 6.1(a),Figure 6.2(a) and Figure 6.3(a) are plotted together in Figure 6.4.

All the figures in this chapter are the results from the real experiments.

a. Original trajectory as reference input

b. Modified trajectory with 40min^{-1} following error as reference input

c. Modified trajectory with 20min^{-1} following error as reference input
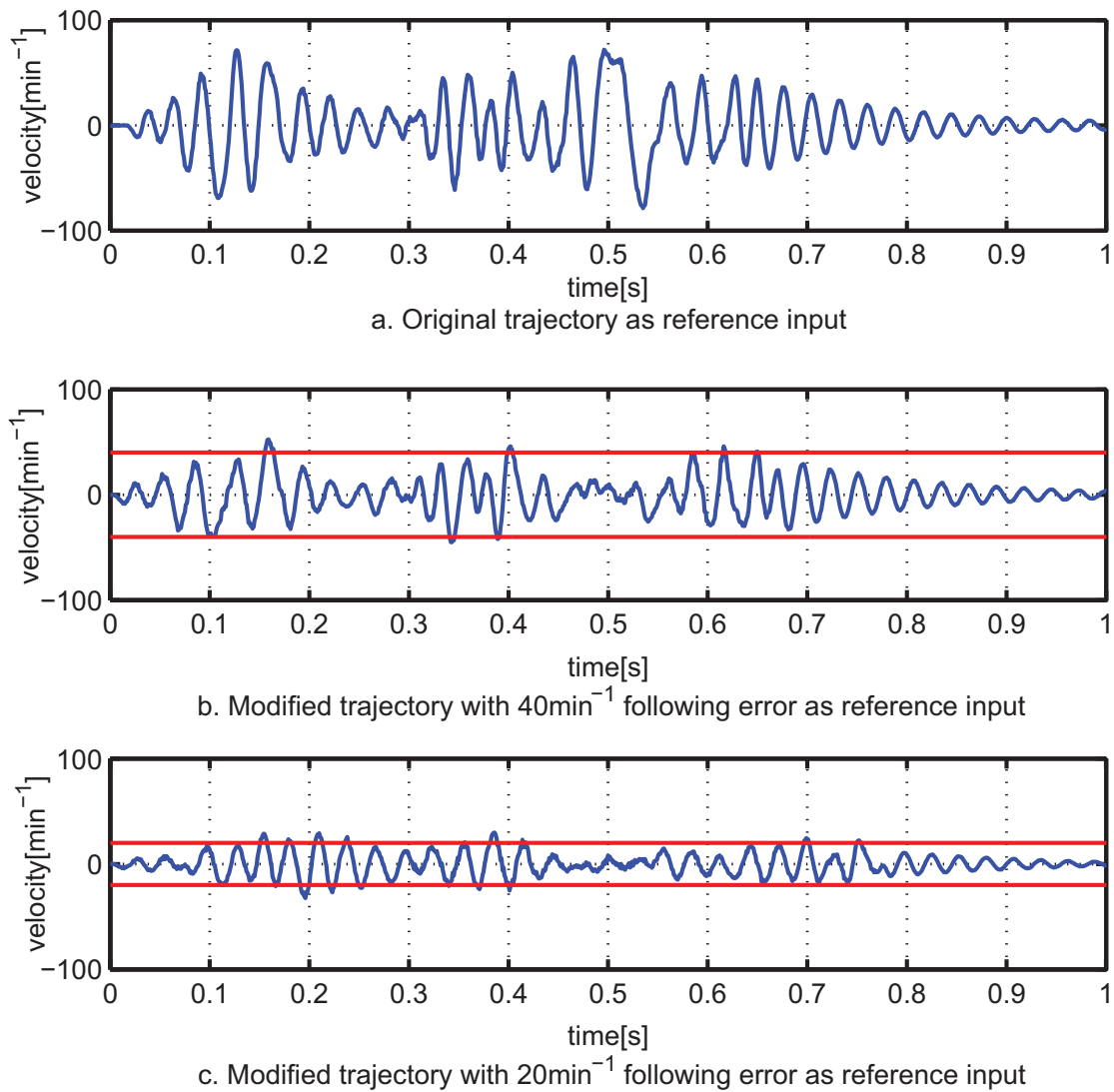
Figure 6.4: Following error of load for the three trajectories in the case of rigid double ratio

CHAPTER 7

Conclusions

Motivated by improving the accuracy and shortening response time of the drive systems with elastic mechanical components, the following areas of research are investigated in this thesis: reducing the vibrations, identifying mechanical parameters of the drive chain, and preventing the vibrations from occuring.

Reducing vibrations is effectively conducted by controllers. Cascaded control loop is widely accepted in the machine tool industries. Normally the parameters of the PI controller in the velocity loop are tuned according to some optimization theory for rigid systems. It is well-known that the parameter of the P controller depends on the total inertia of the drive system. The parameter of I controller depends on the equivalent time of the current control loop. In this thesis, the elasticity property of the driven chain is taken into account in determining the parameters of the PI controller. Simple formulas are developed for the parameters of the PI controller to reduce vibrations. The formulas in equations (3.16) and (3.17) show that the tuning of the PI controller in modern servo drives for elastic systems depends not only on the inertia of the mechanical system but also on the mechanical system's frequency. This also corresponds to engineers' experience in the tuning of controllers of elastic systems. The developed formulas of the PI controller deliver a compromise between response time and accuracy both for the command signal and the disturbance signal. Simulations clearly show that the formulas are very effective in eliminating vibrations for a step input and a step disturbance. The experiments also prove that the PI controller tuned according to the formulas causes less following error than the PI controller that is automatically tuned by the Siemens controller optimization algorithm in Firmware.

Since time is a strict criterion in production engineering, the equations of the PI controller for an elastic system are not the best solution. Input shaper, as a feedforward method, is applied in the cascaded control loop to achieve the time and accuracy requirements. When the input

shaper is applied, the PI controller can be tuned as if the mechanical system is a rigid system. Thus the response of the velocity loop is very fast. The vibrations in the velocity loop can then be eliminated through the input shaper. But it is important to know that this method can only be applied when the system has only a small disturbance. The parameters of the input shaper are set by the equations (3.53) after the analysis of the movement of the poles of the controlled mechanical system. To improve robustness to the frequency change and tuning parameters of the PI controller, another input shaper with equation (3.54) can be added to convolve with the shaper above. Calculations and experiments confirm that the input shaper together with the PI controller gives the most quick and accurate result if the system has no disturbance.

Given the inertia of the motor and the frequency response of the mechanical system, the parameters K_i (spring constant) and J_i (inertia) of the serially connected components of the drive system can be easily identified from equations (4.68), (4.69), (4.70), and (4.71). This identification is suitable for systems with no damping or with little damping, for example damping ratio $\xi < 0.1$, which applies in most cases in the drive systems of machine tools. For damped systems, this identification method can be modified, and provides accurate results for up to 4th order systems. For higher order damped systems, however, efforts are still needed to develop a general equation to identify the parameters of the system. Simulation of the identification of the undamped system proves that the identification method presents quick and accurate results. This method is practice-oriented, as normally in drive systems, the inertia of the motor is known from the motor data sheet, and the frequency response can easily be measured from the firmware supplied with the servo drives. When all the parameters of the mechanical system are known, an exact model of the mechanics can be set up for further use.

Resonance vibrations happen when frequency of the setpoints signal is near or equals the natural frequency of the mechanical system. To prevent such vibrations from occurring, besides the soft control method, the method of eliminating the resonance frequency in the command signal is presented in this thesis. The time-frequency analysis of the command signal is first done by means of Wavelet Transform. Where and how much amplitude error, that is caused by the resonance frequency in the command signal for a second order system, is localized and quantified by wavelet coefficient extraction and synthesis. Compared with the impulse convolution method, wavelet synthesis is much quicker and more precise in the estimation of the following error. When the vibration level calculated from the amplitude

error envelope by the wavelet synthesis is above the limitation set by the user, the command signal (here the trajectory) has to be redesigned.

The redesigning process is an iterative process. By lowering the path limitation of the jerk, acceleration or velocity in the path ranges where the resonance frequency of the mechanical system exists, the vibration due to that frequency can be effectively reduced. Both simulations and experiments verify that the wavelet synthesis method predicts the following error correctly in time and amplitude. They also prove that the redesigned trajectories, based on the information of the wavelet synthesis results, are effective in reducing the vibration level to the user defined level. However, due to the time consideration of the trajectory, and the computation time for the iterative process, it is not practical to reduce the vibration level through the trajectory redesign phase as much as possible. The rest is reduced through controllers.

From reducing vibrations through controllers, to parameter identification of the elastic mechanical drive system, to preventing vibrations through designation of the trajectory, the work in this thesis achieves and assures the aim of getting rid of vibrations in the shortest time for the elastic mechanical system in the whole drive system process.

Appendix

A.1 Calculation of the Test Rig's Parameters

The test rig is composed of two motors, and one rod. The two motors are connected to the rod through couplings. The material and parameters of the rod are:

- Material: Steel with density $\rho = 7.85 * 10^3 Kg/m^3$ and shear modulus $\mu = 82.05 GPa$

- Length: $L = 500mm$

- Diameter: $R = 4mm$

The schematic diagram of the test rig is shown in the following Figure A.1.
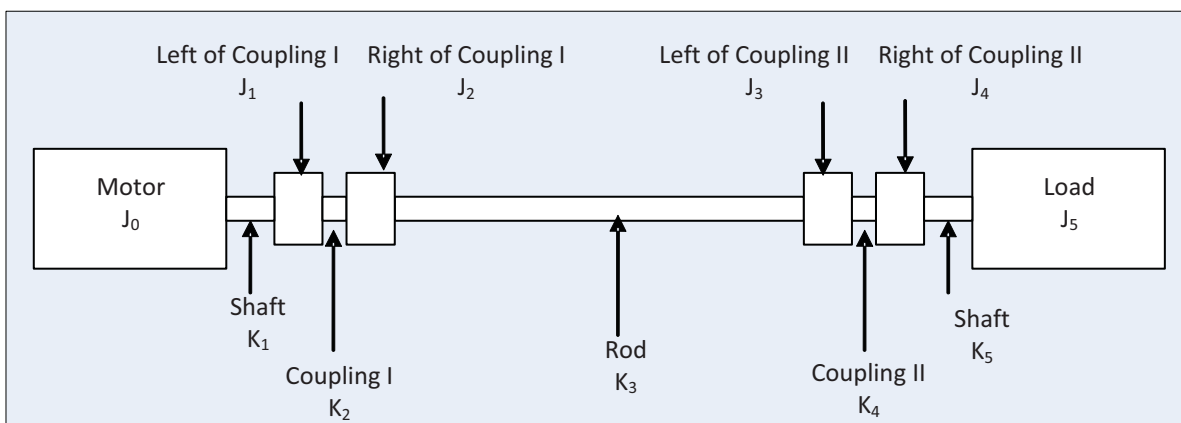

Figure A.1: Schematic of the test rig

Some of the parameters of the mechanical system are given by the data sheet of the motor and coupling:

- Motor data: $J_M = 1.3 * 10^{-3} Kgm^2$;

- Coupling data: $J_C = 2.6 * 10^{-6} Kgm^2$; $K_C = 1.4 * 10^4 Nm/rad$

The calculated parameters of the rod are:

- The moment of inertia of the rod is $J_R = \frac{\pi * L * \rho * R^4}{2g} = 1.6 * 10^{-7} Kgm^2$.

- The torsional stiffness of the rod is calculated as $K_C = \frac{\pi * R^4 * \mu}{2L} = 66 Nm/rad$.

- The torsional stiffness of the outside rod of the motor is $K_R = 1.08 * 10^5 Nm/rad$.

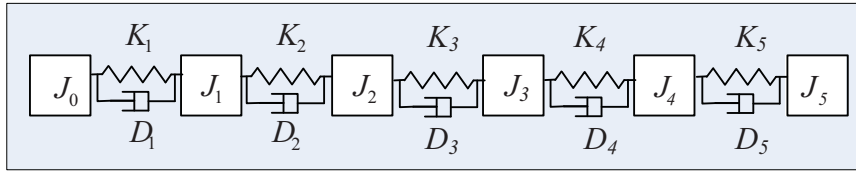This mechanical system can be modeled as the six mass-spring system as in Figure A.2.

Figure A.2: Exact model of the test rig

Now the moment of inertia parameters of the mechanical system can be summarized according to Figure A.2 as:

- $J_0 = J_M = 0.0013 Kgm^2$

- $J_1 = J_C/2 = 1.31 * 10^{-6} Kgm^2$

- $J_2 = J_R/2 + J_C/2 = 1.38 * 10^{-6} Kgm^2$

- $J_3 = J_R/2 + J_C/2 = 1.38 * 10^{-6} Kgm^2$

- $J_4 = J_C/2 = 1.31 * 10^{-6} Kgm^2$

- $J_5 = J_M = 0.0013 kgm^2$

The stiffnesses in the system are:

- spring constant of the outside rod of the motor: $K_1 = 1.08 * 10^5 Nm/rad$

- spring constant of the coupling I: $K_2 = 1.4 * 10^4 Nm/rad$

- spring constant of the connecting rod: $K_3 = 66 Nm/rad$

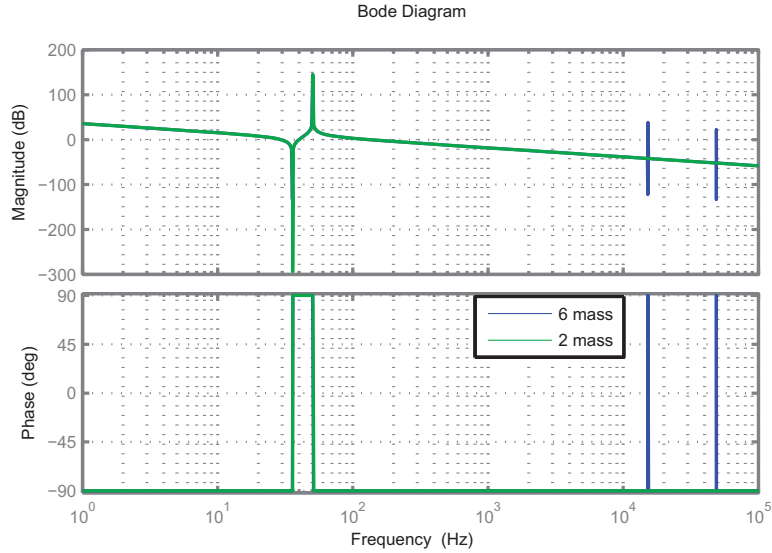- spring constant of the coupling II: $K_4 = 1.4 * 10^4 Nm/rad$

Figure A.3: Bode diagram

- spring constant of the outside rod of the load: $K_5 = 1.08 * 10^5 Nm/rad$

Plot the bode diagram with torque to motor as input and velocity of motor as output in Figure A.3 in the blue curve.

The frequency of the mechanical system can be identified to be : 50Hz, 15215Hz, 15296Hz, 48958Hz and 48958Hz. Except the 50Hz, the other 4 frequencies are very high. They can be ignored. Therefore, a second order system to modify this mechanical system is enough. The simplified schematic diagram and model of the in second order mechanics is shown in Figure A.4.

Figure A.4: Mass-spring-damper model of the test rig
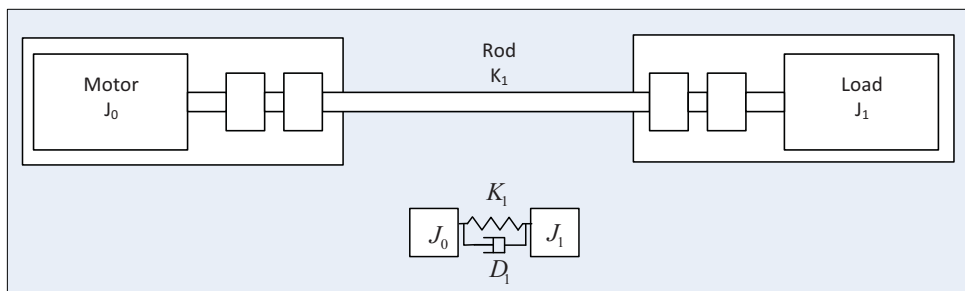
In the above model, the following parameters of the mechanical parameters are applied: $J_0 = 1.3 * 10^{-3} Kgm^2$, $J_1 = 1.3 * 10^{-3} Kgm^2$, $K_1 = 66Nm/rad$. The corresponding bode diagram of the second order model is plotted in Figure A.4 in green curve. It can be seen that in the low frequency range, the second-order and the sixth-order systems are identical.

131

A.2 For fifth order system (n=4)

For $n = 4$, the poles and zeros are (p_1, p_2, p_3, p_4) and (z_1, z_2, z_3, z_4) respectively. The denominator and numerator of the transfer function determined by frequency response are written to

$$f_4(s) = \prod_{i=1}^{4}(s^2 + p_i^2) = s^8 + {}^4a_1 s^6 + {}^4a_2 s^4 + {}^4a_3 s^2 + {}^4a_4, \tag{A.1a}$$

$$g_4(s) = \prod_{i=1}^{4}(s^2 + z_i^2) = s^8 + {}^4b_1 s^6 + {}^4b_2 s^4 + {}^4b_3 s^2 + {}^4b_4. \tag{A.1b}$$

From equations (4.27a), (4.32a) and (4.43a), the denominator is known as in the following equations. From equations (4.27b), (4.32b) and (4.43b), the numerator of the transfer function is also determined as in the following equations:

$$\begin{aligned} f_4(s) &= (s^2 + r_4)(s^6 + {}^3a_1 s^4 + {}^3a_2 s^2 + {}^3a_3) - c_3' c_4 (s^4 + {}^2a_1 s^2 + {}^2a_2) \\ &= s^8 + s^6({}^3a_1 + r_4) + s^4({}^3a_1 r_4 + {}^3a_2 - c_3' c_4) + \\ &\quad + s^2({}^3a_2 r_4 + {}^3a_3 - {}^2a_1 c_3' c_4) + ({}^3a_3 r_4 - {}^2a_2 c_3' c_4). \end{aligned} \tag{A.2a}$$

$$\begin{aligned} g_4(s) &= (s^2 + r_4)(s^6 + {}^3b_1 s^4 + {}^3b_2 s^2 + {}^3b_3) - c_3' c_4 (s^4 + {}^2b_1 s^2 + {}^2b_2), \\ &= s^8 + s^6({}^3b_1 + r_4) + s^4({}^3b_1 r_4 + {}^3b_2 - c_3' c_4) + \\ &\quad + s^2({}^3b_2 r_4 + {}^3b_3 - {}^2b_1 c_3' c_4) + ({}^3b_3 r_4 - {}^2b_2 c_3' c_4). \end{aligned} \tag{A.2b}$$

Mapping equations (A.1a) and (A.2a), as well as equation (A.1b) and (A.2b), the relationships between the coefficients of the transfer functions expressed by different methods are

$$ {}^4a_1 = {}^3a_1 + r_4, \tag{A.3a}$$

$$ {}^4b_1 = {}^3b_1 + r_4, \tag{A.3b}$$

$$ {}^4a_2 = {}^3a_1 r_4 + {}^3a_2 - c_3' c_4, \tag{A.3c}$$

$$ {}^4b_2 = {}^3b_1 r_4 + {}^3b_2 - c_3' c_4, \tag{A.3d}$$

$$ {}^4a_3 = {}^3a_2 r_4 + {}^3a_3 - {}^2a_1 c_3' c_4, \tag{A.3e}$$

$$ {}^4b_3 = {}^3b_2 r_4 + {}^3b_3 - {}^2b_1 c_3' c_4, \tag{A.3f}$$

$$ {}^4a_4 = {}^3a_3 r_4 - {}^2a_2 c_3' c_4, \tag{A.3g}$$

$$ {}^4b_4 = {}^3b_3 r_4 - {}^2b_2 c_3' c_4. \tag{A.3h}$$

From equations (4.46b), (A.3a) and (A.3b), c_1 is calculated as

$$^4a_1 - {}^4b_1 = {}^3a_1 - {}^3b_1 = c_1,$$
$$c_1 = {}^4a_1 - {}^4b_1.$$

From equations (4.45b) and (A.3b), the following equation exists:

$$^4b_1 = {}^3b_1 + r_4 = c_1' + r_2 + r_3 + r_4. \tag{A.4}$$

From equations (4.46b), (4.48) and (A.3d), the following equation can be obtained:

$$^4a_2 - {}^4b_2 = ({}^4a_2 - {}^4b_2)r_4 + ({}^3a_2 - {}^3b_2)$$
$$= c_1 r_4 + c_1(r_2 + r_3) = c_1(r_2 + r_3 + r_4). \tag{A.5}$$

Let we let $x_{11} = \frac{{}^4a_2 - {}^4b_2}{c_1}$, combine this with equation (A.5), x_{11} is also

$$x_{11} = r_2 + r_3 + r_4. \tag{A.6}$$

From equations (A.4) and (A.6), c_1' is

$$c_1' = {}^4b_1 - x_{11}. \tag{A.7}$$

From equations (4.47), (4.51) and (A.3d), the following equation can be obtained:

$$^4b_2 = {}^3b_1 r_4 + {}^3b_2 - c_3' c_4$$
$$= (c_1' + r_2 + r_3)r_4 + (c_1' + r_2)r_3 + c_1' r_2 - c_1' c_2 - c_2' c_3 - c_3' c_4. \tag{A.8}$$

From equations (4.35), (4.48), (4.52), (A.3e) and (A.3f), the following equation is derived:

$$^4a_3 - {}^4b_3 = ({}^3a_2 - {}^3b_2)r_4 + ({}^3a_3 - {}^3b_3) - ({}^2a_1 - {}^2b_1)c_3' c_4 r$$
$$= c_1(r_2 + r_3)r_4 + c_1(r_2 r_3 - c_2' c_3) - c_1 c_3' c_4. \tag{A.9}$$

Let $x_{12} = \frac{{}^4a_3 - {}^4b_3}{c_1}$, combine this with equation (A.9), x_{12} can be written to

$$x_{12} = (r_2 + r_3)r_4 + r_2 r_3 - c_2' c_3 - c_3' c_4, \tag{A.10}$$

From equations (A.8) and (A.10), the following equation is derived:

$$^4b_2 - x_{12} = c_1'r_4 + r_2r_4 + r_3r_4 + c_1'r_3 + r_2r_3 + c_1'r_2 - c_1'c_2 - c_2'c_3 - c_3'c_4$$
$$- r_2r_4 - r_3r_4 - r_2r_3 + c_2'c_3 + c_3'c_4 \tag{A.11}$$
$$= c_1'(c_2' + r_3 + r_4).$$

Let $x_{11}' = \frac{^4b_2 - x_{12}}{c_1'}$, combine this with equation (A.11), x_{11}' is

$$x_{11}' = c_2' + r_3 + r_4. \tag{A.12}$$

From equations (A.6) and (A.12), c_2 is calculated as

$$c_2 = x_{11} - x_{11}'. \tag{A.13}$$

From equations (4.10), (4.34b), (4.45f), (4.51) and (A.3f), the following equation exists:

$$^4b_3 = {}^3b_2r_4 + {}^3b_3 - {}^2b_1c_3'c_4,$$
$$= (c_1'r_3 + r_2r_3 + c_1'c_2' - c_2'c_3)r_4 + c_1'c_2'c_3' - (c_1' + r_2)c_3'c_4.$$

From equations (4.10), (4.36), (4.52), (A.3g) and (A.3h), the following equation is derived:

$$^4a_4 - {}^4b_4 = ({}^3a_3 - {}^3b_3)r_4 - ({}^2a_2 - {}^2b_2)c^3c_4,$$
$$= c_1(r_2r_3r_4 - c_2'c_3c_4 - r_2c_3'c_4),$$

Let $x_{13} = \frac{^4a_4 - {}^4b_4}{c_1}$, combine this with equation (A.14), x_{13} is

$$x_{13} = r_2r_3r_4 - c_2'c_3r_4 - r_2c_3'c_4. \tag{A.14}$$

From equations (A.14) and (A.14), the following equation can be obtained:

$$^4b_3 - x_{13} = c_1'r_3r_4 + r_2r_3r_4 + c_1'c_2'r_4 - c_2'c_3'r_4 + c_1'c_2'c_3' - c_1'c_3'c_4 - r_2c_3'c_4$$
$$- r_2r_3r_4 + c_2'c_3r_4 + r_2c_3'c_4 \tag{A.15}$$
$$= c_1'(c_2'r_4 + r_3r_4 + c_2'c_3' - c_3'c_4).$$

Let $x_{12}' = \frac{^4b_3 - x_{13}}{c_1'}$, combine this with equation (A.15), x_{12}' is

$$x_{12}' = c_2'r_4 + r_3r_4 + c_2'c_3' - c_3'c_4. \tag{A.16}$$

From equations (A.10) and (A.16), the following equation is obtained:

$$x_{12} - x'_{12} = c_2(r_3 + r_4), \tag{A.17}$$

Let $x_{21} = \frac{x_{12} - x'_{12}}{c_2}$, combine this with equation (A.16), x_{21} is

$$x_{21} = r_3 + r_4. \tag{A.18}$$

From equations (A.12) and (A.18), c'_2 is calculated as

$$c'_2 = x'_{11} - x_{21}. \tag{A.19}$$

From equations (4.10), (4.39), (4.57) and (A.3h), the following equation exists:

$$\begin{aligned}{}^4b_4 &= {}^3b_3r_4 - {}^2b_2c'_3c_4 = c'_1c'_2c'_3r_4 - c'_1c'_2c'_3c_4 \\ &= c'_1c'_2c'_3c'_4.\end{aligned} \tag{A.20}$$

Let $x'_{13} = \frac{{}^4b_4}{c'_1}$, combine this with equation (A.20), x'_{13} is rewritten to

$$x'_{13} = c'_2c'_3c'_4. \tag{A.21}$$

From equations (A.14) and (A.21), it is known

$$x_{13} - x'_{13} = c_2(r_3r_4 - c'_3c_4). \tag{A.22}$$

Let $x_{22} = \frac{x_{13} - x'_{13}}{c_2}$, combine this with equation (A.22), x_{22} is rewritten to

$$x_{22} = r_3r_4 - c'_3c_4. \tag{A.23}$$

From equations (A.16) and (A.23), the following equation can be obtained:

$$x'_{12} - x_{22} = c'_2(c'_3 + r_4). \tag{A.24}$$

Let $x'_{21} = \frac{x'_{12} - x_{22}}{c'_2}$, and combine this with equation (A.23), x'_{21} is rewritten to

$$x'_{21} = c'_3 + r_4. \tag{A.25}$$

From equations (A.18) and (A.25), c_3 is now calculated as

$$c_3 = x_{21} - x'_{21}. \tag{A.26}$$

Let $x'_{22} = \frac{x'_{13}}{c'_2}$, and combine this with equation (A.21), x'_{22} is rewritten to

$$x'_{22} = c'_3 c'_4. \tag{A.27}$$

From equations (A.23) and (A.27), it is known that

$$x_{22} - x'_{22} = c_3 r_4. \tag{A.28}$$

Let $x_{31} = \frac{x_{22} - x'_{22}}{c_3}$, and combine this with equation (A.28), x_{31} is rewritten to

$$x_{31} = r_4. \tag{A.29}$$

From equations (A.25) and (A.29), c'_3 is calculated as

$$c'_3 = x'_{21} - x_{31}, \tag{A.30}$$

Let $x'_{31} = \frac{x'_{22}}{c'_3}$, and combine this with equation (A.27), x'_{31} is rewritten to

$$x'_{31} = c'_4. \tag{A.31}$$

From equations (4.10), (A.29) and (A.31), c_4 is finally calculated as

$$c_4 = x_{31} - x'_{31}. \tag{A.32}$$

From equations (A.4), (A.7), (A.13), (A.19), (A.26), (A.30),(A.31) and (A.32) together with the definitions of $x_{11}, x'_{11}, x_{12}, x'_{12}, x_{21}, x'_{21}, x_{13}, x'_{13}, x_{22}, x'_{22}, x_{31}$ and $x'_{31}, c_1, c'_1, c_2, c'_2, c_3, c'_3, c_4$ and c'_4

are summarized as,

$$c_1 = {}^4a_1 - {}^4b_1, \quad x_{11} = \frac{{}^4a_2 - {}^4b_2}{c_1},$$

$$c_1' = {}^4b_1 - x_{11}, \quad x_{12} = \frac{{}^4a_3 - {}^4b_3}{c_1}, \quad x_{11}' = \frac{{}^4b_2 - x_{12}}{c_1'},$$

$$c_2 = x_{11} - x_{11}', \quad x_{13} = \frac{{}^4a_4 - {}^4b_4}{c_1}, \quad x_{12}' = \frac{{}^4b_3 - x_{13}}{c_1'}, \quad x_{21} = \frac{x_{12} - x_{12}'}{c_2},$$

$$c_2' = x_{11}' - x_{21}, \quad x_{13}' = \frac{{}^4b_4}{c_1'}, \quad x_{22} = \frac{x_{13} - x_{13}'}{c_2}, \quad x_{21}' = \frac{x_{12}' - x_{22}}{c_2'}, \quad \text{(A.33)}$$

$$c_3 = x_{21} - x_{21}', \quad x_{22}' = \frac{x_{13}'}{c_2'}, \quad x_{31} = \frac{x_{22} - x_{22}'}{c_3},$$

$$c_3' = x_{21}' - x_{31}, \quad x_{31}' = \frac{x_{22}'}{c_3'},$$

$$c_4' = x_{31}',$$

$$c_4 = x_{31} - x_{31}'.$$

A.3 Following Errors in the Experiments

The following errors of the load response in Figure 6.1 are plotted in Figure A.5.
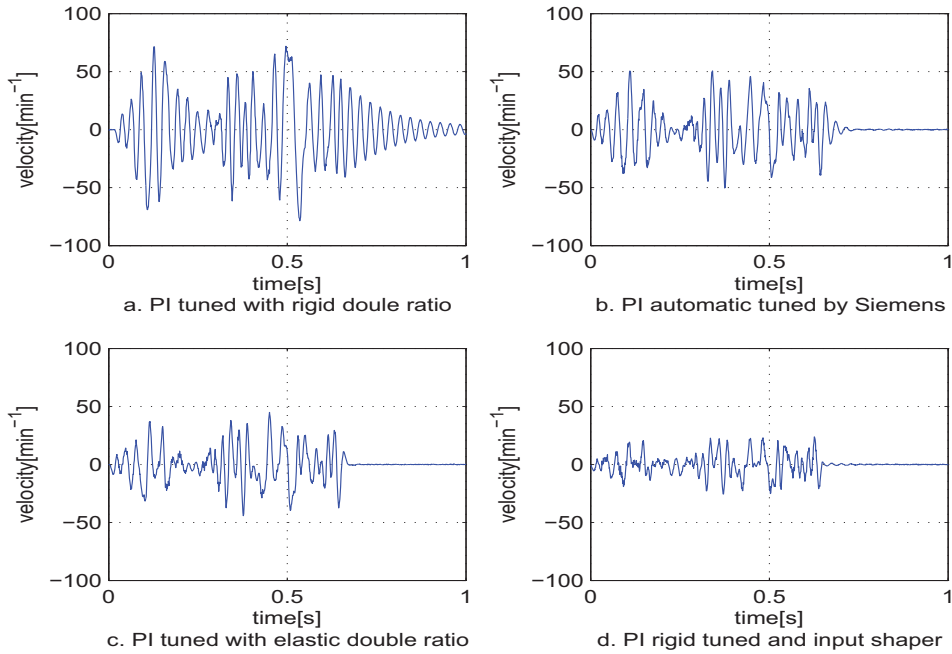
Figure A.5: Load following errors with four controller strategies in the case of time optimal trajectory

The following errors of the load response in Figure 6.2 are plotted in Figure A.6.

Figure A.6: Load following errors with four controller strategies in the case of redesigned trajectory with maximum $40min^{-1}$ following error restriction

The following errors of the load response in Figure 6.3 are plotted in Figure A.7.

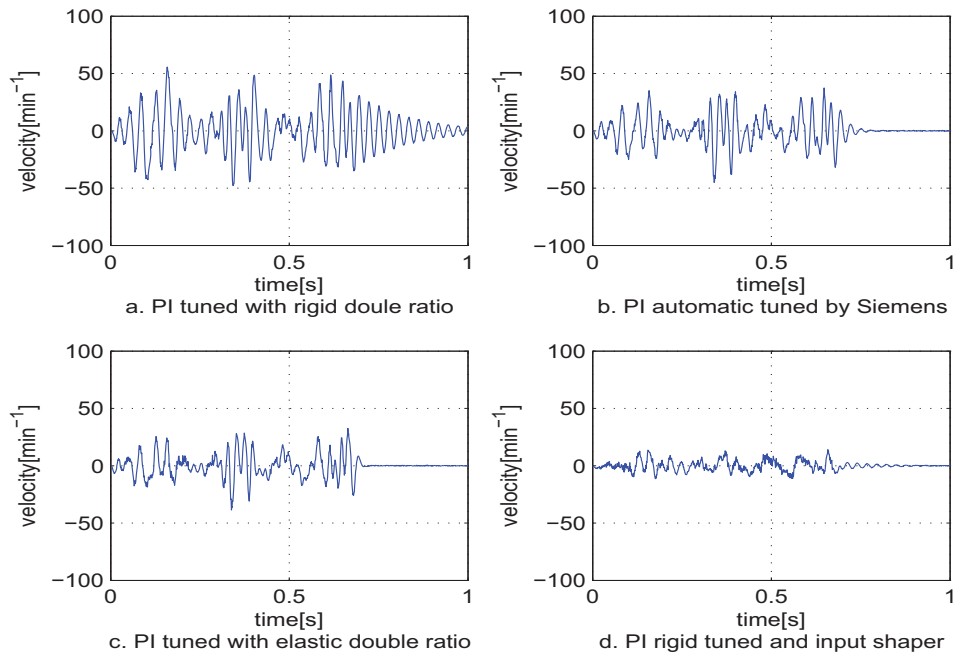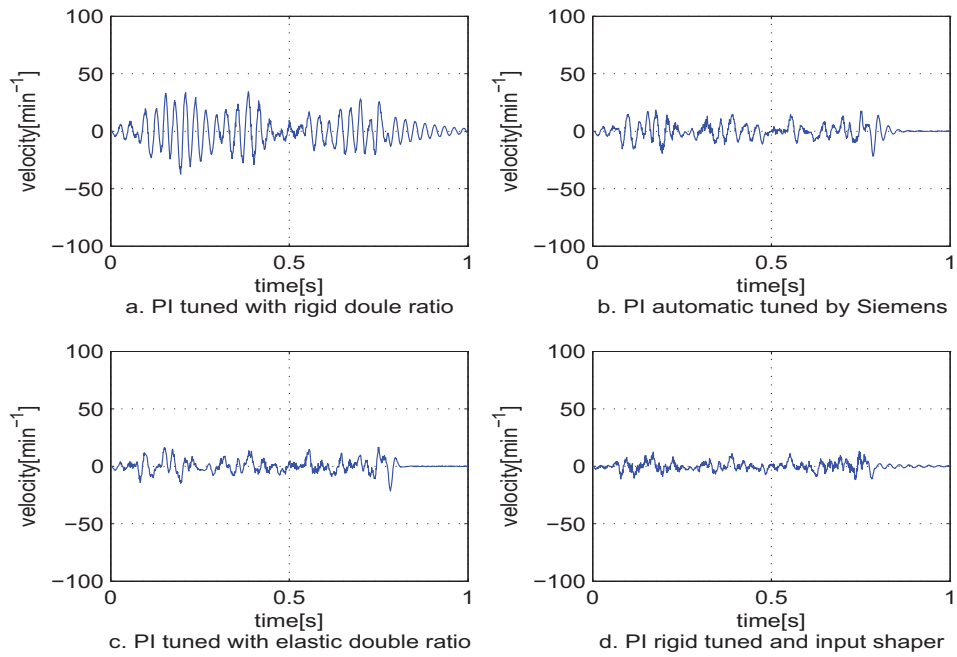**Figure A.7:** Load following errors with four controller strategies in the case of redesigned trajectory with maximum $20 min^{-1}$ following error restriction

References

[1] AHMAD, H., HAMM, C., PAPIERNIK, W., AND TRÖNDLE, H. P. Identifying plant parameters using linear least squares and stochastic techniques. In *International PCIM Europe 2006 Conference* (Nuremberg, Germany, May 2006).

[2] ALLEN, J. Short term spectral analysis, synthesis, and modification by discrete fourier transform. *IEEE Trans. on Acoust., Speech, and Sig. Proc. 25*, 3 (1977), 235–238.

[3] ASHLEY, S. High speed machining goes mainstream. *Mechanical Engineering-CIME May* (1995), 56–61.

[4] BARRE, P., BEAREE, R., BORNEH, P., AND DUMETZ, E. Influence of a jerk controlled movement law on the vibratory behavior of high-dynamics systems. *Journal of Intelligent and Robotic Systems 42* (2005), 275–293.

[5] BEAREE, R., BARRE, P., AND BLOCH, S. Influence of high speed machine tool control parameters on the contouring accuracy - application to linear and circular interpolation. *Journal of Intelligent and Robotic Systems 40* (2004), 321–342.

[6] BOERLAGE, M., TOUSAIN, R., AND STEINBUCH, M. Jerk derivative feedforward control for motion systems. In *Proceedings of the 2004 American Control Conference* (Boston,MA,USA, June-July 2004), pp. 4843–4848.

[7] BRANDENBURG, G., AND PAPIERNIK, W. Feedforward and feedback strategies applying the principle of input balancing for minimal tracking errors in cnc machine tools. In *Proceedings of 4th Workshop on Advanced Motion Control* (Tsu-City, Japan, March 1996), vol. 2, pp. 612–618.

[8] BYRNE, G., DORNFELD, D., AND DENKENA, B. Advancing cutting technology. *CIRP Annals 2003, Manufacturing Technology 52*, 2 (2003), 483–507.

[9] COHEN, L. *Time-Frequency Analysis*. Prentice Hall PTR, Englewood Cliffs, NJ, 1995.

[10] CROCHIERE, R. E. A weighted overlap-add method of short-time fourier analysis/synthesis. *IEEE Trans. on Acoust., Speech, and Sig. Proc. 28*, 1 (1980), 99–102.

[11] CUTFORTH, C. F. An analysis and comparison of frequency-domain and time-domain input shaping. In *American Control Conference* (Philadelphia, PA, June 1998), pp. 3072–3074.

[12] DAUBECHIES, I. The wavelet transform, time-frequency localization and signal analysis. *IEEE Trans. Info. Theory 36* (1990), 961–1005.

[13] DEUR, J., AND PERIC, N. Analysis of speed control system for electrical drives with elastic transmission. In *Proceedings of the IEEE International Symposium on Industrial Electronics* (Bled, Slovenia, July 1999), vol. 2, pp. 624–630.

[14] DUHAMEL, P., AND VETTERLI, M. Fast fourier transforms: A tutorial review and a state of the art. *Signal Processing 19* (1990), 259–299.

[15] EKACHAIWORASIN, R. Design and evaluation of an algorithm for jerk-limited motion control. Master's thesis, Technical University of Hamburg-Harburg, 2005.

[16] ELLIS, G., AND GAO, Z. Cures for low-frequency mechanical resonance in industrial servosystems. In *Proceeding of the IEEE industry application society annual meeting* (Chicago, IL, USA, October 2001), vol. 1, pp. 252–258.

[17] ELLIS, G., AND LORENZ, R. Resonant load control methods for industrial servo drives. In *Proceeding of the IEEE industry application society annual meeting* (Rome,Italy, October 2000), vol. 3, pp. 1438–1445.

[18] FABERT, O., AND SCHMIDT, M. Wavelet filtering with high time-frequency resolution and effective numerical implementation applied on polar motion. *Artificial Satellites-Journal of Planetary Geodesy 38*, 1 (2003), 3–13.

[19] FLEISCHER, M. Adaptive reduced modal model identification for arbitrarily branched multi-inertia traction drive-trains. In *International PCIM Europe 2004 Conference* (Nuremberg, Germany, May 2004).

[20] FLOM, D. G., KOMANDURI, R., AND LEE, M. High speed machining of metals. *Annual Reviews of Material Science 14* (1984), 231–278.

[21] GROSS, H., HAMANN, J., AND WIEGÄRTNER, G. *Electrical Feed Drives in Automation*. Publicis MCD Corporate Publishing, 2001.

[22] IBRAHIM, S., AND MIKULCIK, E. A method for the direct identification of vibration parameters from the free response. *The Shock and Vibration Bulletin 47*, 4 (1977), 183–198.

[23] ISERMANN, R. *Mechatronic systems*. Springer Verlag, 2003.

[24] JONES, D. L., AND PARKS, T. W. Time-frequency window leakage in the short-time fourier transform. *Circuits, Systems, and Signal Processing 6*, 3 (1987), 263–286.

[25] JORDAN, D., MIKSAD, R., AND POWERS, E. J. Implementation of the continuous wavelet transform for digital time series analysis. *Rev.Sci.Instrument 68*, 3 (1997), 1484–1494.

[26] JUANG, J., AND PAPPA, R. An eigen system realization algorithm for modal parameter identification and model reduction. *Journal of Control Dynamics 8* (1985), 620–627.

[27] KAPILA, V., TZES, A., AND YAN, Q. Closed-loop input shaping for flexible structures using time delay control. *Journal of Dynamic System, Measurement and control, 122*, 3 (September 2000), 454–459.

[28] KESSLER, C. Das symmetrische Optimum, Teil I. *Regelungstechnik 6*, 11 (1958), 395–400.

[29] KESSLER, C. Das symmetrische Optimum, Teil II. *Regelungstechnik 6*, 12 (1958), 432–436.

[30] KOZAK, K. *Robust command generation for nonlinear systems*. PhD thesis, Georgia Institute of Technology, 2003.

[31] KOZAK, K., HUEY, J., AND SINGHOSE, W. Performance measures for input shaping. In *Proceedings of 2003 IEEE Conference on Control Applications* (Istanbul, TURKEY, June 2003), vol. 2, pp. 1227–1232.

[32] KYRIAKOPOULOS, K., AND SARIDIS, G. Minimum jerk path generation. In *IEEE International Conference on Robotics and Automation* (Pennsylvania, USA, April 1998), vol. 1, pp. 364–369.

[33] LAMBRECHTS, P., BOERLAGE, M., AND STEINBUCH, M. Trajectory planning and feedforward design for high performance motion systems. In *Americian Control Conference, 2004 Proceedings of the 2004* (Boston, MA, USA, June-July 2004), pp. 4637–4642.

[34] LEWIS, F. L. *Applied Optimal Control and Estimation: Digital Design and Implementation*. Prentice-Hall, New Jersey, 1992.

[35] LIM, S., STEVENS, H., AND HOW, J. Input shaping design for multi input flexible systems. *Journal of Dynamic Systems, Measurement, and Control 121* (September 1999), 443–447.

[36] LJUNG, L. *System identification:theory for the user*. Prentice Hall PTR, 1999.

[37] MACFARLANE, S., AND CROFT, E. Design of jerk bounded trajectories for on-line industrial robot applications. In *IEEE International Conference on Robotics and Automation* (Seoul,Korea, May 2001), vol. 1, pp. 979–984.

[38] MAIA, N., AND SILVA, J. *Theoretical and Experimental Modal Analysis*. Research Studies Press, 1997.

[39] MARKERT, R., AND SEIDLER, M. Analytically based estimation of the maximum amplitude during passage through resonance. *International Journal of Solids and Structures 38*, 10 (2001), 1975–1992.

[40] MERTINS, A. *Signal Analysis*. John Wiley and Sons, 1999.

[41] OWENS, F. J., AND MURRAY, M. S. A short-time fourier transform. *Signal Processing 14*, 1 (1988), 3–10.

[42] PACAS, J., WILLWOCK, S., AND EUTEBACH, T. Parameter-identification of a two-mass-system in the frequency domain. In *International PCIM Europe 2004 Conference* (Nuremberg,Germany, May 2004).

[43] PAO, L., AND CUTFORTH, C. On frequency-domain and time-domain input shaping for multi-mode flexible structures. *Journal of Dynamic Systems, Measurement, and Control 125*, 3 (September 2003), 494–497.

[44] PAPIERNIK, W. Architecture and design of modern cnc/drive systems. In *Official Proceedings of the Thirty-Third International Intelligent Motion Conference* (Nürnberg,Germany, 1996), pp. 271–280.

[45] PAPIERNIK, W. Struktur, Entwurf und Verhalten moderner CNC-Servoantriebe. In *SPS/IPC/Drives 96 Tagungsband* (November 1996), pp. 397–417.

[46] PARK, S., KIM, B., CHUNG, W., AND YOUM, Y. Input preshaping with robust internal-loop compensator for residual vibration suppression of a beam-mass-cart system. In *Control of Vibration and Noise- New Millennium 2000 International Mechanical Engineering Congress and Exposition* (Orlando,Florida,USA, November 2000).

[47] PFEIFFER, F., AND JOHANNI, R. A concept for manipulator trajectory planning. In *IEEE International Conference on Robotics and Automation* (California,USA, April 1986), vol. 3, pp. 1399–1405.

[48] PIAZZI, A., AND VISIOLI, A. Minimum-time system-inversion-based motion planning for residual vibration reduction. *IEEE/ASME Transctions on Mechatronics 5*, 1 (March 2000), 12–22.

[49] PINTELON, R., GUILLAUME, P., ROLAIN, Y., SCHOUKENS, J., AND VAN HAMME, H. Parametric identification of transfer functions in the frequency domain - a survey. *IEEE Transactions on Automatic Control 39*, 11 (November 1994), 2245–2260.

[50] PISLARU, C., FORD, D. G., AND FREEMAN, J. M. Identification of modal parameters affecting the dynamic performance of cnc machine tools. In *Laser Metrology and Machine Performance VI: proceeding of the 6th International Conference and Exhibition on Laser Metrology , Machine Tool, CMM and Robot Performance* (The University of Huddersfield, UK, July 2003), pp. 161–170.

[51] PRITSCHOW, G. On the influence of the velocity gain factor on the path deviation. *CIRP Annals 1996, Manufacturing Technology 45*, 1 (1996), 367–371.

[52] PRITSCHOW, G. A comparison of linear and conventional electromechanical drives. *CIRP Annals 1998, Manufacturing Technology 47*, 2 (1998), 541–548.

[53] PRITSCHOW, G., AND BRETSCHNEIDER, J. A self-tuning controller for digitally controlled electromechanical servo drives in machine tools. *Annals of the CIRP 48*, 1 (1999), 307–312.

[54] RALL, K., ZHANG, X., AND PAPIERNIK, W. Modifizierte Umformung des Eingangssignals für die kreisförmige Trajektorie-Nachführung. *wt, Werkstattstechnik online 11/12*, 94 (2004), 697–701.

[55] RIESWIJK, T. *Robot Trajectory Planning, A Model Based Geometrically Constrained Approach.* PhD thesis, Delft University of Technology, Holland, 1992.

[56] ROMANO, M., AGRAWAL, B. N., AND ZAZZERA, F. B. Experiments on command shaping control of a manipulator with flexible links. *Journal of Guidance,Control and Dynamics 25*, 2 (March-April 2002), 232–239.

[57] SHILLER, Z., AND CHANG, H. Trajectory preshaping for high-speed articulated system. *Journal of Dynamic Systems, Measurement, and Control 117* (September 1995), 304–310.

[58] SHILLER, Z., CHANG, H., AND WONG, V. The practical implementation of time-optimal control for robotic manipulators. *Robotics and Computer-Integrate Manufacturing 12*, 1 (1996), 29–39.

[59] SINGER, N., AND SEERING, W. Preshaping command inputs to reduce system vibrations. *Journal of Dynamic Systems, Measurement and Control 112*, 1 (1990), 71–81.

[60] SINGER, N. C., AND SEERING, W. Design and comparison of command shaping methods for controlling residual vibration. In *Proceedings of the IEEE International Conference on Robotics and Automation* (Scottsdale, May 1989), vol. 2, pp. 888–893.

[61] SINGER, N. C., AND SEERING, W. P. An extension of command shaping methods for controlling residual vibration using frequency sampling. In *IEEE International Conference on Robotics and Automation* (Nice France, May 1992), vol. 1, pp. 800–805.

[62] SINGH, T., AND SINGHOSE, W. Tutorial on input shaping/time delay control of maneuvering flexible structures. In *American Control Conference* (Anchorage, AK,USA, 2002), pp. 1717–1731.

[63] SINGH, T., AND VADALI, S. R. Robust time delay control. *Journal of Dynamic Systems, Measurement, and Control 115*, 2 (1993), 303–306.

[64] SINGHOSE, W., AND CHUANG, T. Reducing deviations from trajectory components with input shaping. In *American Control Conference* (Seattle, WA, USA, 1995), vol. 1, pp. 929–933.

[65] SINGHOSE, W., AND SINGER, N. Initial investigations into the effects of input shaping on trajectory following. In *American Control Conference* (Baltimore,MD,USA, 1994), vol. 3, pp. 2526–2532.

[66] SINGHOSE, W., AND SINGER, N. Effects of input shaping on two-dimensional trajectory following. *IEEE Transactions on Robotics and Automation 12*, 6 (December 1996), 881–887.

[67] SINGHOSE, W. E., SEERING, W., AND SINGER, N. Input shaping for vibration reduction with specified insensitivity to modeling errors. In *Japan-Usa Sym. On Flexible Automation* (Boston,MA, 1996), vol. 1, pp. 307–313.

[68] SMITH, O. Posicast control of damped oscillatory systems. *Proc.of the IRE 45* (September 1957), 1249–1255.

[69] TALLFORS, M. *Parameter Estimation and Model Based Control: Design of Drive Train systems*. PhD thesis, Royal Institute of Technology, Stockholm, Sweden, 2005.

[70] TEOLIS, A. *Computational Signal Analysis with Wavelets*. Birkhäuser, 1998.

[71] TORRENCE, C., AND COMPO, G. P. A practical guide to wavelet analysis. *Bulletin of the American Meteorological Society 79*, 1 (1998), 61–78.

[72] TSE, N., AND LAI, L. Wavelet-based algorithm for signal analysis. *EURASIP Journal on Advances in Signal Processing 2007*, Article ID 38916 (doi:10.1155/2007/38916).

[73] TUTTLE, T., AND SEERING, W. A zero-placement technique for designing shaped inputs to suppress multiple-mode vibration. In *American Control Conference* (Baltimore, MD, June 1994), pp. 2533–2537.

[74] TUTTLE, T., AND SEERING, W. Experimental verification of vibration reduction in flexible spacecraft using input shaping. *Journal of Guidance, Control and Dynamics 20*, 4 (1997), 658–663.

[75] VACCARO, R. *Digital control: A state-space approach*. McGraw-Hill, Inc, 1995.

[76] WECK, M. 3- and 4-contact point spindle bearings - a new approach for high speed spindle systems. *CIRP Annals 2003, Manufacturing Technology 52*, 1 (2003), 311–316.

[77] WILSON, R. G., CALWAY, A. D., PEARSON, E. R., AND DAVIES, A. R. *Technical Report: An Introduction to the Multiresolution Fourier Transform and its Applications*. University of Warwick, UK, 1992.

[78] YOUNKIN, G. *Industrial servo control systems: fundamentals and applications*. CRC Press, 2002.

[79] ZÄH, M., AND BRANDENBURG, G. Das erweiterte Dämpfungsoptimum. *at-Automatisierungstechnik 35*, 7 (1987), 275–283.

[80] ZHANG, X., VÁZQUEZ, C., PAPIERNIK, W., AND RALL, K. Estimating parameters of input shaper in velocity control loop. In *Proceedings of the Eighth International Conference on Electrical Machines and Systems (ICEMS'2005)* (Nanjing, China, September 2005), pp. 1544–1548.

REFERENCES

[81] ZLAJPAH, L. On time optimal path control of manipulators with bounded joint velocities and torques. In *Proceeding of the 1996 IEEE International Conference on Robotics and Automation* (Minneapolis, Minnesota, USA, April 1996), pp. 1572–1577.

Curriculum Vitae

XINMEI ZHANG
Born on 01.Feb.1974
in Lianyungang, China
Nationality: Chinese

EDUCATION AND WORKING EXPERIENCE

05/2007 – now	Bosch Rexroth Electric Drives and Controls, Lohr am Main, Germany
11/2002 – 04/2007	Research assistant leading to a PHD degree at the Institute of Machine Tools, Robotics and Assembly Lines of Technical University of Hamburg-Harburg (TUHH), Hamburg, Germany
10/2000 – 10/2002	Master Degree Study in Mechatronics of TUHH, Hamburg, Germany
10/2000 – 10/2002	Global Engineering Program in Northen Institute of Technology, Hamburg, Germany
06/1999 – 09/2000	Research assistant, Nanjing University of Science and Technology (NJUST), Nanjing, China
09/1996 – 05/1999	Master Degree Study in Advanced Manufacturing from NJUST, Nanjing, China
09/1992 – 08/1996	Bachelor Degree Study in Mechanical Engineering from Huaihai Institute of Technology, Lianyungang, China
09/1981 – 09/1992	Ganyu Primary and High School, Lianyungang, China

LANGUAGES

Chinese:	mother language
English:	fluent
German:	good